LABORATORY INVESTIGATIONS OF EARTHQUAKE DYNAMICS

Thesis by

Kaiwen Xia

In Partial Fulfillment of the Requirements

for the Degree of

Doctor of Philosophy

Advisers:

Prof. Ares J. Rosakis and Prof. Hiroo Kanamori

California Institute of Technology

Pasadena, California

2005

(Defended January 25, 2005)

Acknowledgements

During my enjoyable stay at Caltech, I have got the chance not only to learn the cutting-edgy sciences and technologies but also to know many out-standing researchers.

First of all, I would like to sincerely thank my two advisors: Professor Ares J. Rosakis and Professor Hiroo Kanamori for their support, guidance and tolerance during my Ph.D. study. I believed that I should take the full advantage my experimental background in mechanics and apply it to the study of challenging problems in geophysics. Then it came to me that not many researchers have investigated the dynamics of earthquake experimentally. I did not realize initially though how challenging this problem was but I knew that as a leader in experimental dynamic fracture mechanics, Professor Rosakis is a person that I can rely on. Then one day four year ago I came to his office and told him that idea. To my surprise, he had the same idea long time ago and he was looking for a suitable student to work it out. With Professor Hiroo Kanamori, we started the long journey. I am glad that I did not disappoint them, especially the trust of Prof. Rosakis. We wrote a successful proposal to the National Science Foundation (NSF) and we have been obtaining exciting results. Professor Hiroo Kanamori is an example of traditional scholars who carry out research by themselves during their whole careers. He offered me lots of help during my transition period and afterwards.

I would like to thank other members in my thesis advisory committee, Professor G. Ravichandran, Professor Thomas H. Heaton, Professor Nadia Lapusta, and Professor Jeroen Tromp for their insightful suggestions during my thesis study. Special thanks to Professor Ravichandran, who has been virtually my mentor for years on both academic and non-academic issues. Professor Lapusta shared with

me her useful experience in job-searching in addition to her knowledge of the physics of earthquakes. Professor Heaton is probably one of the most devoted seismologists that I have ever met and he is deeply interested in all of the scientific issues involved in earthquakes. Professor Tromp is a very nice professor in Seismological Laboratory if not the nicest. All of them offered me tremendous encouragement during my Ph.D. studies.

Professor Thomas J. Ahrens took care of me during my first two years of stay at Caltech. We first met in China when I was doing my master degree at the University of Science and Technology in China. He has been a good mentor and friend of me since then. I was lucky to have one of the nicest professors in Seismological Laboratory as my academic advisor, Professor Robert Clayton.

In Seismological Laboratory and in the Graduate Aeronautical Laboratories, I have made many friends and from them, I learned a lot. I would like to thank Dr. Cangli Liu, Dr. Sidao Ni, Dr. Shengnia Luo, Dr. Chen Ji, Dr. Linseng Zeng, Dr. Jing Liu, Dr. Jascha Polet, Dr. Shiming Zhuang, Dr. Luoyu (Roy) Xu, Dr. Yunfeng Zhang, Dr. Yabei Gu, Dr. David Anderson, Dr. Omprakash Samudrala, Dr. Demirkan Coker, Dr. Tae-Soon Park, Dr. Vijay Chalivendra, Dr. Soonsung Hong, Mr. Georgios Lykotrafitis, Mr. Daoyuan Sun, Mr. Lu Xiao, Ms. Zhimei Yan, Ms. Min Chen, Ms. Yin Tan, Ms. Rongjing Zhang, Ms. Min Tao, and Ms. Theresa Kidd. Secretaries to Professor Rosakis, first Ms. Denise Thobe and then Ms. Donna Mojahedi are very professional in taking care of their business. Secretaries in the Seismological Laboratory are a group of most helpful and happiest ladies. Elisa, Viola, Michelle, Sue, Monica and others are members of that unique group. My life at Caltech will be much harder with their help.

I am very fortunate to have my wife, Rui Feng at my side when I was fighting to survive here at Caltech. She offered me support and encouragement especially

when I was in trouble. Our son, Albert is a lucky star to me. I started to make progress in my research during the time we were expecting him. When he was one year old, I got my first important result; when he was two years old, I published my first ever Science paper and I got my other two important results. He is almost three years now, I will put a period to my Ph.D. study and I am expecting another paper in Science. I am sure that he will continue to bring me luck. I would also like to thank my parents and parents-in-law in China who have been helping and supporting me.

Financial support of this work is provided by the National Science Foundation and the Office of Naval Research (monitored by Dr. Y.D.S. Rajapakse).

Abstract

Earthquakes are one of most destructive types of geological hazards. In this thesis I will attempt to understand it through controlled laboratory experiments. The earthquake dynamic rupturing process itself is a complicated phenomenon, involving dynamic friction, wave propagation, and heat production. Because controlled experiments can produce results without assumptions needed in theoretical and numerical analysis, the experimental method is thus advantageous over theoretical and numerical methods.

Our laboratory fault is composed of carefully cut photoelastic polymer plates (Homalite-100, Polycarbonate) held together by uniaxial compression. As a unique unit of the experimental design, a controlled exploding wire technique provides the triggering mechanism of laboratory earthquakes. Three important components of real earthquakes (i.e., pre-existing fault, tectonic loading, and triggering mechanism) correspond to and are simulated by frictional contact, uniaxial compression, and the exploding wire technique. Dynamic rupturing processes are visualized using the photoelastic method and are recorded via a high-speed camera. Our experimental methodology, which is full-field, in situ, and non-intrusive, has better control and diagnostic capacity compared to other existing experimental methods.

Using this experimental approach, we have investigated several problems: dynamics of earthquake faulting occurring along homogeneous faults separating identical materials, earthquake faulting along inhomogeneous faults separating materials with different wave speeds, and earthquake faulting along faults with a finite low wave speed fault core. We have observed supershear ruptures, subRayleigh to supershear rupture transition, crack-like to pulse-like rupture transition, self-healing (Heaton) pulse, and rupture directionality.

1. **For spontaneous rupture along homogeneous faults, we have documented the occurrence of supershear and have explored the conditions under which the subRayleigh to supershear transition occurs**. Supershear ruptures (i.e., rupture speed faster than the shear wave speed of the material) were observed to propagate at a speed close to the longitudinal speed of the material. This observation provided conclusive evidence for the first time of the existence of spontaneous supershear ruptures. We also observed that subRayleigh rupture (i.e., speed slower than the Rayleigh wave speed of the material) may jump to a supershear speed after a finite distance of propagation. Our experiments investigating this transition have confirmed the Burridge-Andrews mechanism, otherwise known as the Mother-daughter crack model.

2. **For spontaneous rupture between dissimilar materials, we observed ruptures propagating bilaterally at different speeds, one at the Generalized Rayleigh wave speed and the other at either a subRayleigh or a supershear speed.** Depending on geometry and load, ruptures were observed indeed propagating at approximately the generalized Rayleigh wave speed in the same direction as that of slip in the more compliant material (positive direction). In the negative direction, we observed either subRayleigh or supershear ruptures depending on the loading condition. Supershear ruptures always propagated at a speed very close to that of P wave in the slower wave speed material.

3. **For spontaneous rupture along faults with a finite fault core (low-velocity zone), we observed for the first time the occurrence of the self-healing (Heaton) pulse.** We simulated the fault core (gauge zone) using a material that is more compliant compared with the material used to simulate the host rock. This is the first experimental attempt to address the earthquake

dynamic process for this type of fault geometry. When the loading level was low, both ruptures in the positive and negative directions were sub-shear ruptures. At high enough loading, the Heaton pulse was found propagating in the negative direction, which is a direction opposite to that suggested by existing numerical simulations. This observation can be used to provide constraints on the nature of physically acceptable available friction models used in numerical simulations.

All of the above described experimental observations are innovative and conclusive. Some of them confirm the results of pre-existing theoretical and numerical works while some of them do not. In addition to comparing with existing theories, we have tried to directly relate our experimental observations to the few available field observations, including supershear, subRayleigh to supershear transition, and self-healing (Heaton) pulse. It is expected that with better seismic networks and other innovative measuring methods, more and more interesting phenomena associated with earthquakes will be identified as we have seen from our experiments. As an example, the subRayleigh to supershear transition has also recently been suggested to exist in natural earthquakes. There are also a few earthquakes that feature both directionality and supershear. The experimentally demonstrated Heaton pulse that we have found may be a general feature in real earthquakes since geological faults always have a core structure. Unfortunately, due to the short duration of such pulses, only high quality strong motion data will be able to conclusively prove its occurrence in a geological setting.

In addition to their value for discovery of new physical phenomena regarding rupture dynamics, the experiments described above have a promising validation component. Indeed, the most poorly understand component in the simulations

of earthquake rupture processes is the nature and consequence of the dynamic frictional laws. A potentially fruitful way to discriminate among the various emerging theories of frictional sliding could involve the numerical modeling of the above experiments by using various frictional laws. The most physically relevant frictional laws would be the ones that result in rupture scenarios that reproduce the rich spectrum of experimentally observed behaviors.

Table of Contents

List of Illustrations and Tables

Number Page Number

Introduction

An earthquake can be considered as a source of information, and the acquisition of which is the subject of seismology (Kostrov and Das 1988). The information conveyed by seismic waves consists of two parts: 1. the excitation of waves at the source of the earthquake and 2. the wave propagation from the source to the station. Consequently, the interpretation of seismic observations requires the solution of two fundamental problems: 1. the determination of the velocity structure of the medium and 2. the determination of the earthquake source parameters.

The practical goal of earthquake seismology is to prevent or reduce human and material losses due to earthquakes by estimating the earthquake hazard at a given site or by forecasting the occurrence of the next strong event. Although this can be done by a purely phenomenological method (i.e., extrapolating available seismic data), the scientific understanding of the earthquake generation process is of primary importance in providing more reliable prediction methodologies. This is the purpose of earthquake source studies, or in other words, the study of the physics of earthquakes.

Substantial progress has been made in the methods of collecting seismic data. Progress in the study of the physics of earthquakes has been slower than progress in seismic data collection. There are many reasons that may account for this. One of the main reasons is that the earth is a complex system. Indeed, there are many factors that may contribute to one single observed feature of earthquake faulting. In order to separate those factors, extremely complete data sets, featuring high spatial and temporal resolution are needed. This is way beyond

current levels of technological and economical resources. Also, in order to extract common features of earthquake faulting, many large earthquakes occurring within a short time are needed. Although this may be fortunate for life on earth, we are usually left with too few events to draw certain conclusions.

The way that we have chosen to overcome some of the above described problems is to perform highly instrumented and accurately controlled laboratory experiments. The experiments were designed in such a way as to resemble the conditions of the naturally occurring phenomena. We then hope that the phenomena produced in the laboratory represent those that occur in nature. In the laboratory we can nucleate as many earthquakes as we want without seismic hazards while the controlled experiments enable us to isolate and study all the possible controlling factors, one by one. The application of cutting-edge, high resolution (temporal and spatial) diagnostics in our experiments is another important enabling feature. The diagnostic methods are in situ and full-field.

The classic block-slider model (direct shear type) may be thought of as the first effort to simulate an earthquake in the laboratory. Based on the observations of stick-slip in rock-sliding tests, Brace and Byerlee proposed that stick-slip may be an important mechanism for shallow earthquakes along pre-existing faults (Brace and Byerlee 1966). Starting in the 1970s, there have been considerable efforts by geophysicists trying to characterize earthquake faulting in the laboratory on simulated faults (Dieterich 1972; Scholz, Molnar, et al. 1972; Wu, Thomson, et al. 1972; Brune 1973; Archuleta and Brune 1975; Johnson and Scholz 1976; Dieterich 1979; Anooshehpoor and Brune 1994; Dieterich and Kilgore 1994; Gu and Wong 1994; Sleep 1995; Brune and Anooshehpoor 1997; Ohnaka, Akatsu, et al. 1997; Blanpied, Tullis, et al. 1998; Olsen, Scholz, et al. 1998; Anooshehpoor and Brune 1999; Ohnaka and Shen 1999; Uenishi, Rossmanith, et al. 1999). Fault

models including saw-cut rock and foam rubber have been studied either quasi-statically (friction) or dynamically (earthquake faulting). Recently, a layer of granular material (sand) was introduced into two saw-cut rocks in order to characterize the effect of the fault gauge on the frictional response of fault systems. The understanding of earthquake dynamics is greatly improves with experimental results conducted using these set-ups. For example, the slip weakening phenomena was demonstrated, the famous state and rate dependent law was formulated based on the experiments, the dependence of normal traction on the slip was examined, the slip pulse was found. In order to examine the fast event in details, we need to modify or improve those design ideas. As will be discussed later, there are some limitations associated with those experimental designs, including edge effects, limited time and spatial resolution, lack of full-field diagnostics, lack of control, etc. Consequently, sometimes it is hard to interpret the experimental data thus obtained under the framework of earthquake dynamics. Furthermore, researchers have only looked at some simplest cases of earthquake faulting, e.g.,, faulting/rupturing along straight interfaces between similar materials. In the real world, the fault can be very complicated geometrically, may separate dissimilar material, and may be inhomogeneous in strength.

The work described in this thesis is the outcome of the interdisciplinary efforts of geophysicists (seismologists) and engineers (fracture mechanicians), and features the first attempt of experimental engineers to experimentally investigate the physics of earthquakes. There are quite a few researchers in the field of the physics of earthquakes who are engineers themselves (such as Kostrov, Freund, and Rice). All of these investigators have approached the subject from either the numerical or the theoretical points of view. Partially due to the great effort of these researchers, seismologists have been able to utilize concepts and models of

engineering dynamic fracture mechanics for the interpretation of seismic data. By doing so they have obtained useful information on the state of static and dynamic stresses, friction, fracture energy, and rupture velocities; information that is key to the understanding of the basic physics of earthquakes. Unfortunately, the theoretical and numerical methods are not enough for the full understanding of the earthquake processes, especially the dynamic earthquake faulting process. As an example, the various rate and state friction laws have been proposed through the years and used in numerical simulations to predict various of different rupture modes (Coker, Lykotrafitis, et al. 2004). Even worse, a single frictional law may yield a host of various rupture predictions by simply choosing different combinations of parameters. Without carefully designed laboratory experiments, it would be difficult to tell which factors dominate the occurrence of observed phenomena in the geological scale.

Before we discuss our plan in detail, we should note that there are fundamental differences in the types of dynamic fracture phenomena that have traditionally been studied by engineers and by seismologists. Perhaps the biggest qualitative difference between the two groups comes from the fact that engineers have almost exclusively been concerned with the dynamic growth of mode-I (opening) cracks rather than mode-II (in-plane shear) ruptures. The historical reason for this preference comes from the fact that most early engineering applications of dynamic fracture involved purely homogeneous (monolithic) materials that do not feature pre-existing crack paths in the form of fault lines or weak joints. In such solids, dynamic cracks can only grow under strictly opening conditions. Indeed, growing cracks are known to curve or kink within a homogeneous solid to ensure that they maintain purely tensile (mode-I) conditions at their tips (Cotterell and Rice 1980; Nemat-Nasser and Horii 1982; Hutchinson and Suo 1992). However, the situation is entirely different in seismological applications.

The earth's crust contains weak interfaces in the form of faults and as such should be viewed as an inhomogeneous system. The system's inhomogeneity arises from the fact that the rupture resistance (or fracture toughness) along the fault is lower than that of the surrounding rock material. That is true even when there are negligible differences in constitutive properties across the fault plane, as in the case of some geologically young faults. It is the presence of both fracture and constitutive inhomogeneities that accounts for the essence of the differences in the types of dynamic cracks and crack behavior relevant to either engineering or to geophysics. The faults typically trap dynamic cracks and constrain such cracks to propagate unstably under primarily mode-II conditions.

The difference in the favored rupture growth mode translates also into substantial differences in the observed maximum attainable rupture velocities between mode-I and mode-II ruptures. In particular, it has long been known that the rupture velocity of tensile (mode-I) cracks in monolithic solids seldom exceeds 40% of C_R, where C_R is the Rayleigh wave speed of the solid (Sharon and Fineberg 1996; Sagy, Reches,, et al. 2001). At about that speed, instability sets in whereby a dynamically growing mode-I crack branches into two or more mode-I branches. In contrast, the rupture velocity inferred for most crustal earthquakes (mode-II ruptures) is about 80-90% of the shear wave speed (C_S) within the layer where slip occurs (Brune 1970). This is substantially higher than for mode-I cracks. Moreover, in a few cases, it has been reported that, at least over a portion of a fault, the rupture velocity could locally become intersonic (supershear), i.e., a speed within the interval between the C_S and the P wave speeds C_P of the surrounding rock (Archuleta 1984; Spudich and Cranswick 1984; Olsen, Madariaga,, et al. 1997; Bouchon, Bouin, et al. 2001; Bouchon and Vallee 2003; Eberhart-Phillips, Haeussler, et al. 2003; Ellsworth, Çlebi, et al. 2004; Koketsu, Hikima, et al. 2004). The inference, however, of intersonic shear rupture has

been met with great caution by the geophysics community because of the absence of direct laboratory evidence supporting the attainment of such extreme crack velocities. In partially addressing this skepticism, a series of recent laboratory studies of shear rupture along coherent (bonded) interfaces, by Rosakis and his co-workers, has revealed the propensity of dynamic interfacial shear cracks to unstably accelerate to high subsonic levels and to often propagate within the intersonic regime (Lambros and Rosakis 1995), i.e., supershear regime. These experiments conducted by using bonded dissimilar (Lambros and Rosakis 1995; Rosakis, Samudrala, et al. 1998; Samudrala and Rosakis 2003) or bonded identical materials (Rosakis, Samudrala, et al. 1999; Samudrala, Huang, et al. 2002), represent the first experimental evidence of intersonic shear rupture in a laboratory setting.

Recognizing the differences and similarities in approach between traditional engineering fracture mechanics and seismology, this thesis describes an interdisciplinary program on "experimental seismology". The goal of this study is to utilize elaborate diagnostic methods, already developed for engineering research, to study, in real-time, the basic physical phenomena governing fault rupture and to address some of the outstanding problems of seismology in the field of the physics of earthquakes. Since seismic faulting occurs spontaneously under tectonic stress with a very fast particle motion in excess of 1 m/s (Brune 1970; Ben-Zion 2001), it is desirable to perform experiments featuring such conditions (e.g., spontaneous rupture and fast sliding speeds). To achieve this, a series of "earthquakes" is triggered in the laboratory to keep track of propagation of seismic waves and of fault ruptures. This is made possible by in situ, optical-based diagnostic techniques combined with a high speed camera. The fault systems are modeled by interfaces between plates, which are held together by friction without adhesives (incoherent faults). External pressure is used to

simulate the tectonic stress (~ 400 bar). The principal direction of pressure will form an acute angle with the fault so as to provide driving force for the rupture process. The normal stress applied on the interface, together with its natural frictional characteristics, also provides the strength of the interface. The dynamic rupture is triggered by an exploding wire mechanism. An analogous convention has been used in the numerical simulations by Andrews and Ben-Zion (Andrews and Ben-Zion 1997) and by Cochard and Rice (Cochard and Rice 2000) to induce rupture by suddenly releasing local pressure at the simulated hypocenter location along a simulated fault plane.

If seismic faulting is indeed appropriately modeled by the dynamic frictional sliding between two solids, our experiments can be used to address many outstanding seismological questions. In the following paragraphs we describe some specific questions that can be addressed.

1. Limiting rupture velocities during spontaneous mode-II sliding

Following the earlier discussion on inferred (through seismic data) mode-II rupture velocities, the planned laboratory earthquake experiments will be used to investigate favorable subsonic and, perhaps, intersonic speed regimes during spontaneous rupturing processes. It should be noted that early experiments on dynamic shear crack growth performed by Rosakis and his coworkers were not motivated by seismological considerations and featured bonded (coherent) interfaces and stress wave loading (induced by impact). In contrast, the current experiments are designed to address the question of limiting rupture velocities in configurations that are designed to mimic spontaneous, rather than wave induced, fault ruptures. The interfaces featured in these configurations are incoherent or frictional with no coherent strength or toughness. The details of the experimental set-up will be discussed in Chapter 1. We will describe the

experimental results and some theoretical models regarding the possible limiting speeds of laboratory earthquake ruptures in Chapter 2. In particular, we will show the conclusive experimental evidence of supershear spontaneous ruptures and, for the first time, we will experimentally describe a unique mechanism that enables a spontaneous rupture, which starts at a 0 speed by definition, to reach the supershear rupture velocity. This mechanism is called the Burridge-Andrews Mechanism that is first proposed by Burridge and later by Andrews based on theoretical and numerical studies (Burridge 1973; Andrews 1976; Andrews 1985).

2. The crack-like versus the pulse-like nature of rupture

As described by Rice (Rice 2001), there are two widely accepted classes of models that provide adequate approximation to source mechanics and have been widely used, through seismic inversion studies, to recover information about the nature and speed of propagating ruptures. The oldest and most classical approach describes rupture through the use of elasto-dynamic shear crack models (Kostrov 1966; Das and Aki 1977; Das, Boatwright, et al. 1988). More recently, models that describe ruptures as 'self-healing' slip pulses have been introduced (Heaton 1990). The question of whether ruptures assume a 'crack-like' or a 'pulse-like' mode and under what circumstances they do so is currently at the center of research activity (Weertman 1980; Heaton 1990; Adams 1995; Andrews and Ben-Zion 1997; Ranjith and Rice 1999; Rice, Lapusta, et al. 2001).

High-speed photography will be used to examine these conditions. At this point, it should be noted that for constitutively homogeneous fault systems, the propensity of a rupture to proceed in a crack-like or a pulse-like manner is thought to depend on the nature of the dynamic frictional law (e.g., rate and state dependent friction acting on the sliding interface). For inhomogeneous fault systems, the strong coupling between normal and shear stresses at the interface of

a bimaterial system is also thought to play a pivotal role in the development and growth of dynamic slip pulses. Indeed, the interaction between slip and normal stress can dramatically reduce the frictional strength and make the constitutively inhomogeneous interfaces mechanically favored surfaces for rupture growth. As described by Ben-Zion (Ben-Zion 2001), the interaction between slip and normal stress allows ruptures to grow in a pulse-like mode under shear stress conditions that are low compared to the nominal frictional strength of the interface. The resulting pulse-like ruptures have properties that are compatible with inferences of short rise-time earthquake slip (Brune 1970; Heaton 1990; Yomogida and Nakata 1994) and have low levels of frictional heat generation.

In addition to the nature of frictional laws and to the presence of elastic property mismatch, geometrical effects are also thought to govern the slip-pulse mode of rupture. In particular some researchers believe (Miyatake 1992; Nielsen, Carlson, et al. 2000) that spatial heterogeneities (e.g., asperity distribution) present on fault planes set the local length scale that promotes slip pulse formation and determines slip duration. The experiments described here are primarily aimed towards the study of the mechanical rather than the geometrical causes of pulse formation. Although the characteristics of slip pulses have been the subject of recent analytical and numerical activity, there are not many visualized pulses in the laboratory (Brune, Brown, et al. 1993; Anooshehpoor and Brune 1999). In Chapter 3, we study the earthquake faulting along faults separating bimaterials and in Chapter 4 we look at the effect of a finite width low-velocity fault core on the earthquake faulting. In these two groups of experiments, we check for the possibility of pulse-like rupturing motivated by recent theoretical and numerical works predicting such a phenomenon. We believe that in the bimaterial case, there is no strong evidence of pulse-like faulting while in the low-velocity fault zone case, we are able to identify the pulse-like ruptures. To our surprise, pulse-

like ruptures propagate in a direction contrary to that suggested in the literature (Ben-Zion and Huang 2002). An explanation for this discrepancy will be attempted.

3. Directionality of rupture and rupture velocity in inhomogeneous fault systems

The recent theoretical and numerical studies mentioned in the previous section (Weertman 1980; Heaton 1990; Adams 1995; Andrews and Ben-Zion 1997; Harris and Day 1997; Ranjith and Rice 1999; Cochard and Rice 2000; Rice, Lapusta, et al. 2001) also predict that if rupture occurs on the boundary between two frictionally held solids having different elastic properties and wave speeds, such a rupture preferentially propagates in the same direction as does the direction of slip in the lower wave speed solid. Since the directionality of fault rupture has a profound influence on the distribution of damage caused by earthquake ground motion, it would be extremely useful if this behavior could be confirmed under controlled laboratory conditions. In most mature faults the elastic properties do vary across the fault (Magistrale and Sanders 1995; Peltzer, Crampe, et al. 1999) and shear wave speeds may also vary by as much as 30% (Cochard and Rice 2000; Ben-Zion and Huang 2002). Recently, Rubin, and Gillard (Rubin and Gillard 2000) studied several thousands of pairs of consecutive earthquakes, that occurred on a segment of the central San Andreas fault south of the Loma Prieta rupture. Among the second events of each pair they found that over 70% more occur to the northwest than to the southwest. They interpret this asymmetry as being a result of the contrast in material properties across the fault. Indeed, at this location of the San Andreas fault, the rock body is more compliant northeast of the fault than it is southwest (Eberhart-Phillips and Michael 1998). The experiments described in Chapter 3 are designed to study the effect of wave speed mismatch on the nature, speed, and

directionality of ruptures propagating along simple inhomogeneous faults. Recognizing the fact that inhomogeneous fault structures involve damaged (low wave speed) fault cores of finite width (Chester and Chester 1998), more complex specimen geometries involving a fault core layer (sandwich-type structures) are described in Chapter 4. The growth of rupture pulses in such sandwich-type fault systems has recently been investigated numerically by Harris and Day (Harris and Day 1997) and by Ben-Zion and Huang (Ben-Zion and Huang 2002). Interesting issues for this geometry are the possible asymmetry and pulse mode of rupturing. We will show that both the bimaterial case and the finite fault core case will lead to asymmetry of earthquake faulting. In Chapter 3, we will show that along the positive direction, which is the sliding direction of the more compliant material, the rupture propagates with a speed that is close to the generalized Rayleigh wave speed. In the negative direction, the rupture is sub-shear or supershear depending on the loading conditions. In Chapter 4, we will show that in both the preferred direction and the opposite direction, the ruptures propagate either at the slow Rayleigh wave speed or the slow shear wave speed.

Chapter 1

Experimental Design of Laboratory Earthquakes

There are not many research groups conducting laboratory experiments in the field of the physics of earthquakes, and even fewer groups doing so in the field of the dynamic earthquake rupturing process. The reason lies in the fact that it is both complicated to design a proper laboratory earthquake model and difficult to conduct the in situ measurements (high speed measurements) that are necessary in the understanding of the whole transient rupturing process. For the few currently existing experimental methods, there are some limitations in either the model design and/or in the choice of diagnostics. Common problems in the model design are rigid body assumption, unavoidable edge effects, using inelastic model materials, and lack of control on the triggering. Common shortcomings in the choice of diagnostics include discrete point measurements (non full-field), and limited spatial and temporal resolution. Consequently, the experimental data are controversial and are difficult to interpret.

In this study, a 2-D laboratory earthquake model is designed by using transparent photoelastic polymers. We control the loading in the experiments so that the deformation of the polymers always remains elastic. The fault is simulated by the frictional contact between polymer plates under far-field loading provided by a hydraulic press. Earthquakes, which are spontaneous ruptures in nature, are triggered in the fault at the location of a simulated hypocenter, and the rupturing processes are recorded using a full-field optical technique (dynamic photoelasticity combined with high-speed photography). We show that rupturing on faults with various geometries and strengths can be studied using this type of

laboratory model and diagnostics. To demonstrate the flexibility of the experimental designs used in this study, results of several earthquake experiments will be shown.

1.1 Introduction

The first effort of simulating earthquakes in the laboratory is the classic block-slider model (direct shear type). Based on the observations in rock sliding tests, Brace and Byerlee proposed that stick-slip may be an important mechanism for shallow earthquakes along pre-existing faults (Brace and Byerlee 1966). The basic assumption of the block-slider model is that rock blocks are rigid, so that edge effects can be ignored. As a result, friction along the interface is uniform and only the displacement history of the slider needs to be measured. In the case of a real crustal earthquake, the normal stress at the depth of 10 km is about 300 MPa and the Young's modulus of rock is about 20 GPa, which leads to strains of the order of 1.5%. If we consider only the average stress drop during earthquakes, which is thought to be in the range of 1-10 MPa (10-100 bar), the corresponding shear strain is in the range of 0.01% - 0.1%. Indeed, the crust is far from being rigid during earthquake faulting. Although the block-slider model tests provide useful insight into some aspects of earthquake mechanics, they should be taken as one of the frictional constitutive experimental configurations instead of a configuration meant to model earthquakes. Indeed, based on the experimental results of Dieterich (Dieterich 1979), the famous state and rate dependent friction law was formulated by Ruina (Ruina 1983) and Rice (Rice 1983).

There are two configurations suitable to produce laboratory earthquakes, namely those of direct shear and of biaxial compression (Wu, Thomson, et al. 1972; Brune 1973; Johnson and Scholz 1976). In order to extract rupture dynamics information from configurations, the rigid assumption should be abandoned.

Indeed, if strain gauges are attached along the fault in a 2-D domain, the dynamic strain history on different points can be measured. With this modification, rupture velocities can be estimated (Wu, Thomson, et al. 1972; Brune 1973; Johnson and Scholz 1976) in addition to the dynamic friction-slip relation (Okubo and Dieterich 1984; Dieterich and Kilgore 1994; Ohnaka and Shen 1999). Strain gauges have sizes of about a few millimeters, and this limits the spatial resolution of the measurements. The technique used to measure the slip history has the same problem (Okubo and Dieterich 1984; Dieterich and Kilgore 1994; Ohnaka and Shen 1999). As a result, the data are point wise, averaged, and hard to explain. For example, although supershear ruptures were suggested by this type of experiment (Wu, Thomson, et al. 1972; Johnson and Scholz 1976; Okubo and Dieterich 1984), this evidence was far from being conclusive due to the quality of the data. Furthermore, since the diagnostics system (the Wheatstone bridge and oscilloscope) was triggered by one of the strain gauge signals and there was no information on the exact time and location of the starting point of earthquake (Hypocenter), the sampling rate was set low enough to capture the whole process. This limits the time resolution of the measurements. Using this type of set-up, the frictional healing and velocity-weakening effects were first observed by Scholz,, et al. (Scholz, Molnar, et al. 1972) and Dieterich (Dieterich 1972).

Recently, two types of modification of the original block-slider model (direct shear) were introduced. The first one involved introducing a granular layer into the interface to simulate the fault core (Gu and Wong 1994), and the second one involved using soft material (foam rubber) and of using multi-point measurements by burying accelerometers inside meter-sized foam rubber blocks (Brune 1973; Brune, Brown, et al. 1993). The first type of test usually ignored the dynamic features of the earthquake, so we will not discuss it in detail here. As to

the second type of test, namely, the "foam model", the usage of slow sound speed material has some advantage over rocks in that: 1. the whole process can be captured without the need of high sampling rate and 2. 3-D effects can be addressed, since it is easy to bury gauges inside the model. However, some serious concerns exist regarding the model material itself exist. These include its non-linear and viscous nature and the special frictional property of the foam rubber (the coefficient of friction can be larger than 1). Regarding their constitutive behavior, foam rubber can sustain large deformations and are not well described by the theory of linear elasticity. This together with their visco-elastic response makes them inappropriate candidates to mimic earthquakes, which occur in much stiffer and more brittle materials, i.e., rocks. Furthermore, like all other direct shear type experiments, it has unavoidable edge effects as first pointed out by Scholz (Scholz, Molnar, et al. 1972). The edge effect can be understood as follows. The direct shear loading force is balanced by the frictional force along the fault, but there is a net angular momentum due to these force pairs. To balance this angular momentum, the normal force along the fault is redistributed so that one end of the fault has a larger normal traction than the other end; consequently, the normal stress and the frictional resistance along the fault are not uniform. For exactly the same reason, in a similar experiment done by Ohnaka and Shen (Ohnaka and Shen 1999), the instability always started from one end of the fault, where the normal force and the frictional resistance are reduced for fairly smooth faults. In these cases the edge effect dominates, instead of the roughness. Nevertheless, the foam rubber model has been producing interesting results (Brune, Brown, et al. 1993; Anooshehpoor and Brune 1994; Brune and Anooshehpoor 1997; Anooshehpoor and Brune 1999).

In order for a natural, large, destructive earthquake to happen, we need at least three important prerequisites working together: proper tectonic loading, a pre-

existing fault and a certain triggering mechanism. The first two prerequisites were addressed fairly well in the previously mentioned models. The triggering mechanism is important for both the earthquake process and the synchronization of high speed diagnostics in a dynamic test. This is usually ignored in most of the past earthquake experiments, except for one particular study specifically targeting the problem of the dynamic triggering of earthquakes by Rayleigh waves (Uenishi, Rossmanith, et al. 1999). In this work, two photoelastic polymer plates of different sizes are held together at their convex sides to form a fault with an extended free surface. Then, a Rayleigh wave pulse is generated on the free surface by a point explosion and this wave propagates along the free surface to the contact part (fault). Depending on the direction of the Rayleigh pulse, it may be able to trigger the dynamic slip of the fault. Also, full-field in situ measurements, which would be helpful to the understanding of the earthquake rupturing process, have never been used before except in the single study we just mentioned.

Earthquake rupture can be thought of as a specific case of spontaneous fracture, which is either Mode-II (in plane shear) or Mode-III (out of plane shear) in type. Spontaneous fracture means a dynamic fracture that is loaded statically and starts to propagate due to some triggering mechanism, which after initiating the rupture, does not further contribute to its growth history (The driving force is contributed by the static pre-load). Even if we consider only the friction (without cohesion) between the two fault surfaces, the earthquake rupture can be modeled mathematically by a cohesive zone fracture model, as we will now discuss. There are two models of the fracture tip in fracture mechanics: the singular model and the cohesive zone model (Freund 1990; Broberg 1999). In the former model, the fracture tip is a mathematical point and the stress state is singular (stressed become infinite as the tip is approached); in the latter model, the fracture tip has a

finite dimension (cohesive zone) and the stress and displacement are finite everywhere and obey certain cohesive zone constitutive laws inside the cohesive zone (process zone). Inside the cohesive zone, the stress decreases from the yielding stress to zero stress at the crack-tip. If we take the friction law (slip-weakening, slip-rate-weakening, or state and rate dependent) as the constitutive law of the cohesive zone, dynamic frictional earthquake ruptures can be treated mathematically the same way as a cohesive zone fracture. In fact, the slip weakening frictional law is an adoption of the Barenblatt cohesive zone model for Mode-I fracture to the Mode-II case (Ida 1972; Palmer and Rice 1973). The striking similarities of earthquake rupture models to engineering fracture models also suggest the possibility for looking to available experimental techniques from fracture mechanics as candidates for the experimental study of earthquake dynamics.

As reviewed by Rosakis (Rosakis 2002), fracture mechanicians are paying more and more attention to the fractures along material interfaces that are becoming common in modern engineering structures and materials. These interfaces usually serve as sites of catastrophic failure of such structures and materials. On a much larger length scale, crustal faults provide natural weak interfaces where earthquake ruptures occur. Experimental methods for dynamic fracture mechanics, such as photoelasticity and Coherent Gradient Sensing (CGS) combined with high-speed photograghy, have been applied successfully by Rosakis and his co-workers in the experimental study of dynamic shear ruptures along a weak plane (Lambros and Rosakis 1995; Rosakis, Samudrala, et al. 1998; Rosakis, Samudrala, et al. 1999; Rosakis, Samudrala, et al. 2000; Coker and Rosakis 2001; Coker, Rosakis, et al. 2003). These diagnostic techniques, which are 2-D in nature, are able to provide full-field in situ stress information. Specifically, the photoelastic method, which measures the maximum in-plane

shear stress contours, is an attractive candidate for the study of shear dominated processes such as earthquake ruptures.

1.2 Experimental Set-up

As discussed above, there are three important factors for an earthquake event: a geological fault (usually pre-existing), far-field tectonic loading, and a certain triggering mechanism. The last factor, addressed very well in numerical simulations as either a local over-stress (Andrews 1976) or a local pressure release (Andrews and Ben-Zion 1997; Cochard and Rice 2000), usually receives less attention in experimental studies. In order to incorporate all of the above three factors for earthquakes and obtain in-situ full-field stress state information, we adopted the following 2-D dynamic photoelastic model.

1.2.1 Photoelastic Fault Model

As shown in Figure1.1, the crust is simulated by a photoelastic plate with a thickness of 9.5 mm (3/8") and 150 mm × 150 mm (6" × 6") in 2-D plane dimensions. The plate is cut into two identical quadrilaterals, the two quadrilaterals are then put together, and the frictional interface is used to simulate a fault. The angle of the fault line to the horizontal will be denoted α while the uniaxial pressure acting at the top and the bottom ends of the sample will be denoted by P. Then the resolved shear traction τ and the normal traction σ along the fault can be expressed in terms of angle α and pressure P as:

$$\tau = P\sin\alpha\cos\alpha, \quad \sigma = P\cos^2\alpha \tag{1.1}$$

To make the connection with geophysics terminology, a dimensionless factor s, which is usually used by seismologists to describe the loading along faults with respect to the strength of the fault (Scholz 2002) is introduced here. By using the

slip weakening frictional model (Palmer and Rice 1973) as in Figure 1.1c, and by denoting the maximum strength of the fault by τ^y and the final strength of the fault by τ^f, this loading factor s is defined by $s=(\tau^y-\tau)/(\tau-\tau^f)$.

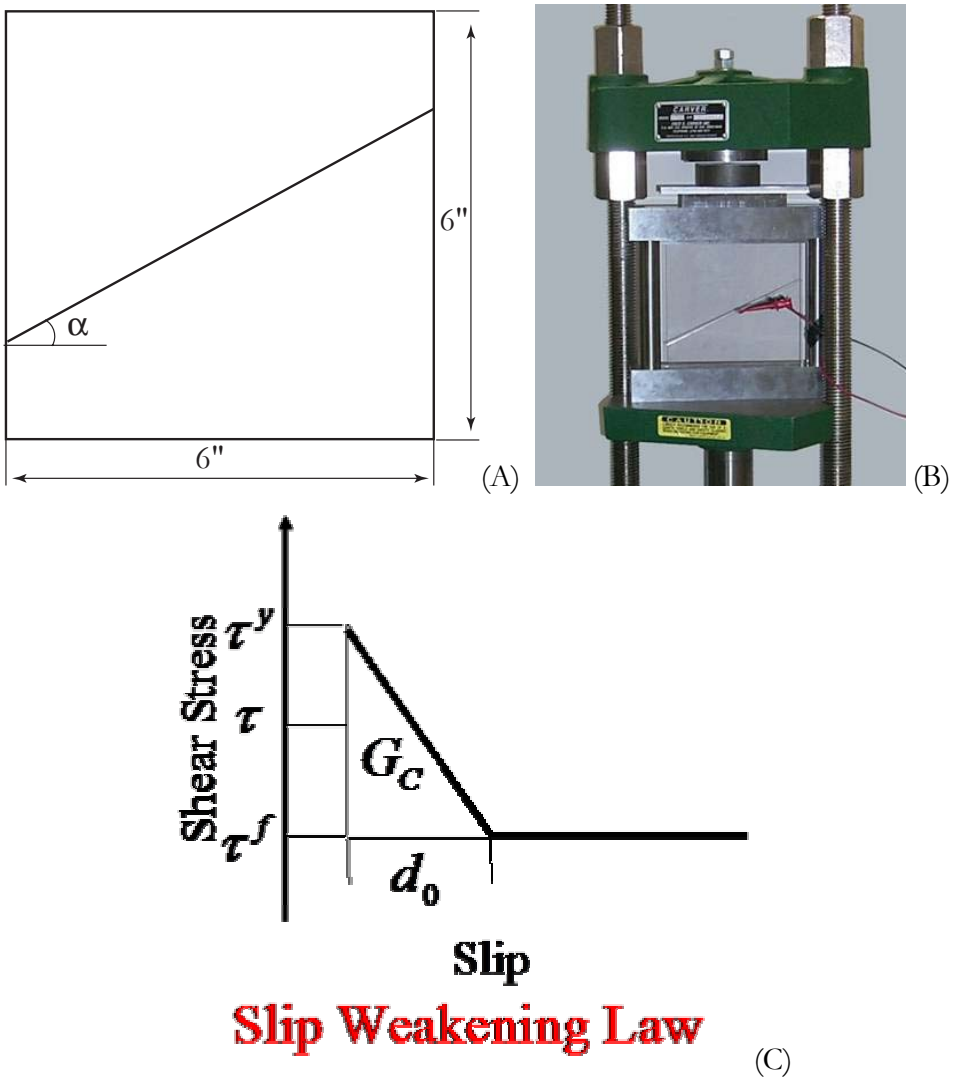

Figure 1.1 Laboratory fault model (A) and the loading fixture inside a hydraulic press (B) (the electronic leads and cables are for exploding wire technique discussed below). (C) Slip weakening frictional law.

In this laboratory fault model, τ^y is the static friction and τ^f is the dynamic friction. Denoting the static and dynamic coefficients of frictions by μ^s and μ^d respectively and by using Equation (1.1), we can express the loading factor s corresponding to the geometry of our experiment in terms of α by:

$$s=[\mu^s\cos\alpha-\sin\alpha]/[\sin\alpha-\mu^d\cos\alpha] \tag{1.2}$$

It is obvious from Equation (1.2) that we can control s and through it the earthquake rupturing process by varying the fault angle α for given frictional properties of the fault in our experiments. The magnitude of the uniaxial pressure P controls the total amount of deformation and total slip.

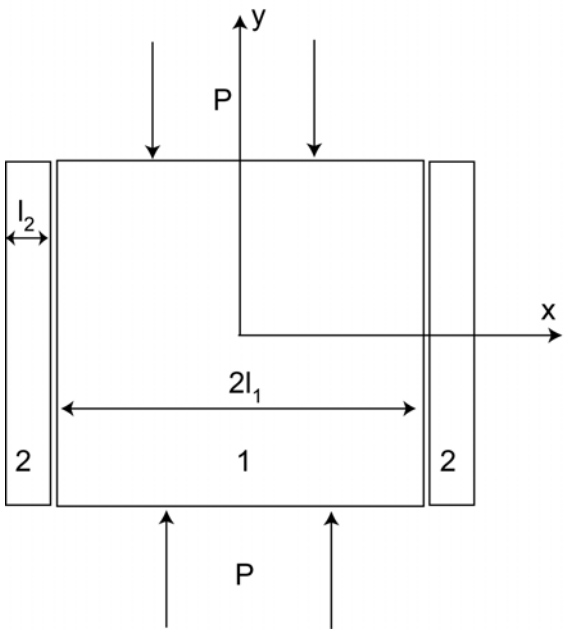

Figure 1.2 Laboratory fault model with confinement.

We are also capable of applying confinement to the specimen to achieve a pseudo-biaxial stress state. As shown in Figure 1.2, we put two stripes (material 2) of the same thickness and length as the specimen (material 1) on both sides of

the specimen. The width of the stripe is l_1 and the half width of the specimen is l_2. The stripe can expand freely in the y direction if we neglect the friction.

The stress-strain relation a for 2-D isotropic solid under plane stress infinitesimal deformation is:

$$\begin{cases} \varepsilon_{xx} = \dfrac{1}{E}(\sigma_{xx} - \nu\sigma_{yy}) \\ \varepsilon_{yy} = \dfrac{1}{E}(\sigma_{yy} - \nu\sigma_{xx}) \\ \varepsilon_{xy} = \dfrac{1}{2G}\sigma_{xy} \end{cases} \tag{1.3}$$

where E is the Young's modulus, G is the shear modulus, and ν is the Poisson's ratio.

For rigid confinement (i.e., material 2 is much stiffer than material 1, hence material 1 can not deform in the x direction), $\varepsilon_{xx}=0$. Using (1.3) and $\sigma_{yy}=P$, we get:

$$\sigma_{xx} = \nu P \tag{1.4}$$

For general confinement, we apply Equation (1.3) to both material 1 and material 2:

$$\begin{cases} \varepsilon^1_{xx} = \dfrac{1}{E_1}(\sigma^1_{xx} - \nu_1\sigma^1_{yy}) \\ \varepsilon^2_{xx} = \dfrac{1}{E_2}(\sigma^2_{xx} - \nu_2\sigma^2_{yy}) \end{cases} \tag{1.5}$$

If the displacement of the stripe along the x direction is denoted by Δx, the strains are given by $\varepsilon_{xx}^2=\frac{\Delta x}{l_2}$, $\varepsilon_{xx}^1=-\frac{\Delta x}{l_1}$.

Noticing that $\sigma_{yy}^1=P$, $\sigma_{yy}^2=0$, $\sigma_{xx}^1=\sigma_{xx}^2=\sigma_{xx}$, (1.5) leads to:

$$\begin{cases}\varepsilon_{xx}^1=-\frac{\Delta x}{l_1}=\frac{1}{E_1}(\sigma_{xx}-\nu_1 P)\\ \varepsilon_{xx}^2=\frac{\Delta x}{l_2}=\frac{1}{E_2}\sigma_{xx}\end{cases} \tag{1.6}$$

Using Equation (1.6), we have $\frac{\varepsilon_{xx}^2}{\varepsilon_{xx}^1}=-\frac{l_1}{l_2}=\frac{E_1}{E_2}\frac{\sigma_{xx}}{\sigma_{xx}-\nu_1 P}$ and eventually:

$$\sigma_{xx}=\nu' P \tag{1.7}$$

where $\nu'=\frac{\nu_1}{\hat{E}/\hat{l}+1}$, and $\hat{E}=E_1/E_2$, $\hat{l}=l_1/l_2$.

In the case of rigid confinement, $\hat{E}=E_1/E_2\to 0$ or $l_2/l_1\to\infty$ holds, Equation (1.7) reduces to Equation (1.4).

In the case of biaxial loading, resulting from confinement, Equation (1.1) and (1.2) can be rewritten as:

$$\begin{cases}\tau=(1-\nu')P\sin\alpha\cos\alpha\\ \sigma=\nu' P\sin^2\alpha+P\cos^2\alpha\end{cases} \tag{1.8}$$

and

$$s = \frac{\mu^s(\nu'\sin^2\alpha+\cos^2\alpha)-(1-\nu')\sin\alpha\cos\alpha}{(1-\nu')\sin\alpha\cos\alpha-\mu^d(\nu'\sin^2\alpha+\cos^2\alpha)} \tag{1.9}$$

1.2.2 The Triggering Mechanism

People have tried to understand the nucleation of earthquakes and indeed, they showed that the nucleation can be understood with proper friction relations (Dieterich 1992; Lapusta and Rice 2003; Uenishi and Rice 2003). Unfortunately, it is impractical to explore the whole process experimentally and instead, we follow the idea of numerics to assume that there are some triggering mechanisms for earthquakes. The triggering can be either a sudden increase of the loading or a sudden decrease of the fault strength. The loading increase case is only possible for a dynamic triggering situation in which an increase of shear stress is provided by stress waves caused by a nearby earthquake. Otherwise, this scenario is unlikely to happen since the tectonic loading rate is very slow and can be approximated as quasi-static loading. Hence it is plausible to assume that triggering is usually due to the local decrease of the fault strength. This can be done either by the flow of pore-fluid into the fault interstice or local catastrophic failure (sudden loss of frictional resistance). Mathematically, they are equivalent to local pressure release and local over-stress respectively. Both mechanisms have been applied in numerical simulations of earthquake rupture dynamics (Andrews 1976; Andrews and Ben-Zion 1997; Fukuyama and Madariaga 1998; Cochard and Rice 2000; Aagaard, Heaton, et al. 2001).

In our laboratory earthquake model, the triggering mechanism is local pressure release, which is achieved by the exploding wire technique shown in Figure 1.3. A capacitor (15 μF, up to 3 kv) is charged by a high voltage power supply. The charging time is determined by the resistance of the charging resistor and the capacity of the capacitor. Upon closing the switch, the electric energy stored in

the capacitor causes a high current (up to thousands of Amperes) in a thin metal wire (buried inside a hole of 0.1 mm in diameter in the interface) for a short duration. The high current turns the metal wire into high pressure, high temperature plasma in less than 10 μs. The expansion of the high temperature, high pressure plasma causes a local pressure release. The adjustable power supply can provide electric potential in a wide range (0~5 kv), and different intensities of explosion can be obtained easily. For the metal wire (Nickel wire, ~0.08 mm in diameter) that we are using, the threshold voltage to explode a 10 mm long wire is about 600 v.

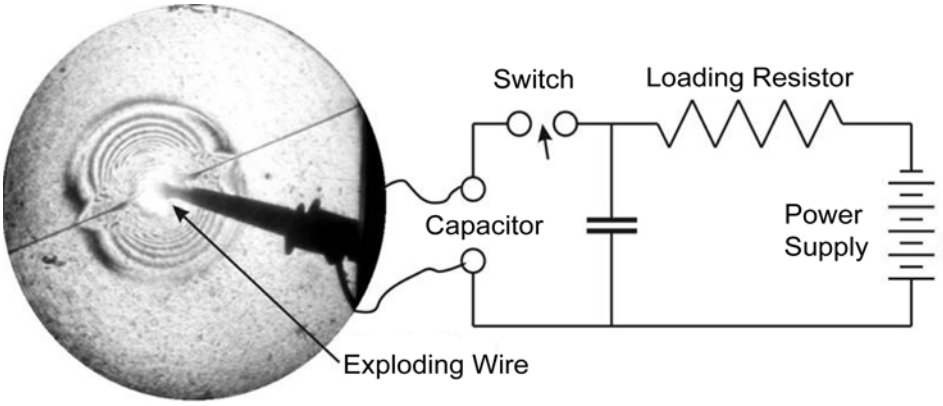

Figure 1.3 Schematic drawing of the exploding wire system coupled with a photoelastic fault model. Isochromatic fringes due to the explosion are visible.

In order to estimate the pressure due to the plasma explosion, the commonly used Grüneisen equation of state (Ahrens 1995) is applied:

$$p_0 - p_x = \frac{\gamma(v)}{v}(E - E_x) \tag{1.10}$$

where γ is the Grüneisen parameter (approximately 1.88 for Nickel), p_0 and E are total pressure and total internal energy, p_x and E_x are cold pressure and cold internal energy due to mechanical interaction of atoms and are negligible, while v is the volume of the material. The total input energy provided by the capacitor is $E_{total}=CV^2/2$, where C is the capacitance (14.7 μF) and V is the electric potential of the capacitor. For the case V = 1 kv, the total energy is then 7.5 J. We can assume then that the part of energy consumed by the mechanical expansion is of the order of 1 J. Since we know the volume of the wire (~10^{-4} cm^3) and can assume an instantaneous explosion, the peak pressure due to explosion can be calculated to be 10 GPa using Equation (1.10). Furthermore, since $t_c=CR$ where R is the resistance of the system (~ 1 Ω, the time of explosion is close to the discharge time constant t_c, which is around 10 μs. This time corresponds to a distance L=10 mm traveled by the sound waves in the plastics sample. The average pressure of the explosion is then:

$$\bar{p}=p_0(L/a)^{-2} \tag{1.11}$$

where a is the radium of the wire or the hole. The average pressure due to the explosion for 1kv is estimated as 1 MPa at a distance 10 mm away from the hole based on equation (1.11). The pressure will decrease more due to unloading from the free surface opened by the explosion and the geometric dispersion effect. The pressure due to the explosion is negligible away (10 mm) from the explosion site (hole) compared with the static loading level (~10 MPa) in our experiments. For this reason, laboratory earthquakes triggered this way can be assumed to be spontaneous ruptures.

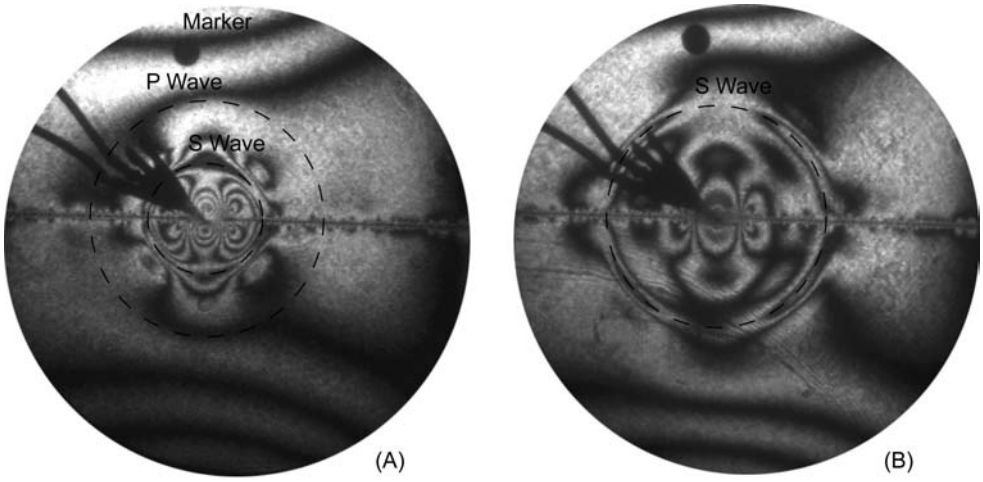

Figure 1.4 Isochromatic fringe patterns for an experiment at two time instances. (A. Pattern at 26 μs and B. Pattern at 34 μs).

Real experimental results support the above arguments (Figure 1.4). In this test, two identical rectangular Polycarbonate plates are held together by uniaxial vertical compressive force of 3000 lbf, which corresponds to a stress of 10 MPa. We set the voltage of the power supply to 1.2 kv and wait for a few minutes to charge the capacitor. Upon the ignition of the explosion, we can identify the P wave and S wave fronts in Figure 1.4A and only the S wave front in Figure 1.4B. This is because the most energy is carried by the S wave and because photoelasticity is mostly sensitive to shear stresses. Noticing that the diameter of the circular marker in the photographs is 1/4", the S wave front in Figure 1.4A is about 10 mm away from the explosion center. Close to the fault, the order of fringe within the S wave front is about 1.

Using the photoelastic relation (discussed below), the peak shear stress is found to be around 0.35 MPa. The peak normal traction along the fault within the S wave front should be around the same order of magnitude. As expected, the magnitude of the stress has decreased as the waves propagated away from the

explosion site (Figure 1.4B). In our experiments, the far-field static uniaxial pressure is of the order of 10 MPa. Hence, the dynamic slip triggered this way can be treated as a spontaneous rupture. In another words, after initiation, the subsequent propagation of the dynamic slip is not controlled by the triggering but by the quasi-static initial far-field loading.

Before the explosion, the shear traction along the fault is less than the maximum static frictional strength. After the explosion, the local normal traction along the fault is reduced and so is the static frictional strength. As a result, the applied shear traction, which is initially smaller than the static frictional strength and unaffected by the isotropic explosion, can be momentarily larger than the reduced frictional strength. The resulting net driving force, defined by the difference between the shear traction and the frictional resistance, will drive the slip along the interface. Furthermore, the slip will reduce the coefficient of friction as described by either the slip-weakening, or the slip-rate-weakening, or the state and rate dependent friction law; in other words, the friction changes from static friction to dynamic frictional strength. If the original shear traction is larger than the dynamic friction, the slip will continue to propagate away from the explosion site (corresponding to the hypocenter of an earthquake) where normal traction reduction due to the explosion is not important any more. In this way a spontaneous rupture or a laboratory earthquake is triggered.

1.2.3 Diagnostics

The diagnostic method used is dynamic photoelasticity. This technique is a classical method to measure the stress state in transparent, birefringent solids (Dally and Riley 1991). Two photoelastic materials, namely Homalite-100 and Polycarbonate are used in this investigation. Relevant properties of several photoelastic materials are listed in Table 1.1

Table 1.1 Summary of optical and mechanical properties of photoelastic materials

Material Property	**Homalite 100**	**Polycarbonate**	**Epoxy**
Young's Modulus E (MPa)	3860	2480	3275
Poisson's Ratio ν	0.35	0.38	0.36
Stress fringe value f_σ (kN/m)	23.6	7.0	11.2
Yielding Stress σ_Y (MPa)	48.3	34.5	55.2
P Wave Speed C_P (km/s)	2.498	2.182	2.548
S Wave Speed C_S (km/s)	1.200	0.960	1.136
Density ρ (kg/m^3)	1230	1129	1200

The stress fringe values are for green light at a wave length 525 nm. The static elastic properties listed in Table 1.1 are from reference (Dally and Riley 1991), and the dynamic elastic properties (wave speeds) were measured using 5 MHz ultrasonic transducers.

A typical set-up of dynamic photoelasticity is shown in Figure 1.5. A polarized laser provides a high intensity beam continuously at a power level of a few watts. The beam is then expanded by a collimator to a size of 100 mm or 130 mm in diameter. The large beam goes through the combination of circular polarizers and the transparent photoelastic specimen, and it is arranged so that an isochromatic fringe pattern is obtained and focused into the camera. The isochromatic fringe pattern obtained from the two-dimensional photoelastic model gives fringes along which the in-plane principle stress difference σ_1-σ_2 is equal to a constant. When the fringe order N is known, the in-plane principle–stress difference can be computed as follows:

$$\sigma_1-\sigma_2=Nf_\sigma/h \tag{1.12}$$

where h is the thickness of the modal material. The high speed camera (Cordin 220) used can take pictures at speeds up to 10^8 frames/sec. In most experiments an inter-frame time of 2-3 μs was used.

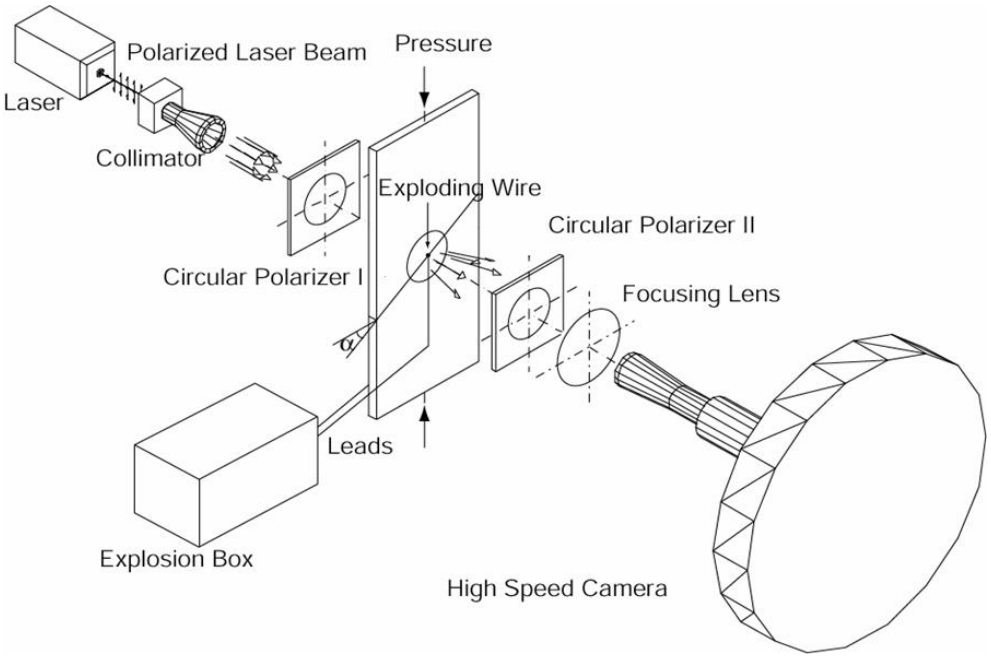

Figure 1.5 The set-up of dynamic photoelasticity combined with dynamic photograghy for laboratory earthquake studies.

1.3 Preliminary Results

A laboratory earthquake photograph taken 28 μs after the triggering is shown in Figure 1.6. In this case, the fault inclination angle was α=25° and the vertical pressure P=7 MPa, with the confining pressure in the horizontal direction at about 3 MPa. The material was Polycarbonate. The figure reveals a rupture propagating bilaterally (two rupture tips) along the fault, indicated by a dashed line. Each rupture-tip is characterized by a concentration of fringes and is

indicated in the figure by an arrow. The ruptures are seen following the circular shear wave front, and the rupture velocity V is close to the Rayleigh wave speed C_R of the material, as determined from the rupture-tip history.

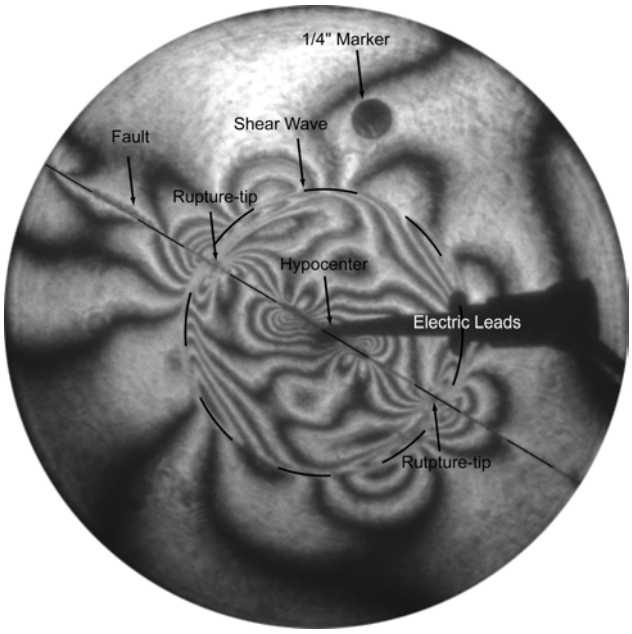

Figure 1.6 A typical isochromatic fringe pattern obtained from the earthquake experiments using Polycarbonate sample. We can see that there are two more stress concentration points close to the hypocenter, which are due to the injected metal powders produced by the explosion.

In Figure 1.7, two isochromatic fringe patterns are shown for an earthquake experiment along a fault with a finite core (1/8"). A fault system is usually composed of stiffer country rocks and a compliant fault core composed of damaged rocks (Ben-Zion and Sammis 2003). Again, the specimen is under far-field uniaxial compression and the fault is orientated at an angle α=20º, with the horizontal direction and far-field loading P=13 MPa. The host country rocks are simulated using Homalite-100 (stiffer) while the fault core is simulated using

Polycarbonate (softer). There are two contact interfaces in this case; we trigger the earthquake faulting in one of the interfaces (upper one). Two ruptures are observed propagating bilaterally at a speed slower than both of the material's shear wave speeds along the fault interface. The detail of the experiments on this type of geometry will be discussed in Chapter 4.

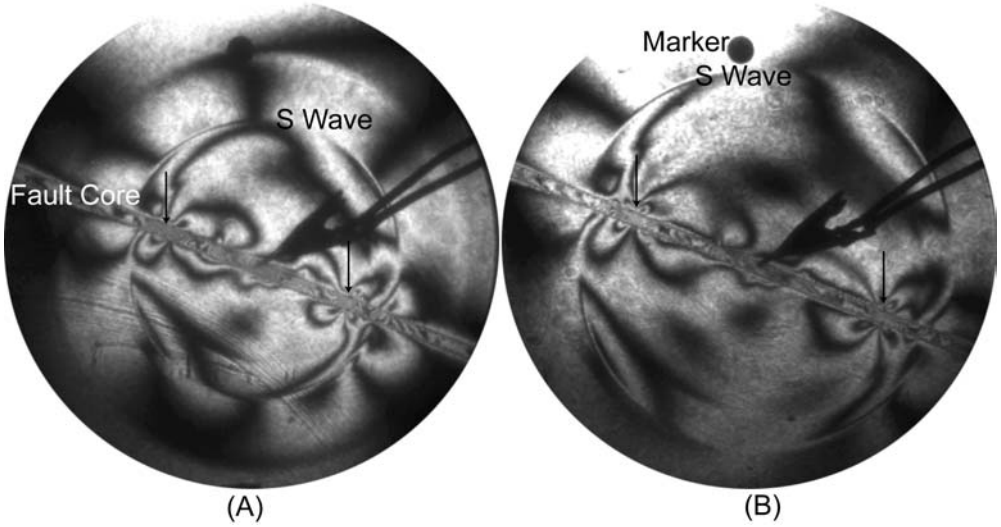

Figure 1.7 Two photographs obtained in a laboratory earthquake experiment for a fault with a finite core at two time instances. (A. Pattern at 32μs and B. Pattern at 44 μs).

In Figure 1.8, the inclination angle of fault α=25° and the uniaxial pressure P=11.5 MPa. We used Homalite-100 as the model material. A rupture-tip is shown propagating to the west along the fault, emitting two Mach wave fronts. The rupture velocity is faster than the shear wave speed C_S of the material and close to the longitudinal wave speed C_P. This rupture velocity is determined from both the rupture-tip history and the Mach cone angle δ (between the Mach cone front and the fault) by using the simple relation $V/C_S=1/\sin\delta$. Detailed discussions of the attainability and conditions of supershear earthquake ruptures

are in Chapter 2. The results described in Figures 1.6-1.8 are only indicative of the wide spectrum of behaviors that will be described in the following chapters.

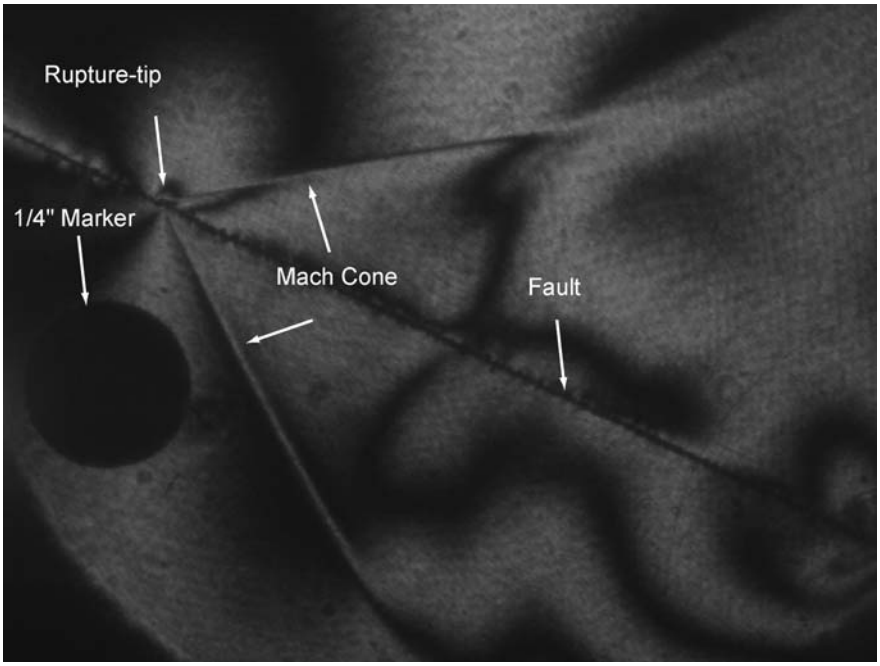

Figure 1.8 Isochromatic pattern shows a supershear rupture obtained in the laboratory earthquake experiment.

1.4 Conclusions and Discussions

In conclusion, we have designed an experimental set-up to simulate earthquake ruptures in the laboratory. Combined with high-speed in situ full-field diagnostics, we are able to obtain accurate measurements of the faulting process, especially the rupture velocities. The set-up is quite flexible. The examples shown demonstrate that this experimental design can be used successfully to address general questions in earthquake dynamics studies.

With slight modifications, we can study the effects of the geometry of the fault plane on earthquake rupturing; we can address the effect of the inhomogeneity of fault strength on earthquake rupturing, and we are able to investigate the mode of earthquake rupturing (i.e., crack mode or pulse mode). This is the first time that spontaneous rupture events simulating natural earthquakes have materialized in a highly controlled laboratory environment.

Chapter 2

Earthquake Rupturing along Faults Separating Similar Materials: SubRayleigh, Supershear, and SubRayleigh-To-Supershear Transition

In this chapter, we concentrate on the earthquake rupturing problem featuring the simplest possible geometry. In this case the earthquake ruptures occur along faults separating identical materials (homogeneous faults). Homalite-100 is the photoelastic material of choice. This material is well approximated by linear elasticity, it is birefringent, and it has a fairly high stress fringe value. Hence it can be used to detect the transient stress field during earthquake rupturing.

Specifically, we will address the question of possible rupture velocities occurring under earthquake type loading conditions. Based on seismic observations, it is believed that the rupture velocity of crustal earthquakes is close to the Rayleigh wave speed, C_R, of crustal rock. However, in a few cases supershear (speed faster than the shear wave speed, C_S, of the rock) ruptures have been suggested for earthquakes. Another related question is that involving the mechanism of reaching supershear speed. Indeed, if we accept the possibility of supershear speeds for earthquake ruptures, how would a rupture transition from a subRayleigh to a supershear speed? Could such rupture be perhaps born supershear?

Having these two questions in mind and using the experimental set-up described in detail in Chapter 1, we conducted around 50 experiments involving the homogeneous fault configurations. In this chapter we present the experimental discovery of the phenomenon of supershear rupture and the visualization of the

mechanism of subRayleigh to supershear transition of laboratory earthquake ruptures. We also probe the parameter space governing the physics of the subRayleigh to supershear transition of dynamic ruptures along incoherent (frictional) interfaces.

2.1 Introduction

The great M_s 8.1 (M_w 7.8) central Kunlunshan earthquake that occurred in Tibet on November 14, 2001, is an extraordinary event from the point of view of both earthquake dynamics and dynamic rupture mechanics. The rupture occurred over a very long, near-vertical, strike-slip fault segment of the active Kunlunshan fault and featured an exceptionally long (400 km) surface rupture zone and large surface slip (Lin, Fu, et al. 2002). In the August 8, 2003 issue of Science, Bouchon and Vallee (Bouchon and Vallee 2003) took advantage of the unusual length of the event and used both seismic waves and geologically observed total slip distribution to infer the rupture velocity history. Although it may not be unique, their modeling suggests speeds that are close to the Rayleigh wave speed, C_R, for the first 100 km of rupture growth, transitioning to a supershear speed for the remaining 300 km of propagation.

Recently, several other seismological reports also pointing to the possibility of supershear ruptures. Such events include the 1979 Imperial Valley earthquake (Archuleta 1984; Spudich and Cranswick 1984), the 1992 Landers earthquake (Olsen, Madariaga, et al. 1997), and most recently the 2002 Denali earthquake in Alaska (Ellsworth, Çlebi, et al. 2004). The 1999 Izmit earthquake in Turkey (Bouchon, Bouin, et al. 2001) is another event featuring a long segment of supershear rupturing. It should be noted here that for all of those examples mentioned above, the supershear ruptures happened only on short patches along the whole rupture length and the results are not conclusive. Bouchon and

Vallee's work is the most recent of a series of papers reporting supershear rupture growth occurring during large earthquake events; moreover it presents the first seismological evidence for transition from subRayleigh to supershear. In this respect it will be shown to be highly relevant to the experiments discussed in this chapter.

The question of whether earthquake ruptures propagate at supershear speeds is still a subject of active debate within the seismological community. This is because of the often insufficient field data as well as the limited resolution and non-uniqueness of the inversion process. A widespread view in seismology speaks of crustal earthquake ruptures mainly propagating at subRayleigh speeds between 0.75 and 0.95 C_R (Kanamori 1994). However, the multiplicity of independently collected evidence warrants further investigations of the mechanics of supershear rupture propagation. Whether and how supershear rupture occurs during earthquakes has an important implication for seismic hazard because the rupture velocity has a profound influence on the character of near-field ground motions (Aagaard and Heaton 2004).

The main goal of this chapter is to report on highly instrumented experiments that mimic the earthquake rupture process and to examine the physical plausibility and conditions under which supershear ruptures can be generated in a controlled laboratory environment. We study spontaneously nucleated dynamic rupture events in incoherent, frictional interfaces held together by the application of far-field tectonic loads. Thus we depart from the body of experimental work that addresses the dynamic shear fracture of coherent interfaces of some intrinsic strength, which are loaded by the application of dynamic, stress wave induced loading (Lambros and Rosakis 1995; Rosakis, Samudrala, et al. 1999; Coker and

Rosakis 2001; Rosakis 2002). A spontaneous rupture is commonly believed to be the closest physical model of an earthquake rupture.

Classical dynamic fracture theories of growing shear cracks have many similarities to the earthquake rupture processes (Freund 1990; Broberg 1999). Such theories treat the rupture front as a distinct point (sharp tip crack) of stress singularity. These conditions are close to reality in cases that feature coherent interfaces of finite intrinsic strength and toughness. The singular approach ultimately predicts that dynamic shear fracture is allowed to propagate either at a subRayleigh wave speed or at only one supershear speed, which is $\sqrt{2}$ times the shear wave speed. As a result, it excludes the possibility of a smooth transition of a steady-state rupture from subRayleigh to supershear speed for a steady-state rupture.

The introduction of a distributed rupture process zone has allowed fracture mechanics to better approximate the conditions that exist during real earthquake events (Ida 1972; Palmer and Rice 1973). Based on this so-called cohesive zone fracture mode, there is a forbidden speed range between C_R, the Rayleigh wave speed, and C_S, the shear wave speed (Burridge, Conn, et al. 1979; Samudrala, Huang, et al. 2002; Samudrala, Huang, et al. 2002). In the subRayleigh speed range all speeds are admissible, but only the Rayleigh wave speed is a stable speed; in the supershear speed range all speeds are admissible, but only speeds larger than $\sqrt{2}\,C_S$ are stable. Ruptures with unstable speeds will accelerate to a stable speed as determined by loading conditions. The theoretical results of the cohesive zone rupture model ultimately predict that earthquake ruptures can propagate either at Rayleigh wave speed or supershear speeds larger than $\sqrt{2}\,C_S$.

Early theoretical results by Burridge (Burridge 1973; Burridge, Conn, et al. 1979), along with numerical results by Andrews (Andrews 1976) and Das and Aki (Das

and Aki 1977) have predicted the possibility of supershear rupture and have alluded to a mechanism (Rosakis 2002) for transition from the subRayleigh to the supershear rupture velocity regime. According to the two-dimensional Burridge-Andrews mechanism, a shear rupture accelerates to a speed very close to C_R soon after its initiation. A peak in shear stress is found sitting at the shear wave front and is observed to increase its magnitude as the main rupture velocity approaches C_R. At that point, the shear stress peak may become strong enough to promote the nucleation of a secondary micro-rupture whose leading edge propagates at a supershear speed. Shortly thereafter, the two ruptures join up and the combination propagates at a speed close to C_P. It is interesting that this transition was also clearly visualized by recent two-dimensional, atomistic calculations of shear rupture in the micro-scale, which provided an impressive demonstration of the length scale persistence of this subRayleigh to supershear rupture transition mechanism (Abraham and Gao 2000). The Burridge-Andrews mechanism is also known as the mother-daughter mechanism in mechanics literature.

For mixed-mode (tensile and shear) ruptures, a different transition model has also been suggested (Geubelle and Kubair 2001; Kubair, Geubelle, et al. 2002; Kubair, Geubelle, et al. 2003). Based on numerical simulation, Geubelle and Kubair suggest that a mix-mode rupture can speed up and cross the forbidden speed range between C_R and C_S continuously. Finally, recent numerical investigations of frictional rupture have identified alternate, asperity based, mechanisms that provide a three-dimensional rationalization of such a transition (Day 1982; Madariaga and Olsen 2000; Dunham, Favreau, et al. 2003). In this case, 3-D effects play an important role in the transition. The rupture front focusing effect provides extra driving to speed up the spontaneous rupture.

The experimental confirmation of the possibility of supershear (intersonic) fracture followed many years after the first theoretical predictions. Indeed, a long series of experiments summarized by Rosakis (Rosakis 2002) showed that intersonic crack growth in constitutively homogenous systems featuring coherent interfaces (interfaces with inherent strength) is possible and may also occur in various combinations of bimaterial systems. However, in all of the various cases discussed by Rosakis (Rosakis 2002), the cracks were nucleated directly into the intersonic regime and there was no observation of a transition from subRayleigh to supershear speeds. This was due to the nature of the impact induced stress wave loading without pre-existing static loading and the nature of the relatively strong coherence of the interface (provided by glue). The major differences between the conditions during earthquake rupture and those fracture experiments have left questions regarding the plausibility of spontaneously generated intersonic rupture in frictionally held, incoherent interfaces unanswered. In addition, earlier laboratory earthquake experiments (Dieterich 1972; Scholz, Molnar, et al. 1972; Brune 1973; Johnson and Scholz 1976; Okubo and Dieterich 1984) dating back to the '70s, which simulated spontaneous rupture in the laboratory, have lacked the spatial and temporal resolution to produce conclusive proof of supershear rupture growth and to investigate the issue of rupture velocity transition.

2.2 Experimental Design

In order to address the above questions, we designed an experimental configuration whose purpose is to simulate earthquake rupture in the laboratory. The exploding wire triggering mechanism shown in Figure 2.1C is inspired by the numerical work of Andrews and Ben-Zion (Andrews and Ben-Zion 1997) and Cochard and Rice (Cochard and Rice 2000). They have used a localized pressure release to trigger rupture in their numerical simulations. Experimentally, it is also

a very convenient way of triggering the system's full-field, high-speed diagnostics (a digital high-speed camera capable of 10^8 frames/sec and a photoelastic set-up Figure 2.1A) that would otherwise have a very hard time capturing an event whose total duration is of the order of 50 μs.

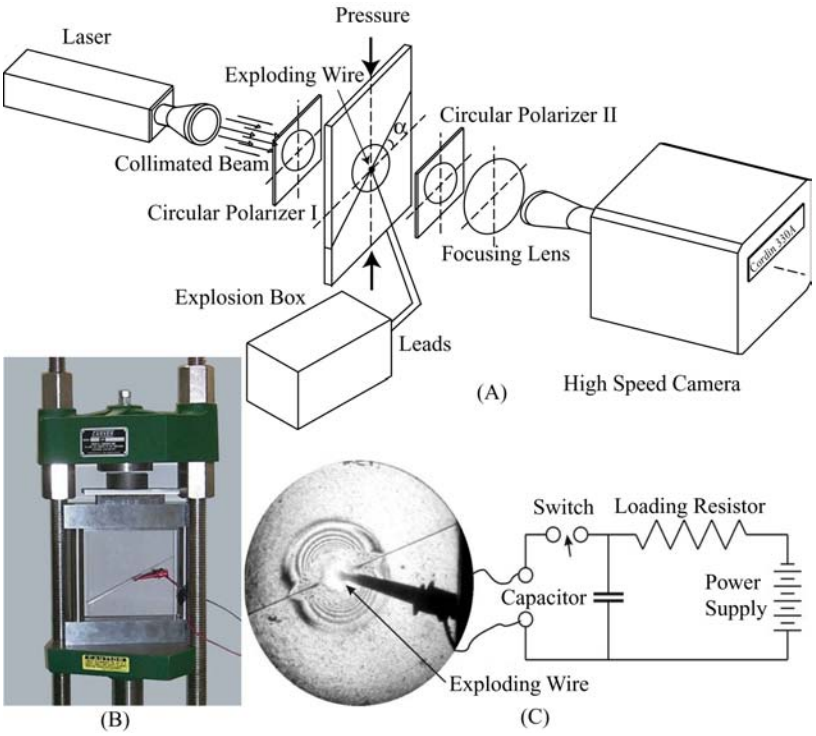

Figure 2.1 The fault system is simulated by using two Homalite-100 plates (shear modulus G =1.4 GPa, Poisson's ration ν=0.34, density ρ =1200 kg/m^3) held together by friction. The far-field tectonic loading is simulated by uniaxial compression exerted at the top and bottom of the system by means of a hydraulic press (B). The earthquake ruptures are triggered by an exploding wire technique (C).

The interface, or fault, is inclined at an angle α to the horizontal promoting strike-slip rupture events. Variations in α are used to vary the level of driving force (resolved shear stress minus dynamic frictional strength) experienced for the rupture after nucleation. As described in chapter 1, a unique aspect of the experimental design is related to the choice of the rupture triggering mechanism, which has not been addressed by previous laboratory earthquake experiments. The dynamic rupture is nucleated at the center of the simulated fault by producing a local pressure pulse in a small area of the interface (Figure 2.1C). A thin wire of 0.1 mm in diameter is inserted in a small hole of approximately the same diameter. An electronic capacitor is then discharged turning the metal into an expanding plasma wave, which triggers the spontaneous rupture. Details of the triggering process can be found in Chapter 1. It is the first time that such a controlled laboratory earthquake rupture has triggered and recorded.

2.3 Experimental Results

A number of experiments featuring a range of inclination angles α and far-field pressure P were performed, and in each of them the rupture process history was visualized in intervals of 2 μs. Depending on these two experimental variables, rupture velocities that are either purely subRayleigh or purely intersonic within the field of view (100 mm) were observed. The rupture events visualized corresponded to symmetric bilateral slip. By carefully controlling the angle α and the loading, the subRayleigh to supershear transition was also captured and the dependence of the transition length on these parameters was investigated.

2.3.1 Purely SubRayleigh and Supershear Earthquake Ruptures

In this section, results of purely subRayleigh and supershear ruptures will be shown. The physics governing the speed regimes will be examined later.

In Figure 2.2, we show two experiments featuring subRayleigh speed ruptures. In all the photographs, we can see clearly the circular shear wave front emitted from the simulated hypocenter. Rupture tips, characterized by the stress concentration (singular points in the photographs), are identified just behind the shear wave front. From the rupture length history, we are able to estimate the rupture velocity. In these two cases, the rupture velocities are very close to the Rayleigh wave speed of the material.

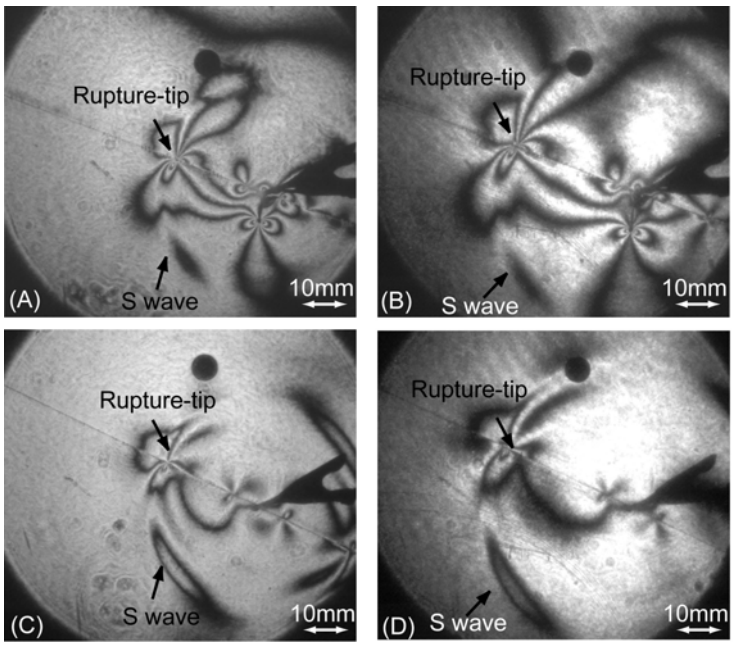

Figure 2.2 Earthquake experimental results of purely subRayleigh cases. A and B are from one experiment with a pressure of P=13 MPa and angle α=20° at the time instants of 28 μs and 38 μs respectively. C and D are from one experiment with a pressure of P=7 MPa and angle α=25° at the time instants of 28 μs and 38 μs respectively. For A and B, we can also identify two mode-I cracked in the lower half of the sample caused by the explosion itself. We expect that the effect of these cracks is localized.

From our experiments with lower inclination angles α and lower magnitude of uniaxial compression pressure P, we observed exactly the same features. This observation is consistent with the field observation of earthquake rupture velocities in general. As we have discussed earlier, in the subRayleigh speed range the only stable rupture velocity is the Rayleigh wave speed according to the cohesive zone model, and it is conformed to here in our experiments.

An interesting observation is that the rupture velocity is always the Rayleigh wave speed of the material. As mentioned, subshear or subRayleigh crustal earthquake ruptures are often observed to propagate at speeds between 0.75 and 0.95 C_R (Kanamori 1994). This discrepancy can be explained by considering the balance between the energy available to drive the rupture and the mode of rupture. In our case, the length of the rupture, l, increases continuously and hence the stress intensity factor K, which is proportional to $\sqrt{l}$ for a given rupture velocity also increases. As a result, the energy available to drive the rupture, which is proportional to l for a given rupture velocity, also increases. Under the theoretical framework of slip-weakening friction law, the resistance due to friction is constant. Hence the rupture will speed up to a stable speed. The only stable speed in the subRayleigh speed range is the Rayleigh wave speed (Burridge, Conn, et al. 1979; Samudrala, Huang, et al. 2002) and that is exactly the speed observed in our experiments. In the case of a real earthquake, due to the finite dimension of the fault, the inhomogeneous nature of the fault strength, and the special friction constitutive behavior, the rupture is often of a fixed length, i.e., it is pulse-like in rupture mode (Heaton 1990). As a result, the energy available to drive the rupture, which is proportional to the crack length for a given rupture velocity, is also constant. Because the resistance of the fault is nearly constant, by equaling the average resistance to the rupture energy release rate, we are able to determine the rupture velocity (Freund 1990). The rupture velocity can be any

value smaller than the Rayleigh wave speed in this case, depending on the value of the resistance and the length of the rupture. This phenomenon was observed in a recent numerical simulation (Dunham and Archuleta 2004).

In Figure 2.3, the inclination angle was kept at 25° while the pressure was increased to 15 MPa. For comparison purposes, the same time instants (28 μs and 38 μs after nucleation) are displayed.

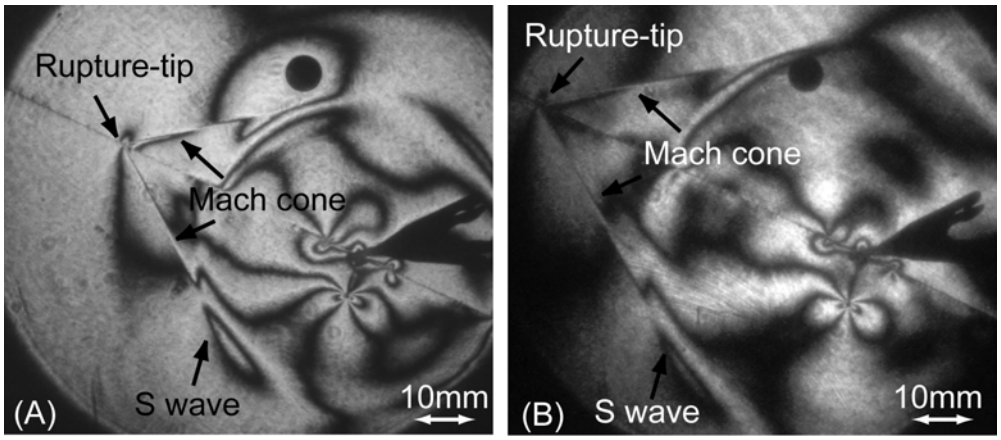

Figure 2.3 Earthquake experimental results of purely supershear case. A and B are from one experiment with the pressure of P=13 MPa and angle α=25° at the time instants of 28 μs and 38 μs respectively.

In this case, the circular traces of the shear wave are also visible and are at the same corresponding locations as in Figure 2.2. However, in front of this circle supershear disturbances (propagating to the left, marked in the photograph as the "Rupture-tip" and featuring a clearly visible Mach cone) are shown. The formation of the Mach cone is due to the fact that the rupture is propagating faster than the shear wave speed of the material. For this case, the sequence of images, other than those at 28 μs and 38 μs, have a very similar form and reveal a disturbance that was nucleated as supershear. The speed history $v(t)$ is

determined independently by either differentiating the rupture length history record or by measuring the inclination angle, δ, of the shear shocks with respect to the fault plane, and using the relation $v=C_S/\sin\delta$. The speed was found to be almost constant and very close to the plane stress P wave speed C_P of the material. This is the first experimental report of the supershear of a spontaneous shear rupture, to our knowledge. The supershear rupture initiated right after the triggering of the earthquake rupture. This is determined from the fact that the Mach cones are nearly tangential to the shear wave front.

In previous experiments involving strong, coherent (inherently strong) interfaces and stress wave loading, stable rupture velocities near $\sqrt{2}\,C_S$ were observed (Rosakis, Samudrala, et al. 1999). This apparent discrepancy can be explained by referring to the rupture velocity dependence on the available energy per unit crack advance within the supershear regime (Samudrala, Huang, et al. 2002). This energy attains a maximum value at speeds closer to $\sqrt{2}\,C_S$ for strong interfaces with a given loading. For weaker interfaces, this maximum moves towards C_P. In our situation, the interface is weak and the driving force (resolved shear minus dynamic friction force) is relatively large and constant. Hence, a rupture velocity close to C_P is expected.

From our above mentioned experimental results, we can see that the attainable rupture velocities depend on both the inclination angle α and the magnitude of uniaxial compression P. Larger angle and higher compression magnitude favors higher rupture velocity.

2.3.2 The Experimental Visualization of the SubRayleigh to Supershear Earthquake Rupture Transition

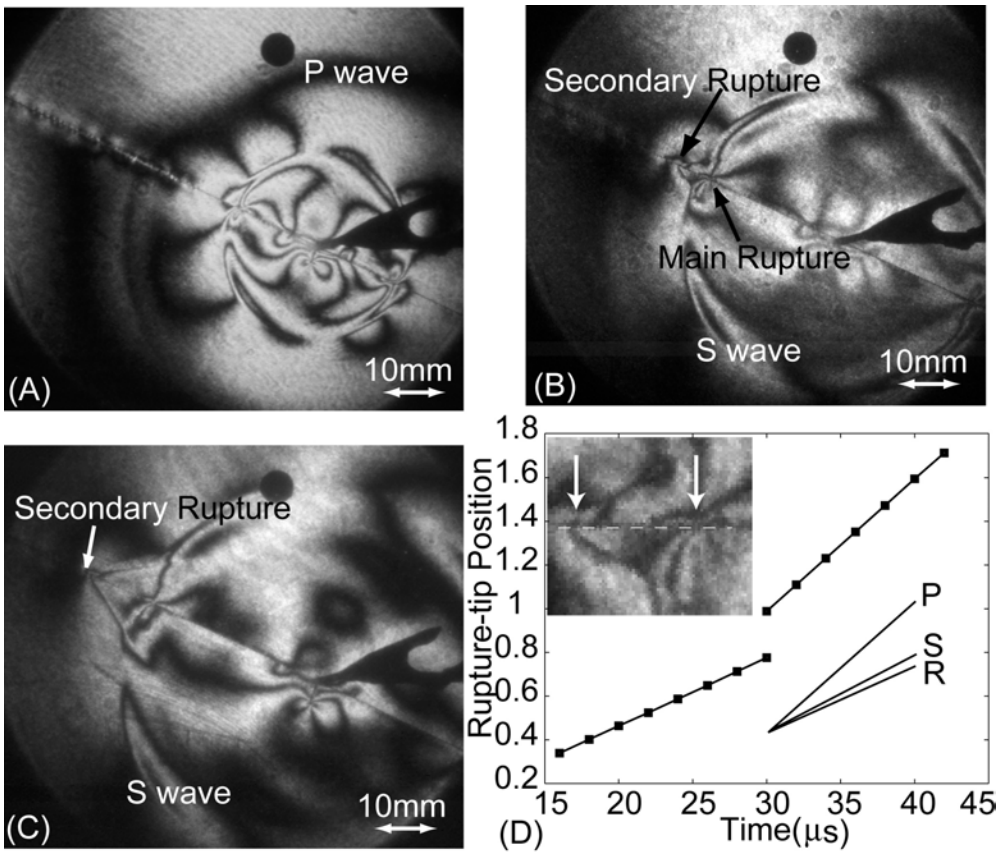

Figure 2.4 Visualization of the subRayleigh to supershear rupture transition.

As discussed earlier, we are interested in investigating how the supershear rupture is nucleated experimentally. For the experimental cases described in the above section, the supershear was nucleated immediately after triggering. Since the rupture velocity is controlled by both the inclination angle α and the magnitude of uniaxial compression P, it is possible for us to vary both of them carefully to suppress or perhaps delay the appearance of supershear rupture. Specifically, we

fix the inclination angle α at 25° and decrease P in order to induce and capture the nucleation process of a supershear rupture.

Figure 2.4A-C corresponds to a case with an intermediate far-field pressure compared to the ones displayed in Figure 2.2C-D and Figure 2.3. Here, the angle is kept the same (25°) and the pressure is decreased to 9 MPa in an attempt to visualize a transition within our field of view (100 mm). Three different time instances of the same rupture event are displayed. In Figure 2.4A, the circular traces of both P and S waves are visible, followed by a rupture propagating at C_R. In Figure 2.4B, a small secondary rupture appears in front of the main rupture and propagates slightly ahead of the S wave front. In Figure 2.4C, the two ruptures coalesce and the leading edge of the resulting rupture grows at a speed of 1970 m/s which is very close to C_p. Figure 2.4D displays the length vs. time of the two ruptures, in which the length scale is directly read from the pictures with the aid of a 1/4" marker in the picture. We compared the slopes to the characteristic wave speeds of the material before and after their coalescence. We also show a magnified view of the secondary rupture as it nucleates in front of the main rupture; both ruptures are indicated by arrows. The transition length L for this case is approximately 20 mm.

Table 2.1 Experimental Results of Transition Length

Test #	**Angle**	**Pressure (MPa)**	**Transition Length L (mm)**
1	25°	9.0	23.2
2	25°	9.1	19.0
3	25°	11.0	17.0
4	25°	12.4	12.1
5	25°	15.0	8.0

In Table 2.1, we list the experiments featuring supershear transition. Test #2 corresponds to the experiment shown in Figure 2.4, in which case the transition length L can be determined easily. Test #5 corresponds to the experiment shown in Figure 2.3, in which case an indirect method is needed to estimate the transition length. This method is described below.

As shown in Figure 2.5, at time T_0, the supershear rupture is nucleated at the intersection of the shear wave front and the fault line (point A). If the transition length $L=\overline{OA}$ is very small, our spatial resolution may not be good enough to measure it accurately. Alternatively a photograph may not have been taken at that instant. Assuming that we can measure the shear wave position and supershear rupture tip position at a later time instance T_1, denoted by B and C respectively, the transition length can be inferred by pure geometry. To do so we observe that relations $\overline{OA}=C_sT_0$, $\overline{OB}=C_sT_1$, and $\overline{OC}=v(T_1-T_0)$ hold provided that the supershear rupture tip also grows at a constant speed $V>C_S$.

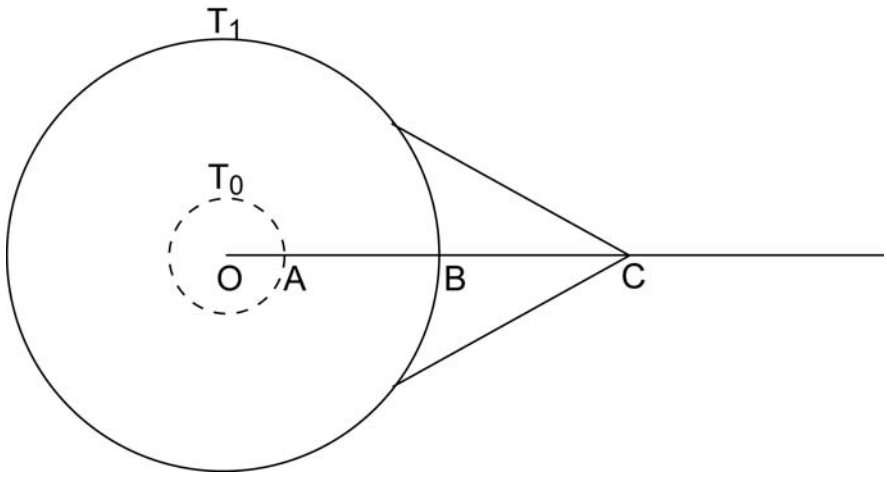

Figure 2.5 Method of estimation transition length L ($\overline{OA}$).

By simple manipulation, we have $\frac{\overline{OC}}{\overline{OB}}=\frac{v}{C_S}(1-T_0/T_1)$, which leads to $T_0=(1-\frac{C_S}{v}\frac{\overline{OC}}{\overline{OB}})T_1$. By multiplying both sides of the last relation by C_S, we get $L=\overline{OA}=C_ST_0=(1-\frac{C_S}{v}\frac{\overline{OC}}{\overline{OB}})C_ST_1=(1-\frac{C_S}{v}\frac{\overline{OC}}{\overline{OB}})\overline{OB}$. Thus, in this relation we are able to estimate the supershear rupture transition length L even if we have not taken any pictures at or before the time instance of the transition. Several results listed in Table 2.1 were obtained using this method. The only assumption is the near constancy of v. The validity of this assumption has been experimentally verified.

2.4 Theoretical Model for the SubRayleigh to Supershear Transition

The above physical picture is comparable with the Burridge-Andrews mechanisms already described in the introduction. Andrews (Andrews 1976; Andrews 1985) quantified this transition in a parameter space spanned by a normalized supershear transition length L/L_c and the non-dimensional driving stress parameter s $[s=(\tau^y-\tau)/(\tau-\tau^f)]$ (described in chapter 1). The parameters τ, τ^y, and τ^f are the resolved shear stress on the fault, the static frictional strength, and the dynamic strength of the fault respectively; they describe the linear slip-weakening frictional law (Ida 1972; Palmer and Rice 1973) used in Andrews' computations.

2.4.1 Uniaxial Loading Condition

We used uniaxial loading in the experiments described in this chapter. With respect to this loading condition and the geometry of our experiment, s (see Equation 1.2) can be expressed as: $s=(\mu^s\cos\alpha-\sin\alpha)/(\sin\alpha-\mu^d\cos\alpha)$, where μ^s and μ^d are the static and dynamic friction coefficients respectively. The Andrews' result can be symbolically written as $L=L_cf(s)$. The function $f(s)$ has been given numerically by Andrews as an increasing function of s, and can be

well approximated by the equation $f(s)=9.8(1.77-s)^{-3}$. The normalizing length L_c is the critical length for unstable rupture nucleation and is proportional to the rigidity G and to d_0, which is defined as the critical or breakdown slip of the slip weakening model. L_C can then be expressed as:

$$L_c = \frac{1+\nu}{\pi}\frac{(\tau^y-\tau^f)}{(\tau-\tau^f)^2}Gd_0 \tag{2.1}$$

By applying the above results to our configuration and by assuming Equation 1.1, the transition length L is found to be inversely proportional to the applied uniaxial pressure P and to be governed by the following general functional form:

$$L=f(s)\left[(1+\nu)/\pi\right]G\left[(\mu^s-\mu^d)/(\tan\alpha-\mu^d)^2\right](d_0/P) \tag{2.2}$$

In Figure 2.6 we display the dependence of the transition length L on pressure from a set of experiments corresponding to the same inclination angle of 25° (s=0.5) and identical surface finish (roughness is about 17 μm). The static frictional coefficient was measured to be $\mu^s=0.6$ using the traditional inclined plane method. In this method, we put one block on top of an inclined plane and increase the inclination angle until the block slides. This way we can measure the critical inclination angle ψ_c. The static coefficient of friction is determined from the relation $\mu^s=\tan^{-1}\psi_c$. To estimate the dynamic frictional coefficient, we increased α from 10° to a critical angle α_c at which slip was initiated under the action of far-field loads and dynamic triggering. We assumed that the shear traction is approximately equal to the dynamic friction at this critical angle α_c. This angle was found to be between 10° and 15° and from which we estimated

the coefficient of dynamic friction to be $\mu^d=0.2$. Using $\mu^s=0.6$ and $\mu^d=0.2$, we can compare our experiment to Andrews' theory as shown in Figure 2.6. Although the theory qualitatively captures the decreasing trends of the experiments, the data exhibits a dependence on pressure that is visibly stronger than P^{-1}.

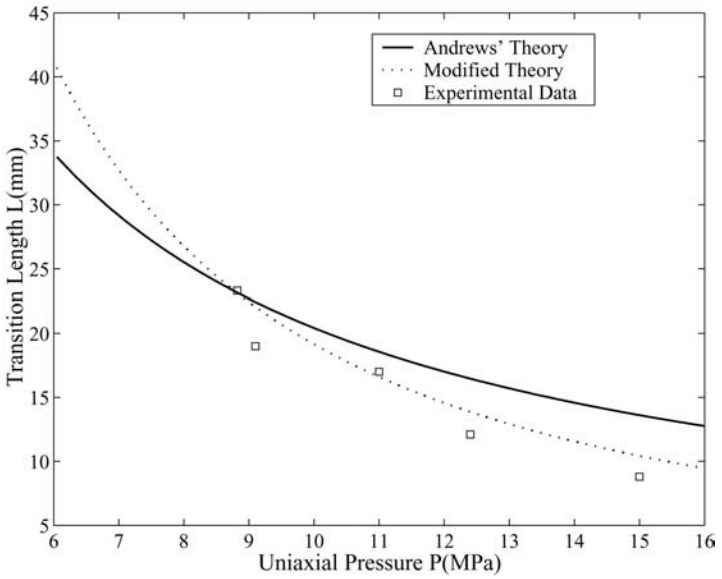

Figure 2.6 Transition length as a function of the far-field load.

A natural way to modify Andrews' results and to introduce some micro-contact physics into the pressure dependence of L is to consider the effect of pressure on the critical breakdown slip d_0. As pointed out by Ohnaka, based on friction experiments on rocks, there exists a linear relation between a characteristic surface length (half-distance between contacting asperities, denoted as D in this case) and the critical slip distance d_0 as (Ohnaka 2003):

$$d_0=c[(\tau^y-\tau^f)/\tau^f]^M D \tag{2.3}$$

where c and M are constants. In addition, D depends on the normal stress, σ, applied on the fault (which is $\sigma=P\cos^2\alpha$ in this case).

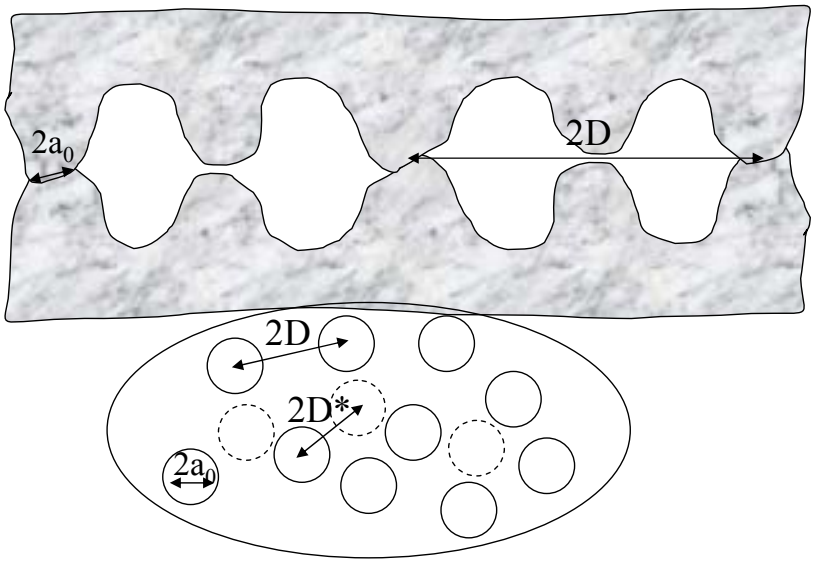

Figure 2.7 Schematic drawing of the micro-contact based frictional model. The top figure is the side view of the contact and the bottom figure is the top view. As the normal force increases, the number of contacts, n, increases.

As shown in Figure 2.7, a classical plastic contact model is used to establish this dependence. In this model the average radius of n contacting asperities is a_0 (assumed as a constant in this model). As the pressure over a macroscopic contact area A ($=n\pi D^2$) is increased, the number of contacts, n, as well as the real contact area A_r ($=n\pi a_0^2$), also increases.

By defining the hardness H as the ratio of the total normal force N to the real contact area A_r (Bowden and Tabor 1986), N can be expressed as:

$$N=HA_r=Hn\pi a_0^2=\sigma A=AP\cos^2\alpha \tag{2.4}$$

Substitution of A and A_r in terms of D and a_0 gives $D=\sqrt{H}a_0\cos\alpha P^{-1/2}$. Using the linear relation between D and d_0, the breakdown slip is further found to depend on the pressure as $d_0 \sim P^{-1/2}$. By substituting the above relations into the expression relating L and d_0/P, discussed above, a modified expression of transition length to pressure that features a stronger dependence ($L \sim P^{-3/2}$) on pressure emerges. As shown in Figure 2.6, this modified relation agrees well with the experimental data presented in this paper for appropriate choices of the parameters of the micromechanics contact model. The explicit form of the functional relation between the transition length and the problem parameters is given as follows:

$$L=f(s)\frac{1+\nu}{\pi}G\frac{\mu^s-\mu^d}{[\sin\alpha-\mu^d\cos\alpha]^2}2c\left(\frac{\mu^s-\mu^d}{\mu^s}\right)^M\sqrt{H}a_0P^{-\frac{3}{2}}\cos^{-1}\alpha \tag{2.5}$$

In Figure 2.8, we applied the Equation (2.5). We take H=240 MPa (it is about three times the compression yielding strength of the material), and the micro-contact radius a_0 are chosen to vary. The best-fit gives the estimation of a_0 as 1.8 μm, which is a reasonable value as compared with the surface roughness.

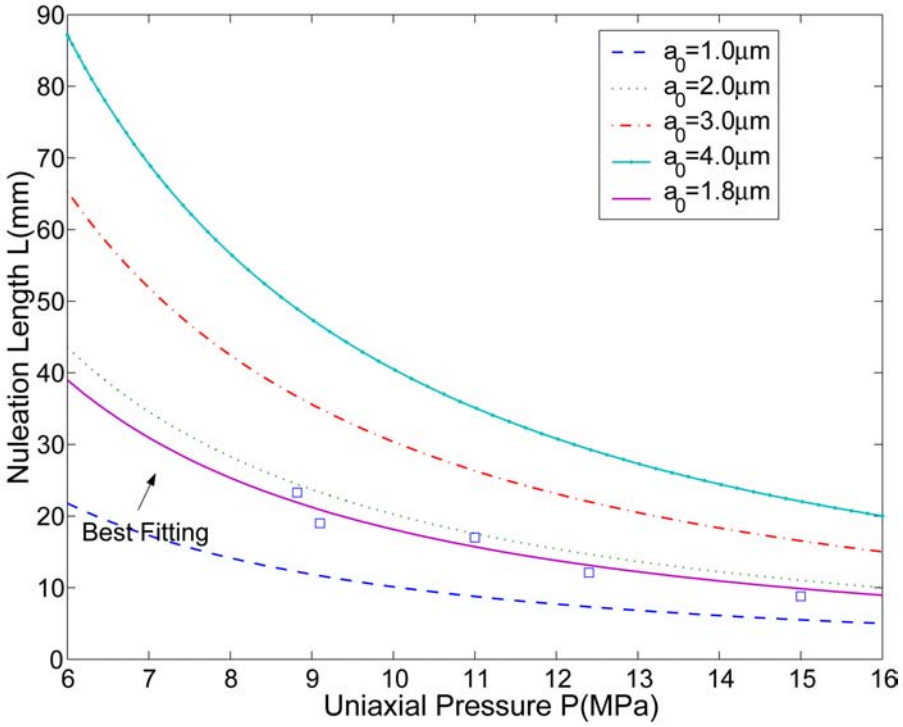

Figure 2.8 The dependence of nucleation length on P in terms of the size of micro-contact radius a_0 using Equation (2.5).

2.4.2 Biaxial Loading Condition

In the earth's crust where natural earthquakes occur, the stress state is always two-dimensional if we assume again that the plane stress state prevails. The stress state can be defined by two principle stresses that are compressive in nature. Let the maximum and minimum tectonic stresses be denoted as $P_1=P$ and $P_2=bP$ respectively, while the angle between the fault plane and P_1 would be $\varphi=90^o-\alpha$ as shown in Figure 2.9.

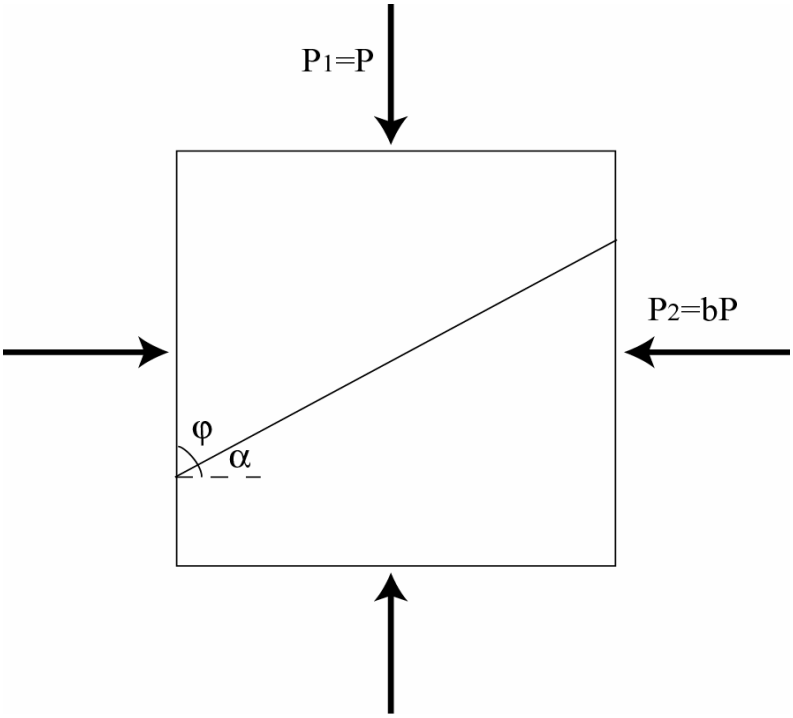

Figure 2.9 The geometry of biaxial loading.

The resolved shear traction τ and the normal traction σ are:

$$\begin{cases} \tau=(1-b)P\sin\alpha\cos\alpha \\ \sigma=bP\sin^2\alpha+P\cos^2\alpha \end{cases} \tag{2.6}$$

Substitute (2.6) into (2.1), we have:

$$L_c=\frac{1+\nu}{\pi}Gd_0\frac{(\mu^s-\mu^d)(\cos^2\alpha+b\sin^2\alpha)}{P\left[(1-b)\sin\alpha\cos\alpha-\mu^d(\cos^2\alpha+b\sin^2\alpha)\right]^2} \tag{2.7}$$

The s parameter $s=(\tau^y-\tau)/(\tau-\tau^f)$ is now:

$$s=\frac{\mu^s(b\sin^2\alpha+\cos^2\alpha)-(1-b)\sin\alpha\cos\alpha}{(1-b)\sin\alpha\cos\alpha-\mu^d(b\sin^2\alpha+\cos^2\alpha)} \tag{2.8}$$

Hence, the transition length L becomes:

$$L=f[s(\alpha)]*L_c=f[s(\alpha)]\frac{1+\nu}{\pi}G\frac{(\mu^s-\mu^d)(\cos^2\alpha+b\sin^2\alpha)}{\left[(1-b)\sin\alpha\cos\alpha-\mu^d(\cos^2\alpha+b\sin^2\alpha)\right]^2}\frac{d_0}{P} \quad (2.9)$$

Finally, using equation (2.3), we have:

$$L=f[s(\alpha)]\frac{1+\nu}{\pi}G\frac{2c(\mu^s-\mu^d)^{1+M}(\cos^2\alpha+b\sin^2\alpha)^{1.5}}{\left[(1-b)\sin\alpha\cos\alpha-\mu^d(\cos^2\alpha+b\sin^2\alpha)\right]^2}(\mu^s)^{-M}\sqrt{Ha_0}P^{-1.5} \quad (2.10)$$

We can then evaluate L (Equation 2.9) in the φ and d_0 space. If in particular we assume the following parameters: $\mu^s=0.6$, $\mu^d=0.2$, $P=50\ \text{MPa}$, $\nu=0.25$, and $G=35\ \text{GPa}$, the result displayed in Figure 2.10 is obtained.

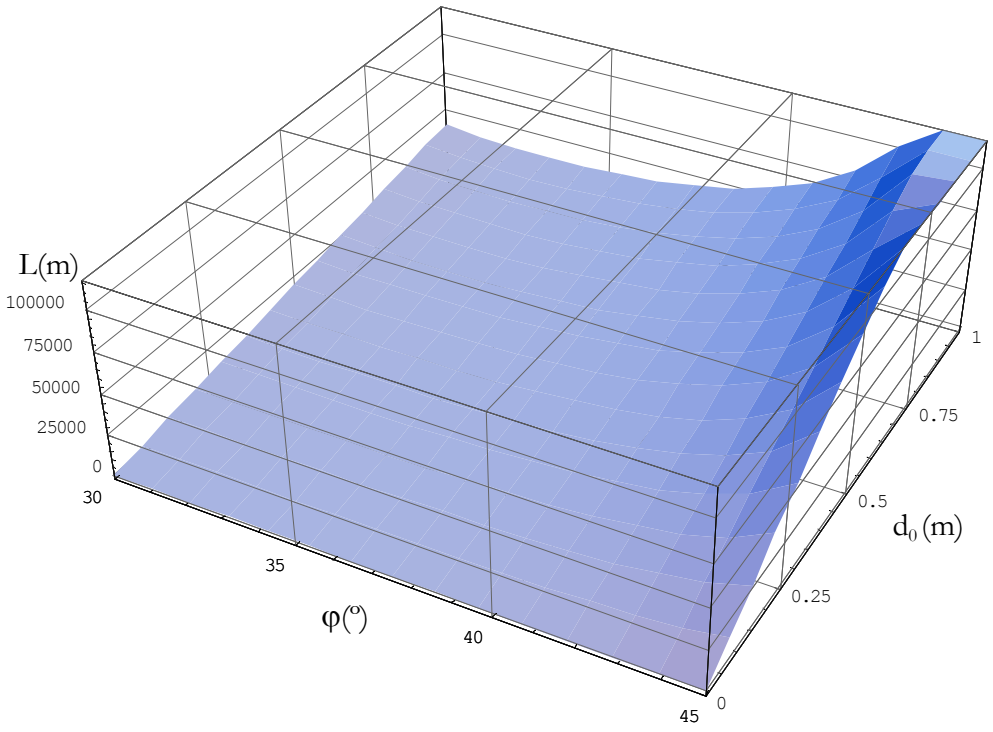

Figure 2.10 The transition length as evaluated for biaxial loading.

Specifically, by taking $d_0 = 0.5$ m and $\varphi = 45^\circ$, we obtained $L = 94$ km. This result is consistent with the transition length for the Kunlunshan earthquake (Bouchon and Vallee 2003). Unfortunately, in order to obtain predictions of the transition length, we need to assume the values of several parameters, which are often very difficult to estimate in specific natural earth settings. However, what is encouraging is that the predictions seem reasonable in an order of magnitude sense. This is true for both the laboratory experiments and for the geophysical length scale. In the next section, we will provide another method to estimate the transition length corresponding to a real earthquake.

2.5 Application to Real Earthquakes

In the above section, we have tried to estimate the transition length for a real earthquake under biaxial loading conditions. Here we will describe another scaling method with fewer parameters and in terms of variables more familiar to geophysicists.

For seismological applications, we rewrite the general form of Equation (2.2) in terms of the effective stress $\tau^e = \tau - \tau^f$, a commonly used and estimated seismological parameter. Equation (2.2) can be rewritten as:

$$L = f(s)(1+\nu)(1+s)Gd_0/\pi\tau^e \qquad (2.11)$$

Application of this equation to both seismic faulting and to laboratory data allows us to scale the transition length L from laboratory to seismological conditions. The effective stress τ^e in our experiment is chosen to be of the same order as that measured in seismology. The ratio of rigidity of the Earth's crust to Homalite is about 25. We estimate L=20 mm from the experiment described in

Figure2.4 (P=9 MPa and α=25°) from which d_0 =10 μm is obtained using Equation (2.2). The values of d_0 for large earthquakes are often estimated as 50 cm to 1 m (Ide and Takeo 1997). If s is approximately the same under laboratory and crustal conditions, the transition length for earthquakes can be estimated to be in the range between 25 and 50 km. Because s can be different and the estimate of d_0 for earthquakes is very uncertain at present, this value should be taken as an order of magnitude estimate. Nevertheless, it is of the same order as that inferred for the Kunlunshan event. The large transition length required for supershear is perhaps one of the reasons that relatively few earthquake events have been observed to feature such high rupture velocities and that all of them correspond to large magnitude earthquakes.

If the tectonic stress is well below the static fault strength (i.e., large s), then the transition length becomes too large for earthquake ruptures to attain supershear. The observation that during several large earthquakes the rupture velocity became very fast, possibly supershear, suggests that the tectonic stress is fairly close to the static fault strength (i.e., small s), which has important implications for the evolution of rupture in large earthquakes.

2.6 Conclusions and Discussions

Using the laboratory earthquake model and high speed, full-field diagnostics, we produced several interesting results for earthquake ruptures along faults separating similar materials. We reported for the first time a supershear rupture speed for earthquake type ruptures (spontaneous in nature) in the laboratory. We also observed the nucleation process of supershear ruptures. Under proper loading conditions, the spontaneous rupture, which initially propagates at a subRayleigh speed, figures out a way to overcome the forbidden speed range between C_R and C_S. This is done by nucleating a secondary rupture at the S wave

front and, afterwards, the two ruptures coalescence as a supershear rupture. This observation confirms the Burridge-Andrews mechanism, which is suggested purely based on theoretical and numerical simulations.

From our experimental results and our theoretical analysis, in order for a spontaneous rupture to propagate at a supershear speed, it is necessary to have proper loading conditions (in terms of s, this means a small s value) and a sufficiently long propagation distance (larger than L). From our simple calculation, the nucleation distance for supershear ruptures for real earthquakes can be of the order of 100 km. This fact can be used to explain the rarity of observations of supershear earthquakes. Another reason for the rarity of supershear ruptures is due to the quality of data and nature of the faults. Low frequency and less accurate data make it difficult to estimate the rupture velocity by inversion. Geological faults are usually inhomogeneous and curved; there are always weak portions available to initiate earthquakes before large enough strain energy to propagate supershear ruptures accumulates.

Chapter 3

Earthquake Rupturing Processes along Faults Separating Different Materials: Generalized Rayleigh Wave Speed, Supershear, and Directionality

For large and mature geological faults, it is highly possible that millions of years of slip would bring rocks of different types and different properties in contact and thus, faults with a material contrast would result. The existence of such a material contrast leads to rich physical phenomena during the earthquake rupturing process. As reviewed by Ben-Zion (Ben-Zion 2001), during the earthquake rupturing on faults separating different materials, the normal traction is coupled to the shear traction. Consequently, in one direction of faulting the normal traction is reduced due to sliding, while in the other direction the normal traction is enhanced. The direction with a reduced normal traction is called the "preferred" direction or "positive" direction, and it is in the same direction of the sliding of the more compliant (slow) material. The other direction is called the "negative" direction.

According to the theoretical and numerical work by Rice and his coworkers, the possible rupture velocity in the positive direction is the Generalized Rayleigh (GR) wave speed if this speed is defined; otherwise, it is close to the slow shear wave speed. The rupture in the opposite direction can propagate at a supershear speed close to the slower P wave speed of the system. This type of directionality of the earthquake rupturing process is primarily due to the material contrast.

In this Chapter, we will design a fault model with a material contrast (bimaterial or inhomogeneous system). The system's constituent solids are chosen so that a generalized Rayleigh wave speed exists. The earthquake ruptures are triggered the same way as described in previous chapters. Our goal is to investigate the effect of the material contrast on earthquake faulting. Especially, we want to investigate the spectrum of possible rupture velocities for earthquakes occurring in inhomogeneous fault systems.

3.1 Introduction

In most mature faults, the elastic properties vary across the fault (Magistrale and Sanders 1995; Peltzer, Crampe, et al. 1999) and the shear wave speeds may also vary by as much as 30% (Cochard and Rice 2000; Ben-Zion and Huang 2002). Recently, Rubin and Gillard (Rubin and Gillard 2000) studied several thousands of pairs of consecutive earthquakes that occurred on a segment of the central San Andreas fault, south of the Loma Prieta rupture. Among the second events of each pair, they found that over 70% more occurred to the northwest than to the southwest. They interpret this asymmetry as being a result of the contrast in material properties across the fault. Indeed, at this location of the San Andreas fault, the rock body is more compliant northeast of the fault than it is southwest (Eberhart-Phillips and Michael 1998).

Theoretical and numerical studies of rupture that employ frictional laws with a constant coefficient of friction (Weertman 1980; Heaton 1990; Adams 1995; Andrews and Ben-Zion 1997; Harris and Day 1997; Ranjith and Rice 1999; Cochard and Rice 2000; Rice, Lapusta, et al. 2001) predict that if rupture occurs on the boundary between two frictionally held solids having different elastic properties and wave speeds, such a rupture preferentially propagates in the same direction as the direction of slip in the lower wave speed solid. Since the

directionality of fault rupture has a profound influence on the distribution of damage caused by earthquake ground motion, it would be extremely useful if this behavior could be confirmed under controlled laboratory conditions. While many of the physical aspects of dynamic rupture (including supershear) are recently becoming progressively clearer in relation to homogeneous faults (Ben-Zion 2001; Rice 2001; Rosakis 2002), the behavior of spontaneously nucleated ruptures in inhomogeneous faults, separating materials with different wave speeds, is experimentally unexplored.

The recent large earthquakes (1999 Izmit and Düzce) and the seismic migration history along the North Anatolian fault may represent a unique field example of the effect of the material contrast across the fault. The 1999 Izmit and Düzce events featured both supershear and subRayleigh rupture branches (Bouchon, Bouin, et al. 2001). Most significantly, they are the last of a series of large ($M \geq 6.8$) earthquakes that have occurred since 1934 in the North Anatolian Fault. These earthquakes have occurred on a rather long and allegedly inhomogeneous fault system (Zor, Sandvol, et al. 2003) that has hosted tens of major migrating earthquakes in the past century. Following the work of Stein, et al (Stein, Barka, et al. 1997) and of Parsons, et al (Parsons, Toda, et al. 2000), tens of large ($M \geq 6.8$) earthquakes occurred over 1000 km along the North Anatolian fault between the 1939 earthquake at Ercinzan and the 1999 Izmit and Düzce earthquakes. Such a long series of earthquakes are believed to be a textbook example of how the transfer of stress from a recent nearby event can trigger the next major event in due time. This presumably happens by adding or transferring stress to the fault segment, which is adjacent to the tips of a segment that has last failed. The stress distribution is highly non-uniform since it occurs in addition to the long term stress renewal and to the pre-existing stress inhomogeneities. However, as much as this model seems to be complete and

convincing, a few questions remain that need to be resolved and are of relevance to the work described here. Such questions are related to structural fault inhomogeneities as we will discuss later.

3.2 Two Types of Ruptures along Inhomogeneous Faults

Inhomogeneous faults separate materials with different wave speeds. When such faults experience spontaneous rupture the equi-bilateral symmetry, expected in the homogeneous case, is broken. This leads to various forms and degrees of rupture directionality. Dynamic rupture along bimaterial interfaces is known to involve substantial coupling between slip and normal stress (Weertman 1980; Ben-Zion 2001; Rice 2001). As a consequence, the relative ease or difficulty for a rupture to propagate in a specific direction along a bimaterial interface is closely related to the degree of mismatch in wave speeds in addition to the faults frictional characteristics. For bimaterial contrast with approximately less than 35% difference in shear wave speeds (as in the case of most natural faults), generalized Rayleigh waves can be sustained. These waves are waves of frictionless contact propagating at a speed, C_{GR}, called the generalized Rayleigh wave speed (Rice 2001).

The 1980 rupture solution by Weertman (Weertman 1980) involves a dislocation like sliding pulse propagating sub-sonically with a velocity equal to C_{GR} along an interface governed by Amonton-Coulomb friction. However, the classical Amonton–Coulomb's description has been shown to be inadequate for addressing fundamental issues of sliding (Ranjith and Rice 2001), since sliding becomes unstable to periodic perturbations. Instability, in the above sense, implies that periodic perturbations to steady sliding grow unbounded for a wide range of frictional coefficient and bimaterial properties (Renardy 1992; Adams 1995). The growth rate is proportional to the wave number. In particular,

when generalized Rayleigh waves exist, Ranjith and Rice (Ranjith and Rice 2001) demonstrate that unstable periodic modes of sliding appear for all values of the friction coefficient. Mathematically, instability to periodic perturbations renders the response of a material interface to be ill-posed (no solution exists to the problem of growth of generic, self-sustained perturbations to steady sliding). The problem is regularized by utilizing an experimentally based frictional law (Prakash and Clifton 1993), in which shear strength in response to an abrupt change in normal stress evolves continuously with time (Cochard and Rice 2000; Ranjith and Rice 2001). In such a case, the problem becomes well-posed and generic self-sustained pulse solutions exist while numerical convergence through grid size reduction is achieved (Cochard and Rice 2000; Coker, Lykotrafitis, et al. 2004). However, despite the fact that this special frictional law provides regularization, self-sustained slip pulses may still grow in magnitude with time. This is a phenomenon that has been demonstrated numerically by Ben-Zion and Huang (Ben-Zion and Huang 2002). Moreover, self-sustained pulses were found to exist and to propagate at discrete steady velocities and at specific directions along the inhomogeneous interface by analytical (Ranjith and Rice 2001) and numerical means (Andrews and Ben-Zion 1997; Cochard and Rice 2000).

Two types of such steady, self-sustained pulses were discovered by Ranjith and Rice (Ranjith and Rice 2001) theoretically. Consistent with Weertmans 1980 analysis (Weertman 1980), the first type corresponds to rupture growth in the direction of sliding of the lower wave speed material of the system. This direction is referred to in the literatures (Ben-Zion 2001; Rice 2001) as the "positive" direction and sometimes as the "preferred" direction (Ben-Zion 2001). The rupture pulses belonging to this type are sub-shear and always propagate with a steady velocity $V = +C_{GR}$, where the plus denotes growth in

the "positive" direction. Thus, in this work we will refer to these rupture pulses as "positive" generalized Rayleigh ruptures and will abbreviate them as "+GR" ruptures. The second type of self-sustained rupture corresponds to growth in the direction opposite to that of sliding in the lower wave speed material of the bimaterial system. This direction is often referred to as the "negative" direction or "opposite" direction (Cochard and Rice 2000). Such ruptures are supershear and they always propagate with a steady velocity that is slightly lower than the P-wave speed of the material with the lesser wave speed ($V= -C_p^2$). Such ruptures are generated for sufficiently high values of the coefficient of friction (Ranjith and Rice 2001) and are less unstable than the "+GR" ruptures described above (Cochard and Rice 2000). In the present paper we will abbreviate such ruptures as "$-P_{SLOW}$" ruptures. This second type of rupture pulse was also studied by Adams (Adams 2001), who showed that the leading edges of these supershear (intersonic) ruptures are weakly singular, a result which is consistent with numerical analysis (Cochard and Rice 2000).

From the point of view of numerics, the early work of Andrews and Ben-Zion (Andrews and Ben-Zion 1997), has brought to light the persistence and interesting properties of rupture pulses of the "+GR" type. This was possible even in the ill-posed context of sliding governed by Amontons-Coulomb friction before much of the theoretical concepts were at hand. In their work, the sliding "+GR" pulses were triggered by a local release of interfacial pressure spread out over a finite region at the interface and over finite time. Surprisingly, no pulses of the second type ("$-P_{SLOW}$" pulses) were excited in these simulations despite the fact that the coefficient of friction was high enough to have permitted their existence as suggested by the modal analysis of Ranjith and Rice (Cochard and Rice 2000). The subsequent numerical simulations of Cochard and Rice (Cochard and Rice 2000), which utilized

modified Prakash and Clifton Law, were able to sequentially excite regularized self-sustained pulses of both types. This was achieved by introducing small changes in the parameters of the friction law and in the geometry of the nucleation zone. At the same time, no simultaneous excitation of both modes was reported. Moreover, the "$-P_{SLOW}$" pulses were found to be slightly more difficult to excite than the "+GR" pulses. However, the degree of relative difficulty was not examined in detail. In partial agreement to the above numerical studies, Harris and Day (Harris and Day 1997) demonstrated the simultaneous existence of both types of sliding modes, propagating in opposite directions during the same rupture event. They considered various bimaterial and tri-layered configurations featuring modest wave speed mismatch and a slip-weakening frictional law. The inconsistency between the different numerical studies may be due to the different friction laws applied. All studies except this of Harris and Day have assumed a constant coefficient of friction (Harris and Day 1997). Here we see the need for experimental analysis because experimental results can be used to judge the physical relevance of various friction laws and to validate various proposed numerical methodologies. It should be emphasized at this point that the goal of some of the early theoretical and numerical studies (Weertman 1980; Adams 1995; Andrews and Ben-Zion 1997; Adams 1998; Cochard and Rice 2000; Ranjith and Rice 2001) was to investigate what kind of unstable slip would develop on a surface which, as judged from conventional friction notions, was superficially stable, in the sense that its friction coefficient, f, did not decrease, or vary otherwise, with slip and/or slip rate. For most brittle solids, however, ample evidence exists that, f does decrease with increase of slip and/or slip rate (or, more fundamentally, f varies with slip rate and contact state). As a result, a proper model for natural faulting along a bimaterial interface should include both a weakening of f and the slip-normal stress coupling effects of the bimaterial situation. Indeed such a

weakening model was included by Harris and Day (Harris and Day 1997). Given the above, it would be an invalid interpretation of the results of the earlier set of papers (Weertman 1980; Adams 1995; Andrews and Ben-Zion 1997; Adams 1998; Cochard and Rice 2000; Ranjith and Rice 2001) to conclude that the rupture (including preference for specific rupture mode) scenarios which they predict constitute the full set of scenarios available to a real earthquake, of which f decreases with increasing slip and/or slip rate. The consistently bilateral nature of rupture predicted by Harris and Day (Harris and Day 1997) is perhaps an indication of the effect of including a slip weakening frictional law in their calculations.

3.3 Experimental Set-up

Our experiments examine the effect of material contrast on the rupture growth of spontaneously nucleated dynamic rupture event hosted by inhomogeneous, frictional interfaces. These interfaces are held together by static, far-field pressure-shear simulating natural tectonic loads. The experiments mimic natural earthquake rupture processes in fault systems, where bimaterial contrast between intact rock masses seldom featured more than a 35% difference in shear wave speeds (Rice 2001).

The experimental set-up is very similar to that described in chapter 1 and subsequently used in our previous study of rupture in homogeneous interfaces (chapter 2). This configuration has proven to be very effective in producing accurate, full-field, and real-time information of generic rupture characteristics that can ultimately be related to the rupture behavior of natural fault systems.

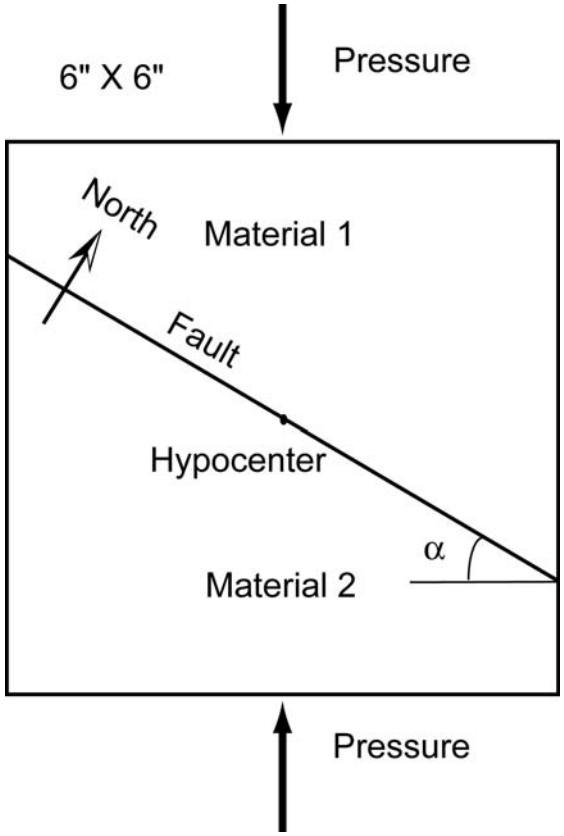

Figure 3.1 Laboratory earthquake fault model composed of two photoelastic plates of the same geometry.

The laboratory fault model is shown in Figure 3.1. The figure shows a Homalite-100 plate (material 1, top) and a polycarbonate plate (material 2, bottom) that are held together by far-field load, P. The higher wave speed material at the top (Homalite-100) has a shear wave speed C_S^1 = 1,200 m/s and a longitudinal wave speed C_P^1 =2,498 m/s. The lower wave speed material at the bottom (Polycarbonate) has a shear wave speed C_S^2 =960 m/s and a longitudinal wave speed C_P^2 =2,182 m/s. The fault is simulated by a frictionally held contact interface forming an angle to the applied load that is varied to mimic a wide range of tectonic load conditions. Spontaneous rupture is

triggered at the hypocenter through the exploding wire mechanism described in chapter 1. The static compressive load P is applied through a hydraulic press. By arbitrary convention, the fault line runs in the east-west direction with the lower wave speed solid located at the south side. As viewed from the camera, a rupture will produce right lateral slip. We use specimens with different roughness in our experiments; we denote one as smooth (roughness is 17 μm) and the other as rough (roughness is 25 μm).

The ratio of shear wave speeds, C_S^1 / C_S^2=1.25, is chosen to be within the naturally occurring bimaterial range so that the interfacial phenomena can be applied to the field observations. In particular, the bimaterial difference is big enough to allow for a high enough growth rate of sliding instabilities and to permit us to clearly distinguish between various wave speeds. Within roughly the same range generalized Rayleigh waves exist as well. The shear wave speeds are directly measured for each material by following the shear wave fronts through high-speed photography and photoelasticity. Photoelasticity, being sensitive to maximum shear stress fields, is perfectly suited for measuring shear wave speeds and for scrutinizing shear-dominated rupture processes in brittle, transparent, and birefringent solids (see discussion in chapter 2). The listed P wave speeds are calculated by using measured values of Poisson's ratios (ν^1 = 0.35, ν^2 =0.38) and by using the listed shear wave speeds. An independent measurement of the P-wave speeds in the plates using ultrasonic transducers has confirmed these listed values to within 5%. The value of C_{GR} can be determined from the equation: $f(V) = (1-b_1^2)a_1 G_2 D_2 + (1-b_2^2)a_2 G_1 D_1 = 0$, where $a_n = \sqrt{1 - V^2/(C_P^n)^2}$, $b_n = \sqrt{1 - V^2/(C_S^n)^2}$, $D_n = 4a_n b_n - (1+b_n^2)^2$, V is the rupture speed, G_n are rigidities of materials, and n=1,2. Substituting the material constants for Homalite-100 and Poly Carbonate into the equation, we get C_{GR}=

0.959 km/s., a value that is extremely close to the shear wave speed of Polycarbonate[1].

3.4 Experimental Results

The dynamic rupture is triggered by means of the exploding wire mechanism, which simulates a localized pressure release at the desired location of the simulated hypocenter. This mechanism has been described in detail in our previous work on rupture of homogenous interfaces (Chapter 2). Experimentally, it is a convenient way of triggering the system's high speed diagnostics. More than 30 experiments featuring different angles, α (20º, 22.5º and 25º), and far-field loading, P (10-18 MPa), were performed and the rupture events were repeatedly visualized in intervals of 3 μs by a digital high speed camera system used in conjunction with dynamic photoelasticity. The higher level of angles was limited by the static frictional characteristics of the interface. Depending on P and on α, three distinct and repeatable rupture behaviors were observed. In all cases, the two separate, semi-circular traces of the shear waves in the two materials were clearly visible as discontinuities in the maximum shear stress field. The ruptures were always bilateral and became progressively asymmetric with time, within the time window of all experiments.

---

[1] As discussed by Rice (Rice 2001), a generalized Rayleigh wave corresponds to frictionless sliding at the interface between two modestly different dissimilar solids, with no opening at the interface. The generalized Rayleigh wave speed, C_{GR}, is the real root of the scalar equation described in section 3.3 and has the properties: $\min(C_R^1, C_R^2) < C_{GR} < \max(C_R^1, C_R^2)$; $C_{GR} < C_S^2 < C_S^1$

In our case, these inequalities become:

$902 \text{ m/s} < C_{GR} < 1,122 \text{ m/s}$, $C_{GR} < 960 \text{ m/s} < 1,200 \text{ m/s}\}$

3.4.1 Case-1, GR Rupture and Sub-shear Rupture

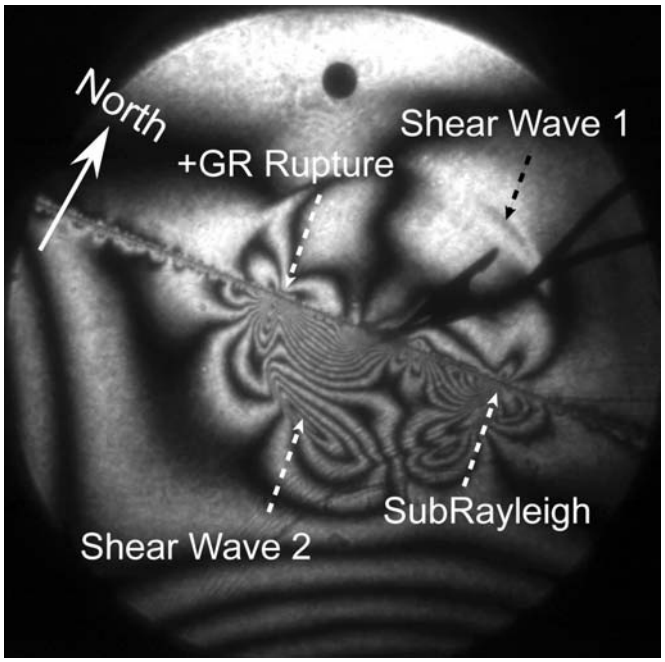

Figure 3.2 The photoelastic patterns for an experiment with α =22.5, P=17 MPa, and smooth surface. Both ruptures to the east and the west are sub-shear. (Case 1)

As shown in Figure 3.2, two distinct rupture tips, one moving to the west and the other moving to the east, with velocities V^E and V^W respectively, are identified by a distinct concentration of fringe lines. For this case (case-1), both tips are seen to propagate at sub-shear velocities $V^E < V^W < C_S^2 < C_S^1$. Differentiation of the rupture length-time histories, obtained from a series of high speed images, allows for the estimation of the rupture velocity histories. On one hand, the rupture moving to the west is the one propagating in the direction of sliding of the lower wave speed material (positive direction). Within experimental error this rupture is found to grow at a constant velocity equal to the speed of the generalized Rayleigh waves (V^W = 950 m/s $\approx +C_{GR}$).

The rupture moving to the east, on the other hand, is the one propagating in the direction opposite to that of sliding in the lower wave speed material (opposite direction). This rupture grows at an almost constant subRayleigh velocity of $V^E = -900$ m/s, which is clearly slower than the Rayleigh wave speed, C_R^2, of the slower wave speed material. The observations were very similar for smaller angles, α, and compressive loads, P, as well. The rupture to the west (positive direction) always propagated with $V^W \approx +C_{GR}$. The rupture to the east remained subRayleigh ($V^E < C_R^1 < C_R^2$). However, its velocity varied continuously across experiments with different load levels and angles. In particular, smaller angles of α (or smaller values of the s factor described in chapter 1) and lower P resulted in V^E being lower fractions of C_R^2. Judging from the number of near-tip fringes per unit area, the eastward moving rupture resulted in a visibly smaller level of stress drop than the one moving to the west.

3.4.2 Case-2, GR Rupture and Supershear Rupture

A very distinct but equally repeatable rupture case (case-2) was observed for higher values of α and P. These conditions correspond to higher values of driving stress or to conditions closer to incipient uniform sliding of the entire interface (smaller values of s). A typical example corresponding to α =25° and P =17 MPa is shown in Figure 3.3. In this case the rupture is still bilateral with a westward tip trailing behind both shear wave traces. This tip moves at a constant velocity $V^W \approx +C_{GR}$ along the "positive" direction. This observation is identical to the situation described above in relation to lower values α and P. The eastward moving tip however is clearly different from the previously described case. Its tip is moving with a velocity faster than both the shear wave speeds. Moreover, its structure, shown in detail in the upper insert of Figure

3.3, is distinctly different to the structure of the subRayleigh, westward moving rupture shown in the lower insert.

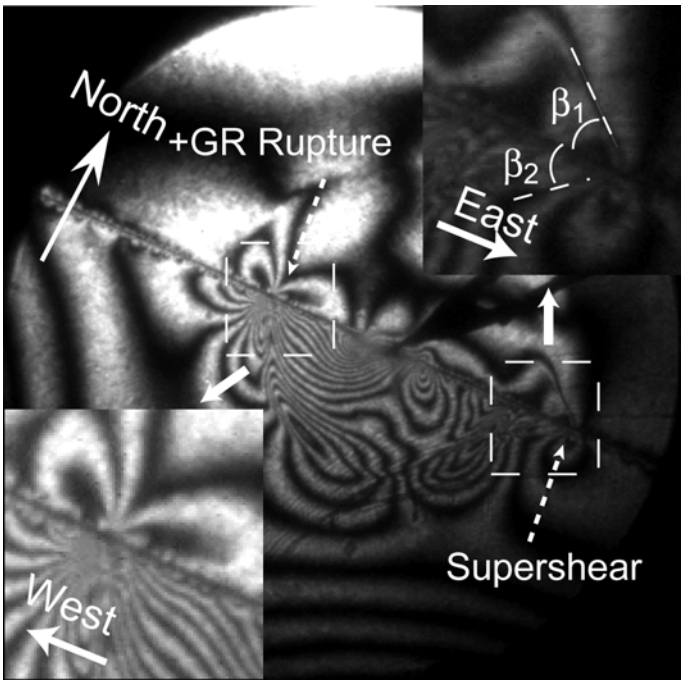

Figure 3.3. For α =25º, P =17 MPa, and smooth surface finish the bilateral rupture features two distinct tips. The one moving to the west (positive direction) has a velocity $V^W = +C_{GR}$, while the one moving to the east (opposite direction) is supershear. (Case-2)

As conclusive proof of its supershear velocity, two distinct shear shock waves are clearly visible. The magnitude of the velocity of the eastward rupture $|V^E|$ is 1920 m/s, which is approximately 12% less than the P-wave speed, C_P^2, of the lower wave speed material. $|V^E|$ is also equal to $1.6\,C_S^1$, or is slightly higher than $\sqrt{2}$ times the shear wave speed of the faster wave speed material. The upper insert in Figure 3.3 shows two clear lines of discontinuity in the maximum shear contours of photoelasticity. Each of these lines (shear shock

waves) is located at two different angles β_1 =41° and β_2 =30°, to the North and to the South of the fault respectively. The two angles β_n (n= 1, 2) are related to the shear wave speeds C_S^n and to the rupture velocity V^E, by $\beta_n = \sin^{-1}(V^E/C_S^n)$. This relation provides independent means of estimating V^E from each individual frame of the high speed camera record without reliance on the less accurate rupture length history. Both methods yield consistent values of V^E =−1920 m/s.

Both cases described above feature westward moving ruptures that are of the "+GR" type. Irrespective of the values of α and P, these ruptures have a constant speed $V^W \approx +C_{GR}$, and they propagate in the "positive" direction. However, those two cases also feature eastward ruptures that are distinctly different in nature. For sufficiently low P and α (or large s), the eastward ruptures, which propagate in the opposite direction, are purely subRayleigh within the time window of our experiments. For large enough P and α however, eastward ruptures propagate in the opposite direction with a constant supershear velocity, which is slightly less than C_P^2 and are thus of the "$-P_{SLOW}$" type.

3.4.3 Case-3, GR Rupture and Sub-shear to Supershear Rupture Transition

To visualize an intermediate situation and a controlled transition from one case to the other within the field of view, P was reduced to 13 MPa (Figure 3.4, A and B). For this case (case-3), figure 3.4 shows a smooth transition from case-1 to case-2 within the same experiment. While the westward rupture remains of the "+GR" type throughout the experiment, the eastward rupture jumps from a constant subRayleigh velocity (−910 m/s) to a constant supershear velocity (−1,920 m/s), and thus transitions to the "$-P_{SLOW}$" type. The rupture length

plot of Figure 3.5 also shows the abrupt transition of the eastward rupture from a subRayleigh velocity to a velocity slightly less than C_P^2. This happens at a transition length, L, which is approximately equal to 25 mm. However, the westward rupture retains its constant $+C_{GR}$ velocity throughout the experiment.

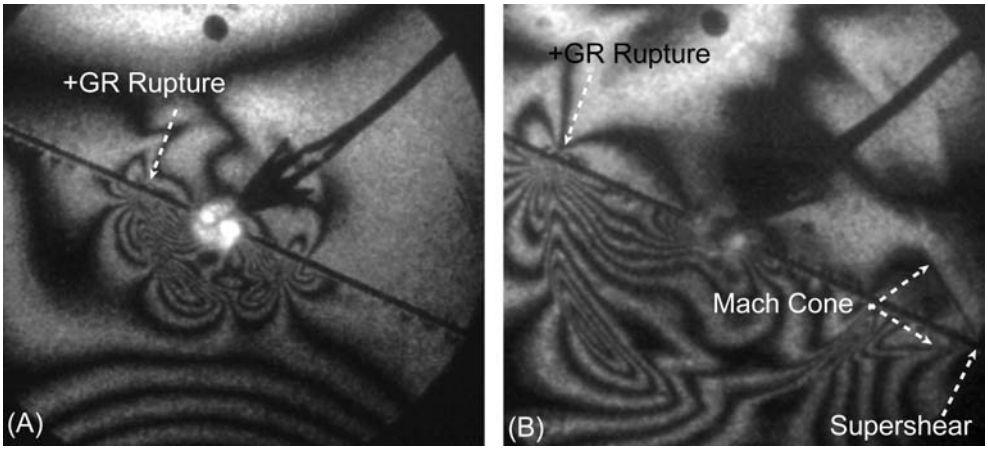

Figure 3.4. Experimental results for α =25º, P =13 MPa, and rough surface showing transition of the eastward moving rupture to supershear. The westward rupture retains a constant velocity $V^W=+C_{GR}$. (Case-3)

The eastward transition behavior of case-3 is qualitatively similar to the one we have discussed (chapter 2) in relation to homogeneous interfaces, while the transition length, L, is also a decreasing function of α and P. Most important to the discussion of the present paper is the observation that the ruptures that propagate to the opposite direction require a certain minimum rupture length before they become supershear. This observation provides a clear intuitive link between super shear growth in the "opposite" direction and large earthquakes. In contrast, no such transition was observed for "positively" growing "+GR"

ruptures irrespective of α, P, and rupture length. As a result, the experiments do not provide an obvious link between "positively" growing ruptures and large earthquakes.

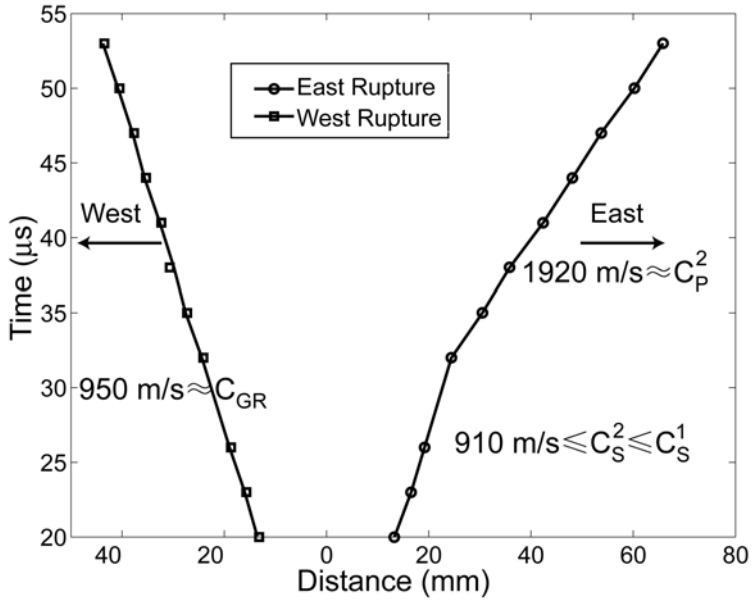

Figure 3.5. Rupture length plot of an experiment for α =25º, P =13 MPa, and rough surface finish.

3.4.4 The Dependence of Transition Length on P

In chapter 2, we have discussed the dependence of the transition length L on the uniaxial pressure P. In the homogeneous case there is a very well defined point for transition, while in the inhomogeneous case the transition point is not always so clear. This difference again is due to the presence of a material contrast. In the homogeneous case, there is an energetically forbidden velocity zone between C_R and C_S ; as a result, the secondary crack is initiated exactly at the shear wave front. In contrast for inhomogeneous faults, the forbidden zone no longer exists and the subshear crack in the opposite direction accelerates to the supershear speed in a smoother way (Figure 3.5). Nevertheless, on occasions we can still

define the transition length where the speed change occurs. The plot of transition length L is in Figure 3.6. L has a weaker dependence on P ($L \sim P^{-0.4}$) than the homogeneous case ($L \sim P^{-1.5}$). This is expected because for the inhomogeneous case, the coupling between the slip and the normal traction causes a dynamic compression locally and thus increases the resistance to the slip locally in the negative direction. On the other hand, the shear traction driving the rupture is constant and hence it takes longer slip to for a crack to reach the supershear velocity.

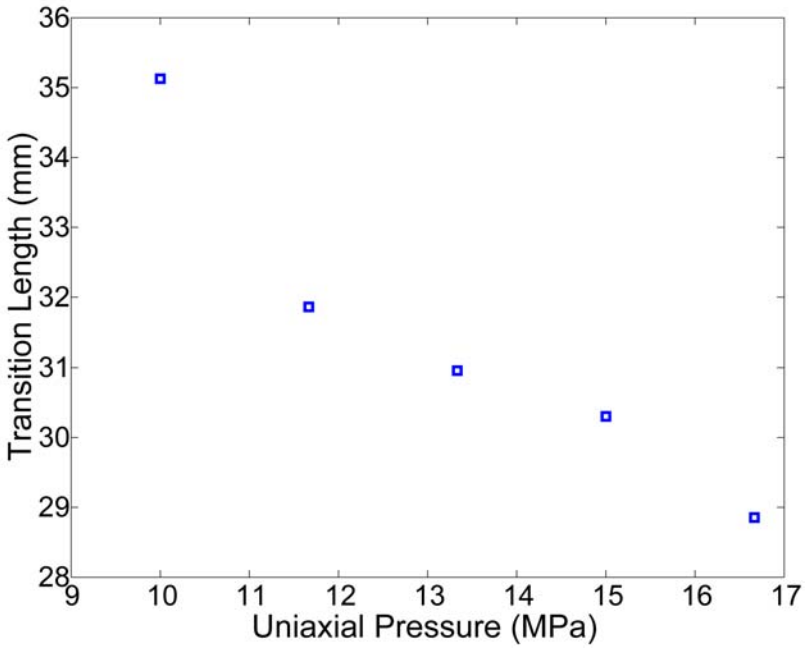

Figure 3.6. Transition length as a function of pressure P for experiments with α=25° and rough surface finish.

We list all the experimental results in Table 3.1. The transition happens only at angle α=25°. For smooth surface, when the angle is smaller than 25°, no transition is achieved within our field of view. For rough surface however, angles smaller than 25° result in no rupture at all.

Table 3.1 Summary of Experimental Results

Surface	Angle α (°)	P (MPa)	West Rupt.	East Rupt.[2]
Smooth	20	10	$\sim C_{GR}$	$\sim C_R^2$
Smooth	20	13	$\sim C_{GR}$	$\sim C_R^2$
Smooth	20	17	$\sim C_{GR}$	$\sim C_R^2$
Smooth	22.5	10	$\sim C_{GR}$	$\sim C_R^2$
Smooth	22.5	13	$\sim C_{GR}$	$\sim C_R^2$
Smooth	22.5	17	$\sim C_{GR}$	$\sim C_R^2$
Smooth	25	10	$\sim C_{GR}$	$\sim C_S^2, \sim C_P^2$
Smooth	25	13	$\sim C_{GR}$	$\sim C_S^2, \sim C_P^2$
Smooth	25	17	$\sim C_{GR}$	$\sim C_S^2, \sim C_P^2$
Rough	25	10	$\sim C_{GR}$	$\sim C_S^2, \sim C_P^2$
Rough	25	12	$\sim C_{GR}$	$\sim C_S^2, \sim C_P^2$
Rough	25	13	$\sim C_{GR}$	$\sim C_R^2, \sim C_P^2$
Rough	25	15	$\sim C_{GR}$	$\sim C_S^2, \sim C_P^2$
Rough	25	17	$\sim C_{GR}$	$\sim C_S^2, \sim C_P^2$

3.5 Comparison of the Experimental Results to Existing Numerical and Theoretical Studies

The experiments described above provide the first full-field and real-time visualization of dynamic frictional rupture events occurring along inhomogeneous interfaces, which feature low wave speed mismatch such that the generalized Rayleigh wave speed can be defined. While it is very difficult to access whether the ruptures are pulse-like, crack-like, or a mixture of the two, the observations confirm the existence of two distinct self-sustained and constant speed rupture modes. These are very similar to the ones that have been theoretically and numerically predicted over the recent years (Weertman 1980; Andrews and Ben-Zion 1997; Cochard and Rice 2000; Ben-Zion 2001;

[2] The east rupture may experience sub-shear to supershear transition. In this case, there are two velocities listed: one before the transition and the other after the transition.

Rice 2001; Ben-Zion and Huang 2002). In particular, a "+GR" type of rupture mode is always excited instantaneously along the "positive" direction of sliding. Furthermore, a "$-P_{SLOW}$" mode is observed as long as the rupture propagating in the "opposite" direction is allowed to grow to sufficiently long distances from the hypocenter. The triggering of the "$-P_{SLOW}$" mode is always preceded by a purely subRayleigh, crack-like rupture whose velocity depends on loading, on geometry , and on the bimaterial characteristics. Therefore, the existence of this preliminary and apparently transient stage is one of the main differences with the numerical predictions (Andrews and Ben-Zion 1997; Harris and Day 1997; Cochard and Rice 2000). However, its existence does not contradict early theoretical studies (Adams 2001; Ranjith and Rice 2001), which only predict self-sustained stable rupture events whose constant velocities relate to the wave speeds of the bimaterial system.

A far more striking difference to some of the numerical predictions (Andrews and Ben-Zion 1997; Cochard and Rice 2000; Ben-Zion and Huang 2002), is the consistent experimental observation of bilateral slip. In contrast to the experiments, the above numerical predictions seem capable only of exciting one or the other of the two self-sustained rupture modes (Cochard and Rice 2000), giving rise to purely unilateral rupture events. They also seem to primarily favor the triggering of the "+GR" mode in low wave speed mismatch bimaterial systems (Andrews and Ben-Zion 1997). This kind of preference has led to the labeling of the "positive" direction as the "favored" rupture direction and of $+C_{GR}$ as the "favored" rupture velocity. These numerical results directly support the closely related notion of ruptured directionality (McGuire, Zhao, et al. 2002). A notable exception to this rule is provided by the early numerical analysis by Harris and Day (Harris and Day 1997), which consistently reports asymmetric bilateral rupture growth in a variety of low speed contrast, in-

homogeneous fault systems. These results are qualitatively very similar to the experimental observations of cases 1 and 2. However, no transition is reported. As briefly discussed by Cochard and Rice (Cochard and Rice 2000), the excitement of various modes or their combinations, may possibly be related to the details of the numerically or experimentally implemented triggering mechanisms. In an attempt to further reconcile the observed differences between various models and the experiments we note that unstable slip rupture propagation has also been observed (Xia, Rosakis, et al. 2004) on Homalite/Homalite and Polycarbonate/Polycarbonate interfaces. Such unstable rupture growth would be possible only if there was a reduction of the friction coefficient with slip and/or slip rate, and hence such reduction must be a property of both materials when sliding against each other. It is then plausible to assume that a similar reduction of friction coefficient occurs along the Homalite/Polycarbonate interface, and to thus infer that its rupture behavior should not be expected to fully correspond to the idealized models of a dissimilar material interface with constant coefficient of friction (Weertman 1980; Adams 1995; Andrews and Ben-Zion 1997; Adams 1998; Cochard and Rice 2000; Ranjith and Rice 2001).

The present experiments neither support exclusivity nor show a strong preference for rupture direction. Although they support the idea that frictional ruptures that grow in the positive direction and will always do so at a specific constant velocity ($V = +C_{GR}$), they still allow for a significant possibility of self-sustained supershear ruptures growing in the opposite direction. This possibility becomes significant, provided that their transient, subRayleigh, (remove comma) precursors grow for a large enough length and are not arrested prior to transitioning to supershear. The requirement of a critical transition length along the "opposite" direction provides a link between large

earthquakes and the occurrence of self-sustained supershear rupture in the "opposite" direction. One perhaps can contemplate the existence of a weak statistical preference for positively growing ruptures, since this link to large earthquakes is absent for "+GR" ruptures.

3.6 Explanation of Earthquake Series on North Anatolian Fault Using the Experimental Results

The 1999, M7.4, Izmit earthquake in Turkey is perhaps a prime example of a recent large earthquake event for which both modes of self-sustained rupture may have been simultaneously present, as is the case in our experiments. The event featured right-lateral slip and bilateral rupture of a rather straight strike-slip segment of the North Anatolian Fault. As reported by Bouchon, et al. (Bouchon, Bouin, et al. 2001), the westward propagating side of the rupture grew with a velocity close to the Rayleigh wave speed, while the eastward moving rupture grew at a supershear velocity that was slightly above the $\sqrt{2}$ times the shear wave speed of crustal rock. Since the laboratory ruptures of the current paper are intentionally oriented similarly to the Izmit event, a direct comparison with the case described in Figure 3.3 becomes possible and it reveals some striking similarities. In addition to featuring right lateral slip and asymmetric bilateral rupture, this case (case-2) featured a subshear westward rupture propagating at $+C_{GR}$. To the east however, the rupture propagated at a velocity slightly lower than C_P^2, which also happens to be equal to $1.6\,C_S^1$ for the particular bimaterial contrast of the experiments. If one interprets the Izmit event as occurring in an inhomogeneous fault with the lower wave speed material being situated at the southern side of the fault (as is in the experiment), the field observations and the experimental measurements of both rupture directions and velocities are very consistent. Moreover, when the bimaterial

contrast is low enough, the differences between C_{GR} and the average of the two Rayleigh wave speeds, $(C_R^1 + C_R^2)/2$, as well as the difference between $1.6\,C_S^1$ and $\sqrt{2}\,(C_S^1 + C_S^2)/2$ would be small enough not to be discriminated by the inversion process, even if the fault geology was completely known. In this respect, the agreement with experiment is as good as it can ever be expected. In addition, viewing the fault as inhomogeneous can explain the choice of direction for both the subRayleigh and the supershear branches respectively. This choice of rupture direction is consistent with both the present experiments and with the theory reviewed in the introduction (Weertman 1980; Adams 2001; Ranjith and Rice 2001).

The 1999 Düzce earthquake can also be interpreted through a similar line of argument used for Izmit. The Düzce rupture also featured right lateral slip (as did all events that occurred in the North Anatolian fault between 1939 and 1999) and it extended the Izmit rupture zone 40 km eastward through asymmetric bilateral slip (Bouchon, Bouin, et al. 2001). Thus similar to the Izmit earthquake, numerical modeling by Bouchon, et al. (Bouchon, Bouin, et al. 2001) indicates subRayleigh westward and supershear eastward rupture fronts. As a result the direct comparison with case-2 described in Figure 3.3 provides an explanation for the two rupture directions and respective velocities, similar to the one given for Izmit. This explanation is of course plausible only if one assumes, once again, that the material to the south of the North Anatolian fault (at its western end) is the lower wave speed solid.

By using similar arguments to the ones used for Izmit and Düzce one can perhaps provide a unified rationalization of the seemingly random rupture directions and rupture velocities of the interrelated series of earthquakes that

occurred since 1939 along the North Anatolian fault and ended in 1999 with the Izmit and Düzce events. The following argument requires the assumption that, in average and along its entire length, the North Anatolian fault features the same type of bimaterial in-homogeneity as the one that has been summarized for Izmit and Düzce. However, rather limited evidence supporting such an assumption is currently available (Zor, Sandvol, et al. 2003). If in some average sense this is true, one would expect that the slight majority (60%) of the large (M≥6.8) earthquake events [i.e., (1939-M7.9), (1942-M6.9), (1944-M7.5), (1951-M6.8), (1957-M6.8), (1967-M7.0)], which featured westward growing ruptures, were probably of the "+GR" type. In other words, this assumption implies that they were classical subRayleigh ruptures that moved with velocity equal to $+C_{GR}$ in the "positive" direction. The remaining ruptures of the series were "irregular" in the sense that they featured dominant eastward growth. As previously detailed, out of the remaining four ruptures of the series, the Izmit and Düzce events were bilateral with a western branch of the "+GR" type (consistent with the others) and an eastward, super-shear branch of the "$-P_{SLOW}$" type. The 1943 and 1949 ruptures were purely unidirectional and eastward moving; however, their rupture velocities are not known. If these ruptures are to be consistent with the remaining events in the sequence, as they have previously been experimentally, then they could also have developed as the "$-P_{SLOW}$" type. This possibility is more likely for the 1943 event that featured over 250km of growth length. As estimated in Chapter 2, this length is much larger than the critical length required for transition to supershear. By observing that the 1943 and the two 1999 (Izmit and Düzce) events were of a higher magnitude than most of the other events of the complete series, as reported by Stein, et al (Stein, Barka, et al. 1997), further supports the assertion that at least three out of four "irregular" events featured partial or total supershear growth along the "opposite" (eastward) direction. The basic support

for this assertion is provided by the experimentally established link between large earthquakes and supershear ruptures growing in the "opposite" direction, and is consistent with the direct evidence of supershear from the two most recent "irregular" events of 1999.

Finally, it should be noted that if earthquakes of lesser magnitude (in the range between M6.4-6.8) are also included in the discussion, the North Anatolian Fault series will feature a weak preference for western propagation. This is not very surprising given the above discussed link between large earthquakes and self-sustained supershear along the opposite direction, a link that does not exist for "positive" (westward growing) "+GR" ruptures. Indeed, in addition to the actual number of ruptures that grew to the east or west, what is of importance here is the actual growth lengths. The results reported by Stein, et al. (Stein, Barka, et al. 1997) show that the total length of westward growth is slightly higher than that of eastward growth. This is again consistent with experiments that show that the self-sustained "+GR" mode is always and instantaneously present after nucleation. In contrast, the self-sustained "$-P_{SLOW}$" mode is often preceded by an unstable sub-shear phase. For smaller earthquakes this unstable phase may never transition to supershear and instead it may be arrested. This in turn would result in a total eastward rupture length, which is slightly shorter than the total western rupture length of the earthquake series.

3.7 Discussions and Conclusions

To investigate the effect of material contrast on the earthquake faulting process, we adopted a fault model made up of two different photoelastic polymer plates. Using the similar experimental design, as we described in chapter 1 and chapter 2, we are able to trigger and observe the dynamic process of earthquake rupturing.

Our results can be summarized as follows: ruptures were always bilateral. In the positive direction the rupture tip propagated at the generalized Rayleigh wave speed, while in the negative direction the rupture tip propagated either at the sub-Rayleigh or at a speed very close to the P wave speed of the slower wave speed solids. In certain cases, a transition from subRayleigh to supershear was documented. Such a transition was only found to occur for the rupture tip growing along the negative direction and has provided a clear link between "negatively" growing ruptures and large earthquakes. Our experimental observations have allowed us to provide a critical appraisal of existing theoretical and numerical results and a unified view of the possible modes of frictional rupture.

Since the inhomogeneous faults are possible in reality, this unified view is very important in the explanation of seemingly "irregular" earthquakes. As an example, we demonstrated how this theory explains observations of the historic sequence of migrating earthquakes along North Anatolian fault.

Chapter 4

Earthquake Rupturing Processes along Faults with a Finite Fault Core (Low-Velocity Zone)

So far, we have exclusively discussed and studied the earthquake faulting process that occurs along a fault with the simplest geometries, i.e., faults that are ideally mathematical straight lines without any internal geometrical structure or strength inhomogeneities. Such an ideal fault can't be found in the real world; instead, one can only define a so-called fault zone with following characteristics: within the fault zone, there is a fault core made up of heavily damaged material with slower wave speeds than that of the host rock, and the thickness of the fault core is about several centimeters. The fault zone is an area of accumulated damage resulting from repeated rupture events through ages.

The existence of a fault core may have a profound influence on the earthquake rupturing process. The fault core thickness provides an intrinsic length scale. This length scale may be related to the pulse width of a pulse-like rupture and may lead to a new mechanism for the pulse mode earthquake faulting in addition to the already proposed mechanisms, including special friction law, material contrast, and inhomogeneity distribution in fault strength (e.g.,, barriers and asperities).

In this chapter, we will systematically examine the effect of a fault core or a finite low-velocity zone on earthquake faulting. We use a set up similar to the one described in detail in Chapter 1. We vary the width of the fault core, the

level of the far field loading, and the inclination angle. The purpose of this chapter is to explore the spectrum of possible rupture velocities and to identify the various modes of rupturing (i.e., crack mode vs. pulse mode) that may occur for faults with a finite core.

4.1 Introduction

It may be too simple to assume that faults are mathematical straight lines without structure, as we did in previous chapters. There are two natural ways to increase the geometrical complexity of the problem. One way is to consider the real two dimensional structure of the fault zone, which is not a straight line of zero width. Another way is to keep the mathematical line feature of the fault, but to allow it to be non-straight. There are a few interesting phenomena that may be triggered by such geometric complexities. These include the development of pulse-like mode of rupturing, and the phenomenon of fault geometry induced arrest of rupture. In this chapter, we will concentrate on the earthquake ruptures occurring along faults with a finite fault core.

According to geological and geophysical observations, the fault zone can be divided into several layers (Ben-Zion and Sammis 2003). From inside out, these are fault core, the adjacent tabular damaged zone, and the surrounding host rock. The two interfaces of the fault core and the tabular damaged zone are called the primary and the secondary slip surfaces. The dimension of the tabular damaged zone is 100's of meters while the dimension of the fault core is not larger than 10's of centimeters. The primary and secondary slip surfaces are a few millimeters of thickness (Chester and Chester 1998; Sibson 2003). One important observation here is that the ratio of the thickness of the fault core to the thickness of the primary slip surface is about 100. Usually, researchers

simplify the structure of the fault zone to a fault core made up of low-velocity material bounded by host rock.

The problem of rupturing along a fault with a finite fault core, or low-velocity zone was numerically studied by Harris and Day by using the standard slip weakening law (Ida 1972; Palmer and Rice 1973), and later by Ben-Zion and Huang using a modified Prakash-Clifton friction law with a constant coefficient of friction (Prakash 1995; Prakash 1998) (Harris and Day 1997; Ben-Zion and Huang 2002). Harris and Day considered the following cases: 1. a fault separating the infinite host rock and low-velocity zone with infinite width (This corresponds to the bimaterial problem considered in the Chapter 3), 2. a fault line bisecting the finite width low-velocity zone that is imbedded within infinite host rock, and 3. a fault separating along one of the two interfaces of the infinite host rock and a low-velocity zone of finite width (Harris and Day 1997). The last configuration is the problem of interest. This reflects our belief that this configuration better resembles what happens in a real fault system. Indeed, based on fracture mechanics theory (Hutchinson and Suo 1992) shear ruptures in layer systems tend to propagate along the material interface.

Harris and Day considered cases where the width of the low-velocity zone (LVD) varied from 200 to 1000 m. Two sets of LVZ characteristic wave speeds were considered (C_P = 5.00 km/s, C_S = 2.89 km/s and C_P = 4.00 km/s, C_S = 2.31 km/s). The characteristic wave speeds of the host rock were taken to be C_P = 6.00 km/s and C_S = 3.46 km/s. Using the generalized Rayleigh wave equation discussed in Chapter 3, we find that for the former case, the GR wave speed is very close to the shear wave speed of the fault core material (C_{GR} = 2.845 km/s); while for the latter case, the GR wave speed is not defined. The significance of the existence of GR wave speed for earthquake faulting along

faults separating bimaterial can be found in the literature (Ben-Zion 2001; Ranjith and Rice 2001; Rice, Lapusta, et al. 2001) and has been discussed in Chapter 3. The mesh size used was equal to 50 m.

Interestingly enough, if we take the dimension of the mesh size as the primary slip surface width and consider the ratio of the width of the low-velocity zone to this dimension, we reached values around 100, which are expected from the field observations. This observation gives us confidence in the similarity of the numerical results of this work to real earthquake faulting. Their study concentrated on the identification of attainable rupture velocities and on the observation of rupture directionality in different material combinations and configurations. Let us first denote the ratio of the shear wave speed of the host rock to that of the fault core (low-velocity zone) by r_S. For cases where $r_S = 1.2$ both ruptures propagating in the positive and negative directions do so at a speed close to the shear wave speed of the low-velocity zone; for the cases where $r_S = 1.5$ the positive rupture propagates at a speed slightly faster than the shear wave speed of the low-velocity zone, while the negative rupture can propagate at a supershear speed. Finally it should be noted that Harris and Day did not produce pulse-like ruptures in none of their simulations on faults with a core structure

The work by Ben-Zion and Huang (Ben-Zion and Huang 2002) examined the possibility of developing a self-sustained, wrinkle-like mode pulse (i.e., Heaton pulse) during rupture growth in a tri-layer system composed of two semi infinite pieces of intact rock surrounding a finite width LVZ. Their frictional law is of the Prakash-Clifton type with a const coefficient of static friction. They found that if there is a finite fault core, rupture along one of the two interfaces between the core and the host rock may take the form of a self-sustained pulse. The pulse

strength is modulated by regular oscillations with period proportional to the width of the core and is amplified at a certain range of such widths. This oscillation is also found by Harris and Day (Harris and Day 1997) using the slip-weakening friction law. Ben-Zion and Huang used a mesh size of 0.25 m, while the width of the low-velocity zone to mesh size ratio varies from 20 to 1000 in their simulations. It is interesting to note that they only monitored the rupture propagation in the positive direction. As we discussed in Chapter 3, this is probably due to the choice of frictional law. Indeed if the frictional resistance is not allowed to vary with slip or slip rate, there seems to be a strong preference for positively growing ruptures along bimaterial interfaces. This preference may indeed persist even in the case of rupture growing at either interfaces between a finite width LVZ and the host rock since the rupture tips of such ruptures are locally bimaterial in nature. In this chapter, we will show in our experiments that experimentally observed ruptures are bilateral and a pulse mode may appear only in the negative direction.

A few reasons have been proposed as being responsible for the occurrence of pulse-like rupture modes of rupture. These include the choice of frictional laws, the existence of bimaterial contrast across the fault as well as the existence of fault strength inhomogeneities. Rice and his coworkers suggested that assuming certain frictional law of the slip rate weakening type, pulse-like earthquake faulting is attainable (Zheng and Rice 1998). In addition to the nature of frictional laws, geometrical effects are also thought to govern the occurrence of pulse modes of rupture. In particular some researchers believe (Miyatake 1992; Nielsen, Carlson, et al. 2000) that spatial heterogeneities (e.g., asperity distribution) that are present on fault planes set the local length scale that promotes slip pulse formation and determines slip duration. Finally the existence of bimaterial contrast is a candidate reason for the promotion of pulses. As described by Ben-Zion (Ben-

Zion 2001), the interaction between slip and normal stress allows ruptures to grow in a pulse-like mode under shear stress conditions that are low compared to the nominal frictional strength of the interface. The resulting pulse-like ruptures have properties that are compatible with the inferences of short rise-time earthquake slip (Brune 1970; Heaton 1990; Yomogida and Nakata 1994) and have low levels of frictional heat generation. The experiments proposed here are primarily aimed towards the study of the mechanically triggered rather than the heterogeneity or frictional law caused pulses. Much like the numerical studies of Ben-Zion and Huang and of Harris and Day, our experiments will study the effect of the presence of low velocity zones of various widths.

Although the characteristics of slip pulses have been the subject of recent analytical and numerical activity, these pulses have not been conclusively visualized in a laboratory setting. An exception to this rule may be provided by experimental indications discussed by Brune and his co-workers (Brune, Brown, et al. 1993; Anooshehpoor and Brune 1999). Using their foam rubber model, Brune and Brown, et al. suggested that the pulse-like earthquake faulting is possible even for the homogeneous case. We need to be very careful with these results because of the choice of foam rubber as the model material. The large deformation behavior of this solid makes it an inappropriate models material for processes that is occurring in very stiff crustal rock. In addition, the normal pressure in their experiment was exerted by the weight of the top foam block, and hence the stress was not uniform across the depth. Finally the material properties of the foam are sensitive to pressure and as a result, the fault model is not homogeneous (different properties exist in the tension and compression sides of interfacial shear). For similar reasons caution should be exercised in the interpretation of the results obtained by Anooshehpoor and Brune in which they

claimed that they observed pulse-like earthquake faulting in a bimaterial fault system.

4.2 Experimental Set-up

The schematic drawing of the laboratory fault model with a finite fault core is shown in Figure 4.1.

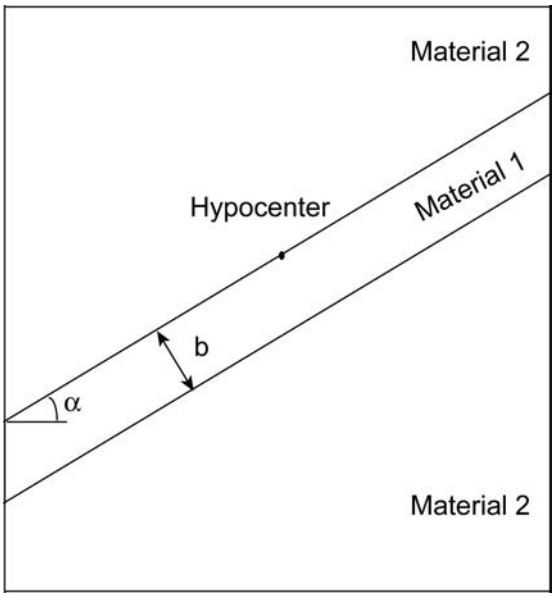

Figure 4.1 The laboratory fault model with a fault core.

The fault core has a width of b and the other two identical plates are cut of a 6" by 6" plate. The out of plane thickness of the composite plate is equal to 3/8". This fault model can be thought as a fault core embedded in infinite host rock because we only record the earthquake rupture process before the waves are reflected back from the specimen boundaries. There are two parallel interfaces formed by the host rock and the fault core, as shown in Figure 4.1; we only trigger rupture in one of them. The sliding interface is referred to as the primary slip zone and the other interface is referred to as the secondary slip zone in real faults (This interface never ruptured during our experiments.). We

use Homalite 100 as the host rock, which is material 2 in Figure 4.1, and Polycarbonate as the fault core, which is material 1 in Figure 4.1. Homalite has a shear wave speed C_S^1 = 1200 m/s and a longitudinal wave speed C_P^1 =2,498 m/s. Polycarbonate has a shear wave speed C_S^2 =960 m/s and a longitudinal wave speed C_P^2 =2,182 m/s. The shear wave speed ratio of Homalite to Polycarbonate is r_S =1.25. This case lies between the two cased studied by Harris and Day and closer to the smaller (r_S=1.2) case. As we have discussed in Chapter 3, the GR wave speed is defined for the material combination of Polycarbonate and Homalite. Hence our experimental results can be compared with the one of then numerically studied cases (r_S=1.2). The width of fault core b ranges from 1/8" to 1/2". The primary slip surface width, which is twice the average asperity height in our case, is around 50 μm. The ratio of the fault core width to the width of the primary slip zone ranges from 63.5 to 254. This range is consistent with field observations.

The loading direction is vertical and the fault core is inclined at an angle α to the horizontal axis. In our experiments, we can vary the loading level, the inclination angle, and the fault core width b. We use the exploding wire technique to trigger the earthquake faulting at the simulated hypocenter location. The details of the principles of the exploding wire technique can be found in Chapter 1. Interestingly, if we trigger the earthquake along one interface, it never jumps to the other one. This may be obvious since the shear waves emitted from the rupture tips are unloading waves as far as the second interface is concerned. Rupture jumping is possible only if we deliberately arrest the faulting on the first interface; the stress will accumulate around the stop location and thus it may be large enough to trigger earthquake faulting in a nearby fault. This is called a dynamic triggering problem (Brodsky, Karakostas,

et al. 2000; Gomberg, Bodin, et al. 2003). Rutpure jumping or dynamic triggering is possible in the real world because there are barriers along the faults and fault systems that are usually made up of several faults in parallel. The jumping happened for the Landers and Hector Mine earthquakes (Wald and Heaton 1994; Ji, Wald, et al. 2002).

4.3 Experimental Results

We vary the angle of inclination α, the magnitude of uniaxial pressure P, and the width of the fault core b in our experiments. In the following, we will present experimental evidence of the occurrence of a pulse mode of rupturing, the effect of varying the fault core width b on faulting, and the effect of the magnitude of far-field loading P on faulting. The experimental results show that for high enough pressure and a high enough angle α, the self-healing pulse-like mode of rupturing is possible in the opposite direction of earthquake rupturing.

4.3.1 The Effect of Fault Core on Faulting and On Wave Propagation Characteristics

In order to qualitatively demonstrate the effect of the presence of a low velocity fault core qualitatively, in Figure 4.2, we show photographs taken from four experiments with the same inclination angle α (17.5°), under the same uniaxial loading (13 MPa), and at the same time instance after triggering for two different types of material configurations.

In specimens to the left (Figure 4.2 A and C) are composed of identical constituents (Polycarbonate host rocks and fault core) while the specimens to the right (Figure 4.2 B and D) are composed of different constituents (Homalite host rock and Polycarbonate fault core). In both cases ruptures are initiated at

one interfaces corresponding to the primary slip interface. Two core widths are shown. The top two (Figure 4.2 A and B) feature a wide (1/2") core while in the bottom two (Figure 4.2 C and D) the core is half that width.

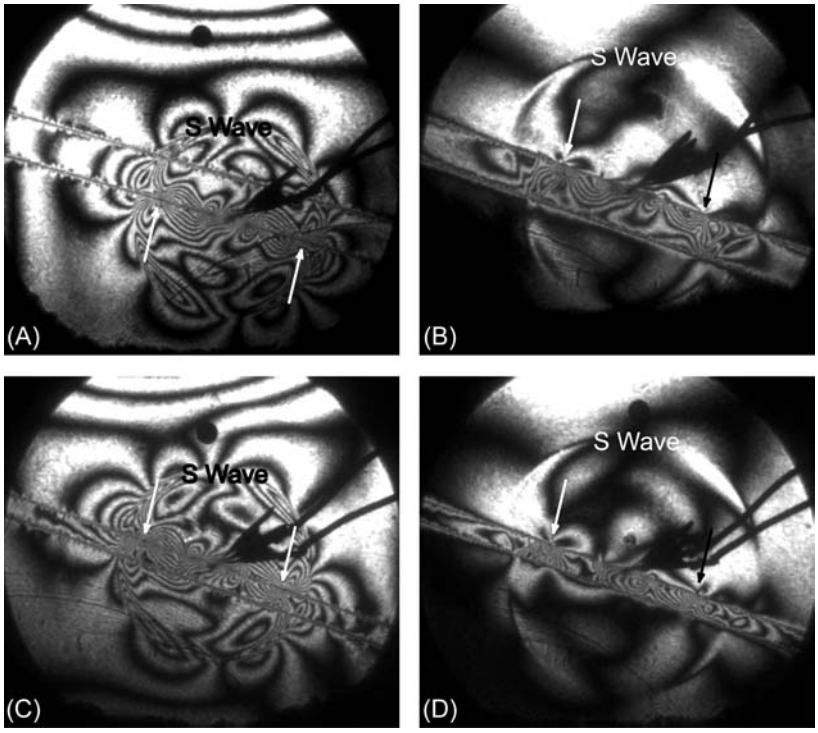

Figure 4.2 Photographs taken at the same time instant after the triggering for experiments with and without fault core. Arrows indicate rupture tips. (P=13 MPa and angle α=17.5°)

In Figures 4.2A and C there are no material contrast across the fault. We can easily identify two ruptures propagating bilaterally along the interface where the hypocenter is located for each case. The earthquake ruptures and the emitted waves are symmetric. The rupture propagated at a speed very close the Rayleigh wave speed. It is interesting to note that the other interface for each case has no visible effect on the rupturing process within the resolution of the

diagnostics method. In Figures 4.2B and D we can see that the shear wave fronts above and below the fault core feature different radii and the patterns unlike the previous case, lose their radial symmetry. The shear wave front in the lower Homalite plate is delayed by the low-velocity zone or fault core made of Polycarbonate. In these two cases the rupture velocities are close to the Rayleigh wave speed of Polycarbonate. In Figure 4.2B we can also identify the "head" waves inside the fault core connecting the two shear wave fronts in the host rock. This head wave is not clear in Figure 4.2D due to the limitation of the spatial resolution of the diagnostics method.

4.3.2 Visualizing Crack-like and Pulse-like Ruptures

In this section we present the first evidence of the creation of pulse-like ruptures in fault systems with a finite fault core. Here we concentrate on specimens composed of Homalite plates (host rock) and Polycarbonate cores of two different widths (1/2" and 1/4"). In what we will see follow the problems geometrical (α, b) and load (P) parameters will be changed and the resulting rupture modes (crack-like or pulse-like) will be contrasted. In the following figures, we indicate the shear wave fronts and the rupture tips by using white arrows. Figure 4.3 contrasts two otherwise identical cases (P=17 MPa, b=1/4") featuring two different angles (α=22.5º for A and α=25º for B). In Figure 4.3 A we see two distinct rupture tips, indicated by the single arrows, propagating to the right (negative direction) and to the left (positive direction) of the hypocenter. As the angle is increased to 25º, the rupture to the right (negative direction) splits into two parts that are visible through the observation of two points of stress concentration. These points are indicated by the two arrows and growing with speeds close to C_{GR}. Our interpretation of this split is as follows: the front tip separates the domain of sliding and sticking, while the trailing tip separates the domain of sliding and healing. According to this

interpretation these two tips enclose a self-healing, propagating slip pulse, which is reminiscent of a Heaton pulse.

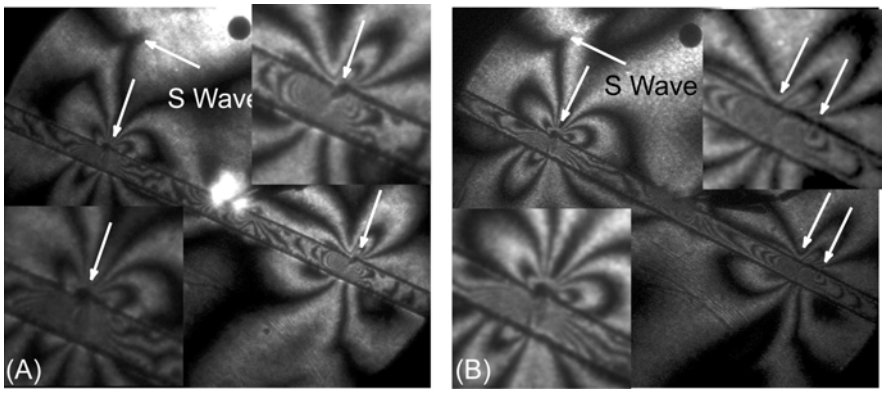

Figure 4.3 Generating a pulse mode through angle increase. Lower insert is the magnification of left rupture tip and upper insert is for the magnification of right rupture tip.

A similar phenomenon is illustrated in Figure 4.4. This figure contrasts two otherwise identical cases (α=25º, b=1/2") that feature two different applied stresses (P=10 MPa for A and P=17 MPa for B). Here again an increase of P results in the creation of a self-healing pulse propagating to the right along the negative direction.

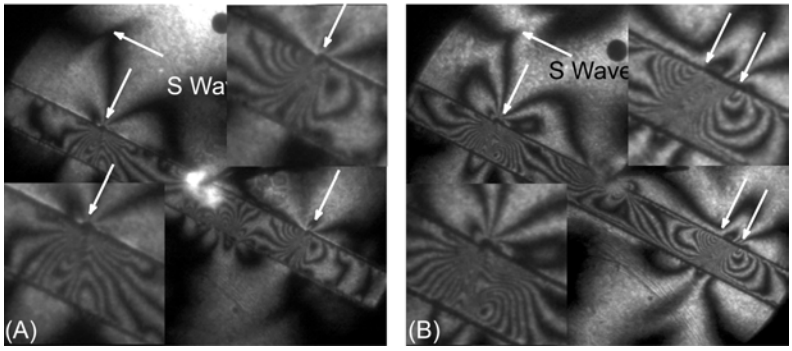

Figure 4.4 Generating a pulse mode through load increase. Lower insert is the magnification of left rupture tip and upper insert is for the magnification of right rupture tip.

It is clear from the above figures that higher angles and pressures facilitate the generation of a pulse-like rupture mode that propagates (in both cases) along the negative direction. The rupture tip propagating along the positive direction always remains crack-like.

4.3.3 The Birth and Growth of the Slip Pulse

In order to demonstrate the nucleation and growth of a slip pulse, we present a time sequence of pictures (Figure 4.5) taken from a single experiment. The inter-frame time is 3 μs while the first frame corresponds to 38 μs after triggering. The uniaxial pressure is 17 MPa, the inclination angle is 25°, and the fault core width b=1/8" for this experiment. As we can tell from the figures, the rupture in the positive direction (left) is always propagating at a speed close to the generalized Rayleigh wave speed of the system. The rupture in the negative direction is a standard single rupture initially (Figure 4.5A to C) and starting from Figure 4.3D we can identify two rupture tips the same way as we have discussed above.

An interesting observation is that the pulse length is approximately constant within the field of view of our experiment (~120mm). The pulse propagates at a speed close to the generalized Rayleigh wave speed of the system. The rupture tip history plot corresponding to this experiment is shown in Figure 4.6. The time-distance plot to the right clearly features a distinct point in which the rupture moving in the negative direction splits into two and becomes a stable pulse of constant width.

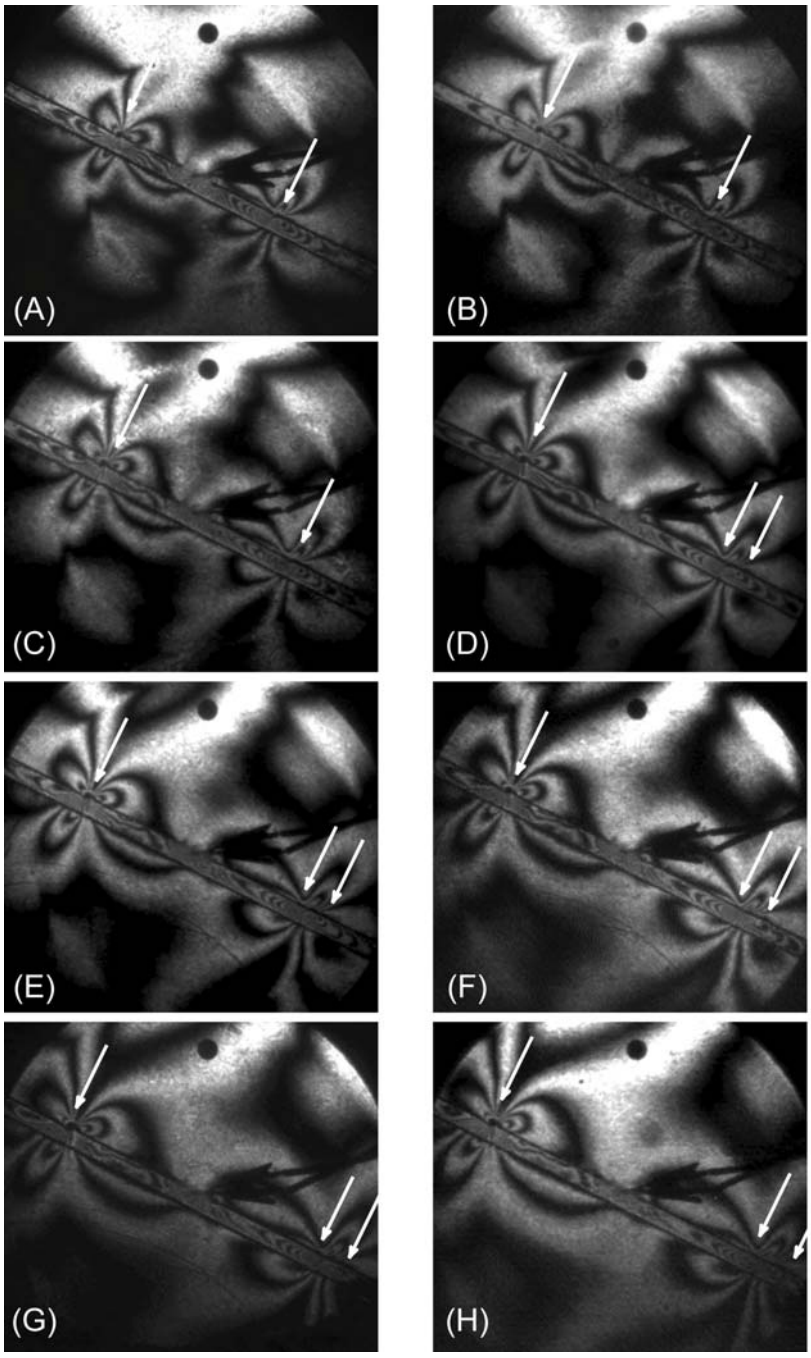

Figure 4.5 Photograph sequence from one experiment showing the birth of a self-sustained pulse (P=17 MPa, α=25°, b=1/8").

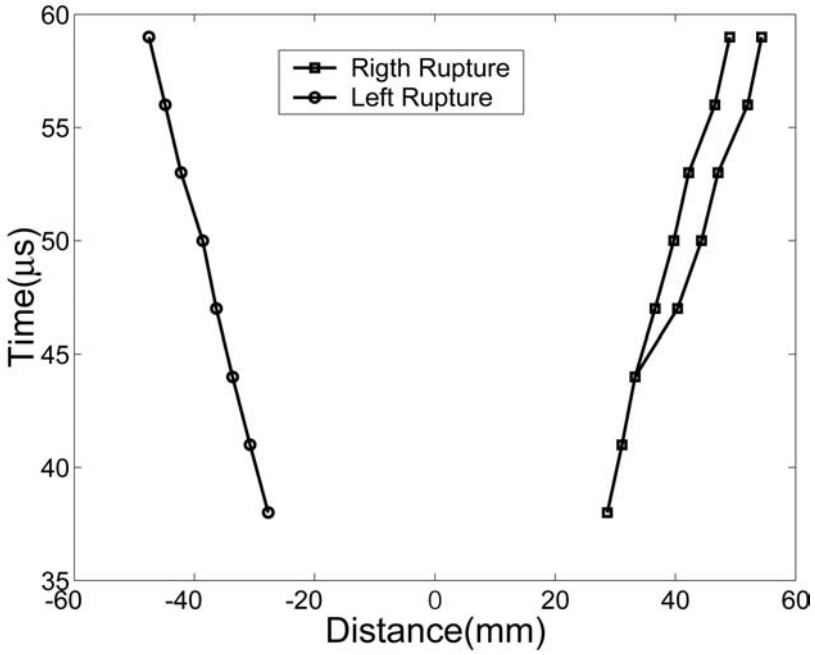

Figure 4.6 The rupture tip history of the experiment shown in Figure 4.5 (P=17 MPa, angle α=25°, and b=1/8").

4.3.4 The Effect of the Fault Core Width b on Faulting

To study the effect of the width of the fault core b on earthquake rupture mode selection, we contrast the isochromatic photographs of different experiments at the time instance after triggering with the same inclination angle (α=25°) and far-field uniaxial loading (P=17 MPa). This is done in Figure 4.7.

The three figures all features "left" propagating ruptures that are all crack-like and "right" propagating rupture that are pulse-like. The width of the pulse-like ruptures is approximately 6.4 mm and is independent of the width of the fault core.

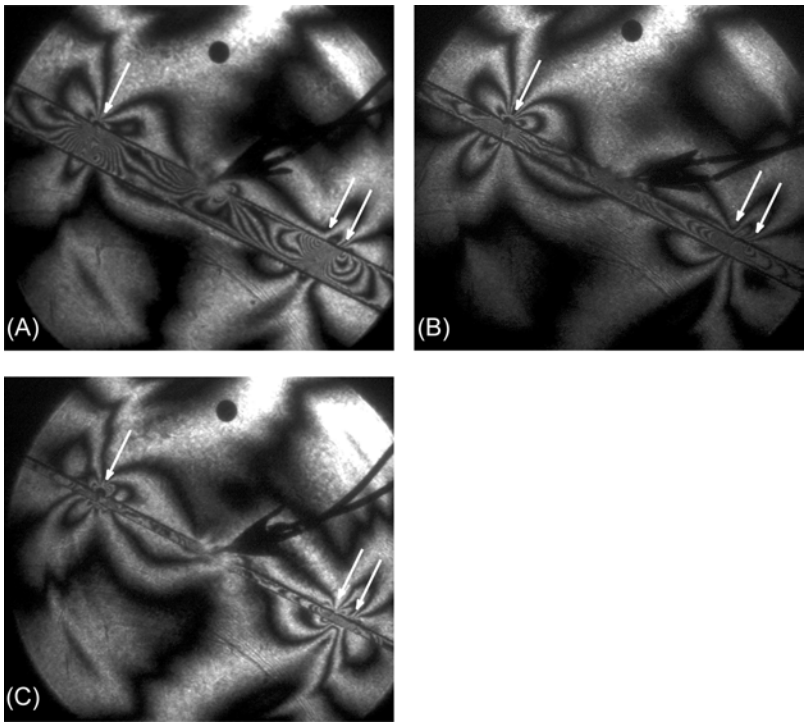

Figure 4.7 The effect of the width of the fault core b on earthquake faulting (Arrow indicates rupture tip). A (b=1/2"), B (b=1/4"), C (b=1/8").

4.3.5 The Effect of the Far-field Loading P on Rupture Speeds

To illustrate the effect of the far-field loading on earthquake faulting along faults with finite fault core, we show the isochromatic photographs taken at the time instance after the triggering with the same inclination angle (α=25°) and the same width of the fault core (b=1/8") in Figure 4.8. The three cases correspond to various compressive loads P (13, 17 and 20 MPa).

When the pressure level is low, as in Figure 4.8A, both the left and right ruptures are crack-like ruptures propagating at the Rayleigh wave speed of Polycarbonate (~900 m/s). For both the intermediate and high pressure level, as in Figures 4.8B and C, the left rupture is a crack mode rupture propagating at the generalized Rayleigh wave speed of the system (959 m/s) this rupture never

exceed C_{GR}. The rupture to the right, on the other hand, transitions from a crack-like to a pulse-like mode in a manner similar to that shown in Figure 4.6. After transition both rupture tips propagate at speed closet to $+C_{GR}$. This suggests that high enough loading is needed for the nucleation and growth of both the regular +GR rupture in the positive direction and the sub-shear pulse-like rupture in the opposite direction for given inclination angle, α.

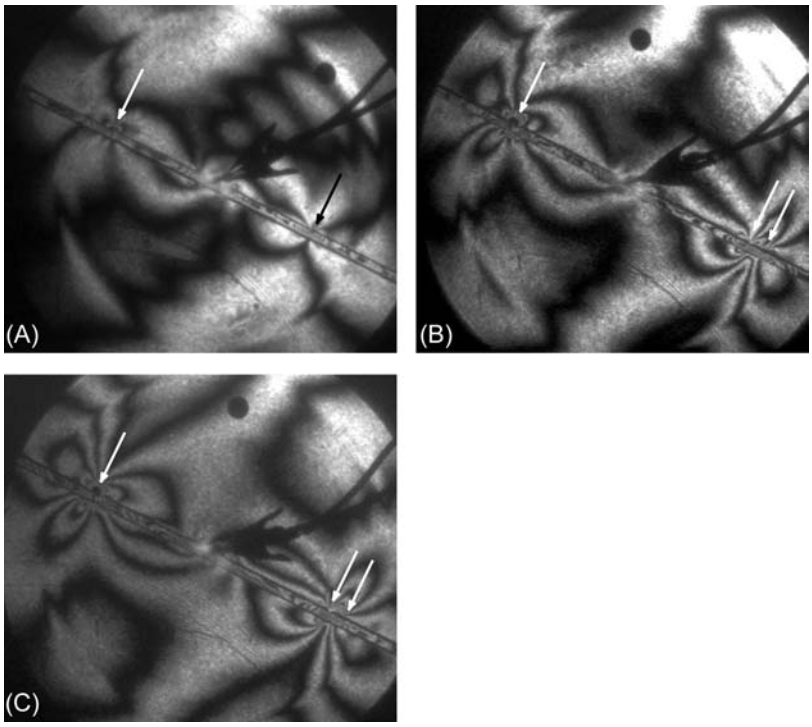

Figure 4.8 The effect of far-field loading on earthquake faulting along faults with a finite fault core (Arrow indicates rupture tip). A (P=13 MPa), B (P=17 MPa), C (P=20 MPa).

4.3.6 The Sub-shear to Supershear Transition and the Birth of an Unstable Pulse

In this section we report on an observation of rupture transition to supershear. In Figure 4.9, we present a time sequence of photographs of an experiment with

P=20 MPa, angle α=25° and d=1/8". In this experiment, we applied the highest level of compression. In all figures, the left ruptures are always crack-like and always grow at the generalized Rayleigh wave speed of the system. The right ruptures on the other hand start as crack-like and soon develop into pulse-like rupture after a certain growth distance. From Figure 4.9A-D, we can see that the width of the pulse is no longer constant but it increases with time. This fact can be seen clearly from Figure 4.10.

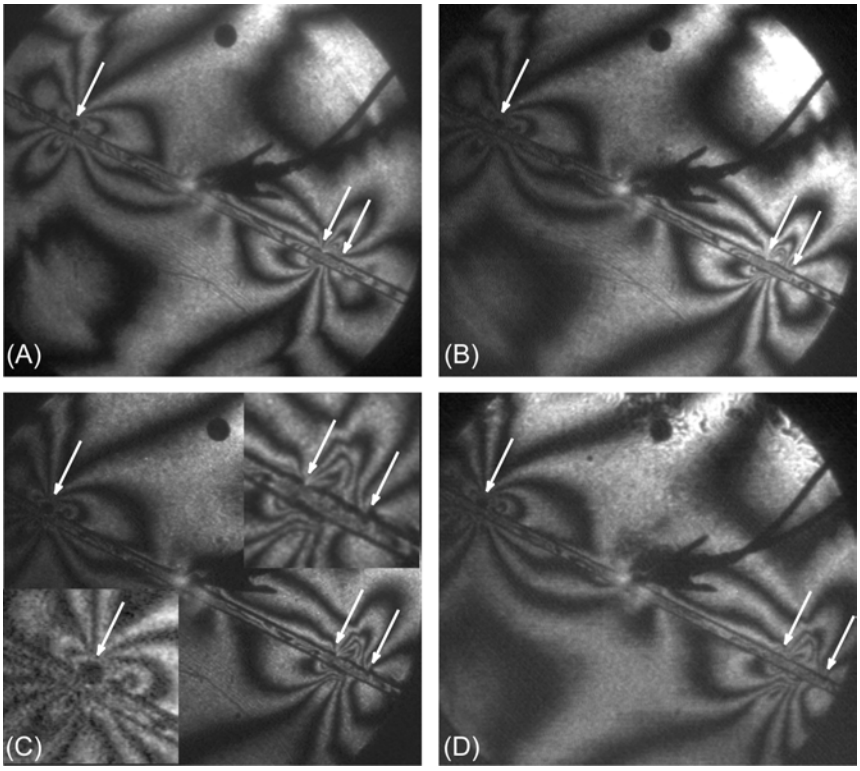

Figure 4.9 Photograph sequence from one experiment showing self-sustained pulse speed transition (P=20 MPa, angle α=25° and d=1/8"). A. 42 μs, B. 45 μs, C. 48 μs, D. 52 μs. In C, lower insert is the magnification of left rupture tip and upper insert is for the magnification of right rupture tip.

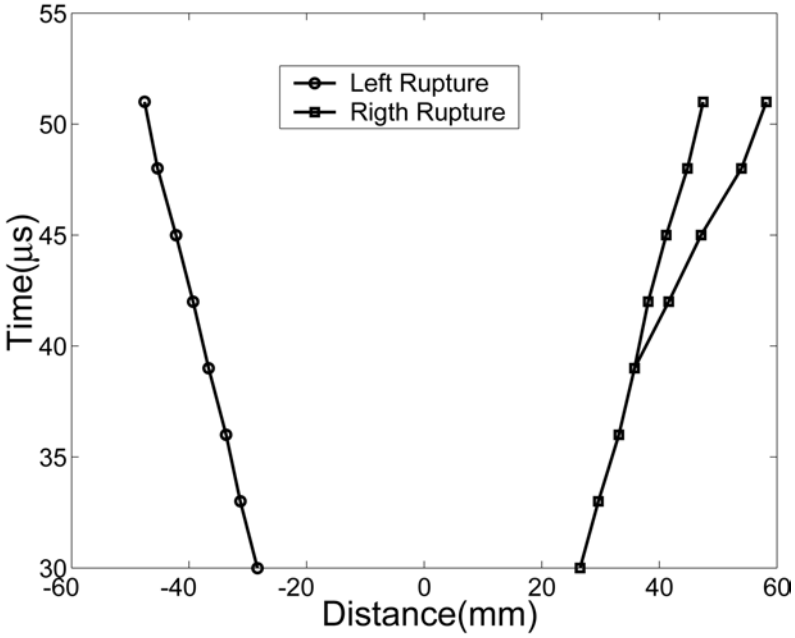

Figure 4.10 The rupture tip history of the experiment shown in Figure 4.8 (P=20 MPa, angle α=25°, and b=1/8").

Figure 4.10 shows the rupture length plot of the experiment shown in Figure 4.9. After nucleation of the pulse-like rupture (growing in the negative direction), the trailing edge of the pulse remains at the generalized Rayleigh wave speed, while the leading edge propagates at a supershear wave speed close to the P wave speed of Polycarbonate. This is consistent with the observation in Chapter 3 for bimaterial systems, where it was shown that a rupture tip moving in the negative direction transitions to a supershear speed close to $-P_{SLOW}$. Since we have not observed this supershear phenomena for experiments with lower pressure, it seems that there exists a critical pressure for given core width b and inclination angle α, beyond which the leading edge of the slip pulse propagates at a supershear wave speed right after the nucleation of the pulse-like mode. We can not exclude the possibility that there is a jump in rupture speed of the leading edge from the generalized Rayleigh wave speed to a supershear speed close to $-P_{SLOW}$ as we have shown in previous chapters. As in

the bimaterial case, the crack-like rupture propagating in the positive direction remains insensitive to the load level. The load however, greatly affects both mode and speed of the rupture growing to the right (positive direction). Here again we have the notion of a critical length or lengths of rupture growth after which the two transitions occur. One transition is a transition of mode and the other is a transition of speed. In the examples that we presented both of these transitions occurred simultaneously. The existence of this critical transition length provides a connection between large earthquake and growth in the negative direction.

Finally, the experimental results are summarized in Table 4.1.

Table 4.1 Summary of Experimental Results

α(°)	b(")	P(MPa)	Pulse-like	Left Rupture	Right Rupture[3]
25	1/8	20	Yes	$\sim C_{GR}$	$\sim C_P^2$
25	1/8	17	Yes	$\sim C_{GR}$	$\sim C_{GR}$
25	1/8	13	No	$\sim C_{GR}$	$\sim C_{GR}$
25	1/4	17	Yes	$\sim C_{GR}$	$\sim C_{GR}$
25	1/4	13	No	$\sim C_{GR}$	$\sim C_{GR}$
25	1/2	17	Yes	$\sim C_{GR}$	$\sim C_{GR}$
25	1/2	10	No	$\sim C_{GR}$	$\sim C_{GR}$
22.5	1/8	17	Yes	$\sim C_{GR}$	$\sim C_{GR}$
22.5	1/8	13	No	$\sim C_{GR}$	$\sim C_{GR}$
22.5	1/4	17	No	$\sim C_{GR}$	$\sim C_{GR}$
22.5	1/4	13	No	$\sim C_{GR}$	$\sim C_{GR}$
20	1/2	13	No	$\sim C_{GR}$	$\sim C_{GR}$
20	1/4	13	No	$\sim C_{GR}$	$\sim C_{GR}$
20	1/8	13	No	$\sim C_{GR}$	$\sim C_{GR}$
17.5	1/2	13	No	$\sim C_R^2$	$\sim C_R^2$
17.5	1/4	13	No	$\sim C_R^2$	$\sim C_R^2$

[3] There are two edges of the pulse-like rupture; the trailing pulse always propagates at C_{GR}. The listed values are rupture velocities of the leading rupture.

4.3.7 Comparison of Experiments with Available Numerical Results

There are no good field examples available for us to compare with our experiments. In addition the two existing numerical simulations (Harris and Day 1997; Ben-Zion and Huang 2002) relevant to our configurations are seem too primitive to provide complete explanations of the host of behaviors that we observed experimentally. However in this section we will attempt to perform some rudimentary comparisons.

There are indeed some similarities of our results to those of Harris and Day (Harris and Day 1997) for the case r_s=1.2 where generalized Rayleigh wave speed in defined. In this case the numerical results predict rupture moving in the positive direction that feature speed close to $+C_{GR}$. Along the negative direction both the numerical simulations and our experiments show that the supershear ruptures are possible. It is noteworthy to observe that such supershear rupture appear only in the negative direction. The supershear rupture velocity in both studies consistently points to the P wave speed of the slower fault core. The main difference consists in that we observed pulse-like ruptures along this direction whose leading edge propagates at a supershear speed. In contrast they only report the occurrence of strictly crack-like supershear modes. A closer look at the nature of the frictional law used by them may provide an explanation for the discrepancy.

The main difference between our results and Ben-Zion and Huang's numerical results is that the experimentally identified pulse-mode of rupture propagates in a different direction from what they suggested(Ben-Zion and Huang 2002). They only suggested the pulse-like rupture propagating in the positive direction while we did not have clear evidence to support that. The reason for these

discrepancies also remains obscure. Perhaps the choice of frictional law will provide the clue for that.

4.4 Conclusions and Discussions

In order to address the effect of the existence of a finite fault core on earthquake faulting, we have designed a laboratory fault model composed of two materials with different characteristic wave speeds. We use the material with the faster speeds to simulate the host rock and the material with the lower wave speeds to mimic the fault core.

We performed a series of experiments to understand the influence of geometrical and loading parameters involved in the problem (the inclination angle α, far-field loading P, and the fault core width b) on rupture mode and speed history. The results show that larger inclination angles, higher far-field loading and smaller fault core width facilitate the generation of faster speed ruptures and the birth of pulse-like ruptures that grow along the negative direction. In contrast, along the positive direction, our experiments consistently predict a crack-like rupture propagating at $+C_{GR}$ irrespective of parameter values.

The observed pulse-like mode of rupturing and its speed transition behavior are two new experimental results that question the validity of existing theoretical concepts that have emerged through numerical modeling. The discrepancies of the results of these models to the experiments will stimulate the search for more physically sound dynamic friction laws

Chapter 5

Summary and Future Work

Spontaneous rupture along incoherent (frictional) interfaces is the closest model for real earthquakes. In my thesis work, I designed a unique experimental set-up to investigate the dynamic process during spontaneous ruptures. Using this set-up, I have studied spontaneous earthquake ruptures in homogeneous faults, inhomogeneous faults, and faults with a finite core. Several interesting phenomena have been observed for the first time. These include the observation of spontaneous generated supershear ruptures, of the subRayleigh to supershear rupture transition, directionality in inhomogeneous faults, of the generalized Rayleigh wave speed ruptures, and of pulse-like ruptures. These laboratory observations have been used to explain a number of field observations and, are able to settle several long-standing debates in the field of the physics of naturally occurring earthquakes. This experimental set-up can also be used to address other issues in the field of earthquake dynamics; a few examples will be discussed in the section on future work.

5.1 Summary of the Thesis Work

There are three important components that are characteristics of naturally occurring earthquakes: a pre-existing fault, proper tectonic loading, and a certain triggering mechanism. Not all of these components have been fully considered in previous laboratory earthquake studies. In our laboratory earthquake model, we simulated the fault using the frictional contact between two polymer plates. We used uniaxial compression provided by a hydraulic press to mimic the far-field tectonic loading. As a special design of the whole

study, we applied an exploding wire technique to trigger the dynamic earthquake faulting by providing a local release of pressure at pre-determined location on the simulated fault. We controlled the magnitude of the explosion to ensure that it is negligible compared to the static loading and hence the rupture process is spontaneous in nature.

Our laboratory earthquake set-up has several advantages over more traditional set-ups used in experimental seismology. First, it addressed the triggering mechanism explicitly. The triggering design was shown to be very controllable and negligible in controlling the kinetics of during the rupturing process and it is also a very convenient way to trigger the high speed diagnostic system. Secondly, we have used a state-of-art diagnostics and full-field method that feature high spatial and temporal resolution. Traditional diagnostic methods, such as strain gauges and transducers, can be easily incorporated into a model to provide additional data sets as shown in the section on future work. Finally, we are able to trigger the rupture within the typical length scale of a laboratory specimen (~ 150 mm) because of the choice of the polymer as the material of choice. There are two reasons to use the polymer as model material: (a) it is birefringent as required by the diagnostics and (b) it is more compliant than rock so that the critical length of rupture nucleation is short (< 10 mm) for the loading levels used (~ 10 MPa). Being brittle it is aslo very well described yb the linear theory of elasticity and features infinitesimal deformations prior to the onset of rupture. This is a condition that allows us to perform desired comparison with both field data and available analysis.

Using the experimental set-up and diagnostics, we have made the following discoveries:

1. **For spontaneous earthquake type rupture along an interface separating similar materials, we observed supershear and the subRayleigh to supershear transition** (Chapter 2). Supershear ruptures (speed faster than the shear wave speed of the material) were observed to propagate at a speed close to the longitudinal speed of the material. This observation provided the first conclusive evidence of a supershear laboratory earthquake rupture. We also observed that a subRayleigh rupture (speed slower than the Rayleigh wave speed of the material) jumped to a supershear speed after a finite distance of propagation. This transition mechanism confirmed the Burridge-Andrews mechanism, also known as the Mother-daughter crack model. This transition mechanism, which has never been observed experimentally before, serves as a physical rationalization of creation for supershear ruptures during spontaneously occurring earthquake ruptures, which always start at a subRayleigh speed. We have discussed some relevant field evidence supporting supershear rupture and the subRayleigh to supershear transition.

2. **For spontaneous rupture between dissimilar materials, we observed ruptures propagating bilaterally at different speeds, one at the Generalized Rayleigh wave speed and the other at either subRayleigh or supershear speed** (Chapter 3)**.** Spontaneous ruptures were observed propagating approximately at generalized Rayleigh wave speed in the same direction as that of slip of lower velocity solid. In the opposite direction, we observed either subRayleigh or supershear ruptures depending on the loading condition. Here we provided the first conclusive, experimental evidence supporting theoretical and numerical results by Rice, Harris, and their coworkers. Using our experimental observation, we tried to explain the seismic history on the North Anatolian Fault. With proper assumption of the material contrast, we rationalized the seemingly contradicting observations.

3. **For spontaneous rupture along faults with a finite fault core (low-velocity zone), we have observed and described, for the first time, the occurrence of a self-healing "Heaton" pulse** (Chapter 4)**.** We simulated the fault core using a material with wave speeds that are lower than the material used to simulate the host rock. This is the first experimental attempt to study this fault geometry. When the loading level is low, both ruptures in the positive and opposite directions are subshear ruptures. At high enough loading, a Heaton pulse was found to be nucleated and to propagate in the negative direction, which is a direction different from that suggested by existing numerical simulations. This pulse became supershear as the load was increased drastically. The rupture propagating along the positive direction always remained crack-like and grew at the generalized Rayleigh wave speed. This observation can be used to validate available friction models. We propose to construct a frictional model that is able to reproduce our experiment, before we apply it to numerical simulations in a geological length scale.

5.2 Future Work

In the previous section, we showed several exciting experimental results obtained by using our set-up. These results however only represent the first step towards the full understanding of the physics of earthquakes and it is time for us to make substantial progress. So far, we have only studied straight faults that are homogeneous in strength. We have also only recorded the transient stress field associated with the rupturing process. The following proposed projects are intended to loosen these constraints.

5.2.1 Effect of Inhomogeneities of Fault Strength on Faulting (Barrier and Asperity)

Based on the seismological observation, the barrier and asperity model were proposed by Das and Kanamori respectively (Das, Boatwright, et al. 1988). In order to check the influence of barrier and asperity on rupturing, we will use simulated barriers and asperities in the laboratory fault model. The laboratory fault model itself can be homogenous, inhomogeneous, or sandwich. We will apply glue and lubricant to small patches of the fault. Patches with glue correspond to barriers and patches with lubricant correspond to asperities (Figure 5.1). Transducers will also be used to obtain seismic waves; we will check the signature of barriers and asperities on seismic waves.

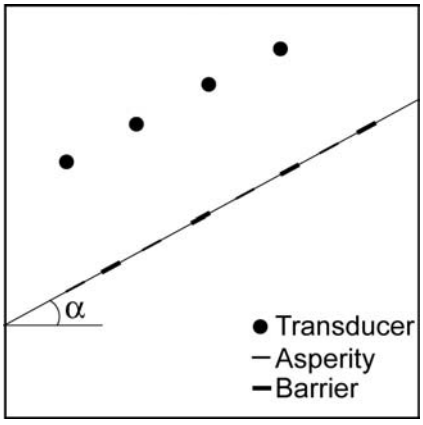

Figure 5.1 Fault model with barriers and asperities.

5.2.2 Effect of Fault Steps on Faulting (Dynamic Triggering and Rupture Arrest)

Natural faults usually have some steps or jogs. Depending on the force produced during the earthquake faulting, there are two types of steps, namely dilatational and compressive (Figure 5.2). The propagating earthquake rupture may be facilitated or delayed at steps (Sibson 1985; Harris and Day 1993). The

jumping of a rupture to a neighboring fault (no fault connecting them), which is sometimes called dynamic triggering, can also be studied.

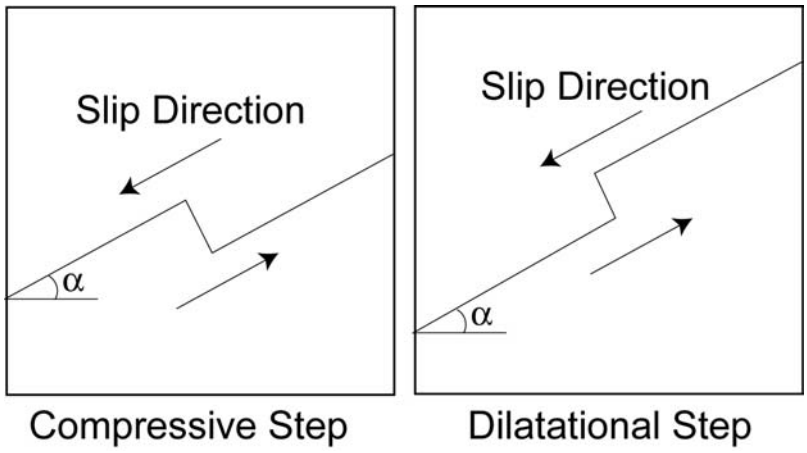

Figure 5.2 Faults with steps.

5.2.3 Direct Measurements of Slip History

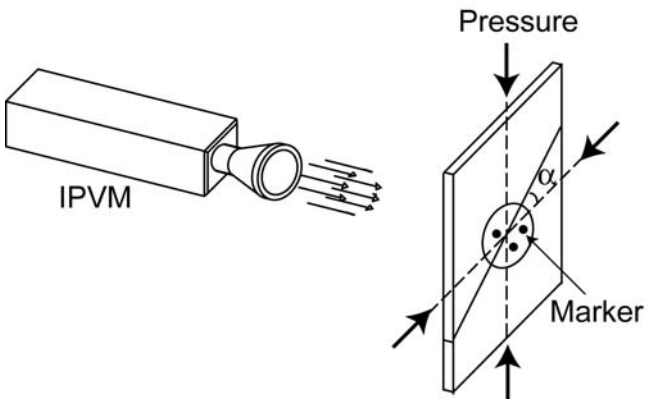

Figure 5.3 Schematic of the measurement of slip history

The direct measurement of the slip history at points close to the fault and at a very high frequency is very important to the understanding of the rupturing process; it also provides a link of the laboratory earthquake to the real

earthquake, through the comparison of slip data measured in the laboratory and that measured by high speed (up to 1 Hz) Global Positioning System (GPS) (Larson, Bodin, et al. 2003). An In-Plane Velocity Meter (IPVM) is currently available in our laboratory.

IPVM can remotely measure the in-plane velocity of a small optical marker (reflector) attached onto the specimen surface (see Figure 5.3) at high spatial and temporal resolutions. Using this method, we would be able to directly check the rupture mode, i.e. pulse-like or crack-like and to obtain signatures of "ground" velocity and acceleration at various locations away or adjacent to the fault.

5.2.4 Direct Measurements of Transient Temperature Increase (Heat Production and Flash Heating)

The heat production during earthquakes has been a long-standing problem in the community of geophysics. The paradox of heat flow in the San Andres Fault is still not resolved (Lachenbruch and Sass 1980). A remote, high speed thermometer, uses the principle of radiation, can be applied to measure the transient temperature increase during earthquakes. A high speed infrared camera capable of 1 million frames per second, which has recently been developed by Prof. Rosakis and Ravichandran would be perfect for this task. The experimental set-up is similar to that shown in Figure 5.3. This experiment can also be used to check the idea of flash heating, proposed by Rice to explain the low dynamic frictional resistance during natural earthquakes.

5.3 Conclusion

In summary, inspired by the success of laboratory earthquake experiments during my Ph.D. study, I have proposed several problems that can be

investigated in the near future. I strongly believe that it is time for us to make significant progress in the direction of laboratory earthquakes. We can combine all these measurements together with cooperative efforts from numerical and theoretical researchers to obtain a better physical picture of the faulting process.

BIBLIOGRAPHY

Aagaard, B. T. and T. H. Heaton (2004). "Near-source ground motions from simulations of sustained intersonic and supersonic fault ruptures." Bulletin of the Seismological Society of America **(submitted)**.

Aagaard, B. T., T. H. Heaton,, et al. (2001). "Dynamic earthquake ruptures in the presence of lithostatic normal stresses: Implications for friction models and heat production." Bulletin of the Seismological Society of America **91**(6): 1765-1796.

Abraham, F. F. and H. J. Gao (2000). "How fast can cracks propagate?" Physical Review Letters **84**(14): 3113-3116.

Adams, G. G. (1995). "Self-excited oscillations of two elastic half-spaces sliding with a constant coefficient of friction." Journal of Applied Mechanics-Transactions of the Asme **62**(4): 867-872.

Adams, G. G. (1998). "Steady sliding of two elastic half-spaces with friction reduction due to interface stick-slip." Journal of Applied Mechanics-Transactions of the Asme **65**(2): 470-475.

Adams, G. G. (2001). "An intersonic slip pulse at a frictional interface between dissimilar materials." Journal of Applied Mechanics-Transactions of the Asme **68**(1): 81-86.

Ahrens, T. J., Ed. (1995). Rock physics and phase relations: a handbook of physical constants. Washington, D.C., American Geophysical Union.

Andrews, D. J. (1976). "Rupture Velocity of Plane Strain Shear Cracks." Journal of Geophysical Research **81**(32): 5679-5687.

Andrews, D. J. (1985). "Dynamic Plane-Strain Shear Rupture with a Slip-Weakening Friction Law Calculated by a Boundary Integral Method." Bulletin of the Seismological Society of America **75**(1): 1-21.

Andrews, D. J. and Y. Ben-Zion (1997). "Wrinkle-like slip pulse on a fault between different materials." Journal of Geophysical Research-Solid Earth **102**(B1): 553-571.

Anooshehpoor, A. and J. N. Brune (1994). "Frictional Heat-Generation and Seismic Radiation in a Foam Rubber Model of Earthquakes." Pure and Applied Geophysics **142**(3-4): 735-747.

Anooshehpoor, A. and J. N. Brune (1999). "Wrinkle-like Weertman pulse at the interface between two blocks of foam rubber with different velocities." Geophysical Research Letters **26**(13): 2025-2028.

Archuleta, R. J. (1984). "A Faulting Model for the 1979 Imperial-Valley Earthquake." Journal of Geophysical Research **89**(NB6): 4559-4585.

Archuleta, R. J. and J. N. Brune (1975). "Surface Strong Motion Associated with a Stick-Slip Event in a Foam Rubber Model of Earthquakes." Bulletin of the Seismological Society of America **65**(5): 1059-1071.

Ben-Zion, Y. (2001). "Dynamic ruptures in recent models of earthquake faults." Journal of the Mechanics and Physics of Solids **49**(9): 2209-2244.

Ben-Zion, Y. and Y. Q. Huang (2002). "Dynamic rupture on an interface between a compliant fault zone layer and a stiffer surrounding solid." Journal of Geophysical Research-Solid Earth **107**(B2): art. no.-2042.

Ben-Zion, Y. and C. G. Sammis (2003). "Characterization of fault zones." Pure and Applied Geophysics **160**(3-4): 677-715.

Blanpied, M. L., T. E. Tullis,, et al. (1998). "Effects of slip, slip rate, and shear heating on the friction of granite." Journal of Geophysical Research-Solid Earth **103**(B1): 489-511.

Bouchon, M., M. P. Bouin,, et al. (2001). "How fast is rupture during an earthquake? New insights from the 1999 Turkey earthquakes." Geophysical Research Letters **28**(14): 2723-2726.

Bouchon, M. and M. Vallee (2003). "Observation of long supershear rupture during the magnitude 8.1 Kunlunshan earthquake." Science **301**(5634): 824-826.

Bowden, F. P. and D. Tabor (1986). The friction and lubrication of solids. Oxford, Clarenden Press.

Brace, W. F. and J. D. Byerlee (1966). "Stick-Slip as a Mechanism for Earthquakes." Science **153**(3739): 990-&.

Broberg, K. B. (1999). Cracks and Fracture. San Diego, Academic Press.

Brodsky, E. E., V. Karakostas,, et al. (2000). "A new observation of dynamically triggered regional seismicity: Earthquakes in Greece following the August, 1999 Izmit, Turkey earthquake." Geophysical Research Letters **27**(17): 2741-2744.

Brune, J. N. (1970). "Tectonic Stress and Spectra of Seismic Shear Waves from Earthquakes." Journal of Geophysical Research **75**(26): 4997-&.

Brune, J. N. (1973). "Earthquake Modeling by Stick-Slip Along Precut Surfaces in Stressed Form Rubber." Bulletin of the Seismological Society of America **63**(6): 2105-2119.

Brune, J. N. and A. Anooshehpoor (1997). "Frictional resistance of a fault zone with strong rotors." Geophysical Research Letters **24**(16): 2071-2074.

Brune, J. N., S. Brown,, et al. (1993). "Rupture Mechanism and Interface Separation in Foam Rubber Models of Earthquakes - a Possible Solution to the Heat-Flow Paradox and the Paradox of Large Overthrusts." Tectonophysics **218**(1-3): 59-67.

Burridge, R. (1973). "Admissible Speeds for Plane-Strain Self-Similar Shear Cracks with Friction but Lacking Cohesion." Geophysical Journal of the Royal Astronomical Society **35**(4): 439-455.

Burridge, R., G. Conn,, et al. (1979). "Stability of a Rapid Mode-Ii Shear Crack with Finite Cohesive Traction." Journal of Geophysical Research **84**(NB5): 2210-2222.

Chester, F. M. and J. S. Chester (1998). "Ultracataclasite structure and friction processes of the Punchbowl fault, San Andreas system, California." Tectonophysics **295**(1-2): 199-221.

Cochard, A. and J. R. Rice (2000). "Fault rupture between dissimilar materials: Ill-posedness, regularization, and slip-pulse response." Journal of Geophysical Research-Solid Earth **105**(B11): 25891-25907.

Coker, D., G. Lykotrafitis,, et al. (2004). "Frictional sliding modes along an interface between identical elastic plates subject to shear impact loading." Journal of the Mechanics and Physics of Solids (In Press).

Coker, D. and A. J. Rosakis (2001). "Experimental observations of intersonic crack growth in asymmetrically loaded unidirectional composite plates." Philosophical Magazine a-Physics of Condensed Matter Structure Defects and Mechanical Properties **81**(3): 571-595.

Coker, D., A. J. Rosakis,, et al. (2003). "Dynamic crack growth along a polymer composite-Homalite interface." Journal of the Mechanics and Physics of Solids **51**(3): 425-460.

Cotterell, B. and J. R. Rice (1980). "Slightly Curved or Kinked Cracks." International Journal of Fracture **16**(2): 155-169.

Dally, J. W. and W. F. Riley (1991). Experimental Stress Analysis. New York, McGraw-Hill, Inc.

Das, S. and K. Aki (1977). "Numerical Study of 2-Dimensional Spontaneous Rupture Propagation." Geophysical Journal of the Royal Astronomical Society **50**(3): 643-668.

Das, S., J. Boatwright,, et al., Eds. (1988). Earthquake Source Mechanics. Geophysical monograph ; 37. Washington, American Geophysical Union.

Day, S. M. (1982). "3-Dimensional Simulation of Spontaneous Rupture - the Effect of Nonuniform Prestress." Bulletin of the Seismological Society of America **72**(6): 1881-1902.

Dieterich, J. H. (1972). "Time-Dependent Friction as a Possible Mechanism for Aftershocks." Journal of Geophysical Research **77**(20): 3771-&.

Dieterich, J. H. (1979). "Modeling of Rock Friction .1. Experimental Results and Constitutive Equations." Journal of Geophysical Research **84**(NB5): 2161-2168.

Dieterich, J. H. (1992). "Earthquake Nucleation on Faults with Rate-Dependent and State- Dependent Strength." Tectonophysics **211**(1-4): 115-134.

Dieterich, J. H. and B. D. Kilgore (1994). "Direct Observation of Frictional Contacts - New Insights for State-Dependent Properties." Pure and Applied Geophysics **143**(1-3): 283-302.

Dunham, E. M. and R. J. Archuleta (2004). "Evidence for a Supershear Transient during the 2002 Denali Fault Earthquake." Bulletin of the Seismological Society of America **(submitted)**.

Dunham, E. M., P. Favreau,, et al. (2003). "A supershear transition mechanism for cracks." Science **299**(5612): 1557-1559.

Eberhart-Phillips, D., P. J. Haeussler,, et al. (2003). "The 2002 Denali fault earthquake, Alaska: A large magnitude, slip-partitioned event." Science **300**(5622): 1113-1118.

Eberhart-Phillips, D. and A. J. Michael (1998). "Seismotectonics of the Loma Prieta, California, region determined from three-dimensional V-p, V-p/V-s, and seismicity." Journal of Geophysical Research-Solid Earth **103**(B9): 21099-21120.

Ellsworth, W. L., M. Çlebi,, et al. (2004). Processing and Modeling of the Pump Station 10 Record from the November 3, 2002, Denali Fault, Alaska Earthquake. Eleventh International Conference of Soil Dynamics and Earthquake Engineering, Berkeley, California, Jan. 7-9.

Freund, L. B. (1990). Dynamic Fracture Mechanics. Cambridge ; New York, Cambridge University Press.

Fukuyama, E. and R. Madariaga (1998). "Rupture dynamics of a planar fault in a 3D elastic medium: Rate- and slip-weakening friction." Bulletin of the Seismological Society of America 8**8(**1): 1-17.

Geubelle, P. H. and D. V. Kubair (2001). "Intersonic crack propagation in homogeneous media under shear- dominated loading: numerical analysis." Journal of the Mechanics and Physics of Solids 4**9(**3): 571-587.

Gomberg, J., P. Bodin,, et al. (2003). "Observing earthquakes triggered in the near field by dynamic deformations." Bulletin of the Seismological Society of America 9**3(**1): 118-138.

Gu, Y. J. and T. F. Wong (1994). "Development of Shear Localization in Simulated Quartz Gouge - Effect of Cumulative Slip and Gouge Particle-Size." Pure and Applied Geophysics 1**43(**1-3): 387-423.

Harris, R. A. and S. M. Day (1993). "Dynamics of Fault Interaction - Parallel Strike-Slip Faults." Journal of Geophysical Research-Solid Earth 9**8(**B3): 4461-4472.

Harris, R. A. and S. M. Day (1997). "Effects of a low-velocity zone on a dynamic rupture." Bulletin of the Seismological Society of America 8**7(**5): 1267-1280.

Heaton, T. H. (1990). "Evidence for and Implications of Self-Healing Pulses of Slip in Earthquake Rupture." Physics of the Earth and Planetary Interiors 6**4(**1): 1-20.

Hutchinson, J. W. and Z. Suo (1992). Mixed-Mode Cracking in Layered Materials. Advances in Applied Mechanics, Vol 29. 2**9: 6**3-191.

Ida, Y. (1972). "Cohesive Force across Tip of a Longitudinal-Shear Crack and Griffiths Specific Surface-Energy." Journal of Geophysical Research 77(20): 3796-&.

Ide, S. and M. Takeo (1997). "Determination of constitutive relations of fault slip based on seismic wave analysis." Journal of Geophysical Research-Solid Earth 102(B12): 27379-27391.

Ji, C., D. J. Wald,, et al. (2002). "Source description of the 1999 Hector Mine, California, earthquake, part I: Wavelet domain inversion theory and resolution analysis." Bulletin of the Seismological Society of America 92(4): 1192-1207.

Johnson, T. L. and C. H. Scholz (1976). "Dynamic Properties of Stick-Slip Friction of Rock." Journal of Geophysical Research 81(5): 881-888.

Kanamori, H. (1994). "Mechanics of Earthquakes." Annual Review of Earth and Planetary Sciences 22: 207-237.

Koketsu, K., K. Hikima,, et al. (2004). "Joint inversion of strong motion and geodetic data for the source process of the 2003 Tokachi-oki, Hokkaido, earthquake." Earth Planets and Space 56(3): 329-334.

Kostrov, B. V. (1966). "Unsteady Propagation of Longitudinal Shear Cracks." Pmm Journal of Applied Mathematics and Mechanics 30(6): 1241-&.

Kostrov, B. V. and S. Das (1988). Principles of Earthquake Source Mechanics. Cambridge ; New York, Cambridge University Press.

Kubair, D. V., P. H. Geubelle,, et al. (2003). "Analysis of a rate-dependent cohesive model for dynamic crack propagation." Engineering Fracture Mechanics 70(5): 685-704.

Kubair, D. V., P. H. Geubelle,, et al. (2002). "Intersonic crack propagation in homogeneous media under shear- dominated loading: theoretical analysis." Journal of the Mechanics and Physics of Solids 50(8): 1547-1564.

Lachenbruch, A. H. and J. H. Sass (1980). "Heat-Flow and Energetics of the San-Andreas Fault Zone." Journal of Geophysical Research 85(NB11): 6185-6222.

Lambros, J. and A. J. Rosakis (1995). "Development of a dynamic decohesion criterion for subsonic fracture of the interface between two dissimilar materials." Proceedings of the Royal Society of London Series a-Mathematical Physical and Engineering Sciences 451(1943): 711-736.

Lambros, J. and A. J. Rosakis (1995). "Dynamic Decohesion of Bimaterials - Experimental-Observations and Failure Criteria." International Journal of Solids and Structures 32(17-18): 2677-&.

Lapusta, N. and J. R. Rice (2003). "Nucleation and early seismic propagation of small and large events in a crustal earthquake model." Journal of Geophysical Research-Solid Earth 108(B4): art. no.-2205.

Larson, K. M., P. Bodin,, et al. (2003). "Using 1-Hz GPS data to measure deformations caused by the Denali fault earthquake." Science 3**00(**5624): 1421-1424.

Lin, A. M., B. H. Fu,, et al. (2002). "Co-seismic strike-stip and rupture length produced by the 2001 M-s 8.1 Central Kunlun earthquake." Science 2**96(**5575): 2015-2017.

Madariaga, R. and K. B. Olsen (2000). "Criticality of rupture dynamics in 3-D." Pure and Applied Geophysics 1**57(**11-12): 1981-2001.

Magistrale, H. and C. Sanders (1995). "P-Wave Image of the Peninsular Ranges Batholith, Southern California." Geophysical Research Letters 2**2(**18): 2549-2552.

McGuire, J. J., L. Zhao,, et al. (2002). "Predominance of unilateral rupture for a global catalog of large earthquakes." Bulletin of the Seismological Society of America 9**2(**8): 3309-3317.

Miyatake, T. (1992). "Numerical-Simulation of 3-Dimensional Faulting Processes with Heterogeneous Rate-Dependent and State-Dependent Friction." Tectonophysics 2**11(**1-4): 223-232.

Nemat-Nasser, S. and H. Horii (1982). "Compression-Induced Nonplanar Crack Extension with Application to Splitting, Exfoliation, and Rockburst." Journal of Geophysical Research 8**7(**NB8): 6805-6821.

Nielsen, S. B., J. M. Carlson,, et al. (2000). "Influence of friction and fault geometry on earthquake rupture." Journal of Geophysical Research-Solid Earth 1**05(**B3): 6069-6088.

Ohnaka, M. (2003). "A constitutive scaling law and a unified comprehension for frictional slip failure, shear fracture of intact rock, and earthquake rupture." Journal of Geophysical Research-Solid Earth 1**08(**B2): art. no.-2080.

Ohnaka, M., M. Akatsu,, et al. (1997). "A constitutive law for the shear failure of rock under lithospheric conditions." Tectonophysics 2**77(**1-3): 1-27.

Ohnaka, M. and L. F. Shen (1999). "Scaling of the shear rupture process from nucleation to dynamic propagation: Implications of geometric irregularity of the rupturing surfaces." Journal of Geophysical Research-Solid Earth 1**04(**B1): 817-844.

Okubo, P. G. and J. H. Dieterich (1984). "Effects of Physical Fault Properties on Frictional Instabilities Produced on Simulated Faults." Journal of Geophysical Research 8**9(**NB7): 5817-5827.

Olsen, K. B., R. Madariaga,, et al. (1997). "Three-dimensional dynamic simulation of the 1992 Landers earthquake." Science 2**78(**5339): 834-838.

Olsen, M. P., C. H. Scholz,, et al. (1998). "Healing and sealing of a simulated fault gouge under hydrothermal conditions: Implications for fault healing." Journal of Geophysical Research-Solid Earth 1**03(**B4): 7421-7430.

Palmer, A. C. and J. R. Rice (1973). "Growth of Slip Surfaces in Progressive Failure of over- Consolidated Clay." Proceedings of the Royal Society of London Series a- Mathematical Physical and Engineering Sciences 3**32(**1591): 527-548.

Parsons, T., S. Toda,, et al. (2000). "Heightened odds of large earthquakes near Istanbul: An interaction-based probability calculation." Science 2**88(**5466): 661-665.

Peltzer, G., F. Crampe,, et al. (1999). "Evidence of nonlinear elasticity of the crust from the Mw7.6 Manyi (Tibet) earthquake." Science 2**86(**5438): 272-276.

Prakash, V. (1995). "A pressure-shear plate impact experiment for investigating transient friction." Experimental Mechanics 3**5(**4): 329-336.

Prakash, V. (1998). "Time-resolved friction with applications to high-speed machining: Experimental observations." Tribology Transactions 4**1(**2): 189-198.

Prakash, V. and R. J. Clifton (1993). Time resolved dynamic friction measurements in pressure-shear. Experiemental techniques in the dynamics of deformable solids. K. T. Ramesh. New York, Applied mechanics division, ASME. 1**65: 3**3-48.

Ranjith, K. and J. R. Rice (1999). "Stability of quasi-static slip in a single degree of freedom elastic system with rate and state dependent friction." Journal of the Mechanics and Physics of Solids 4**7(**6): 1207-1218.

Ranjith, K. and J. R. Rice (2001). "Slip dynamics at an interface between dissimilar materials." Journal of the Mechanics and Physics of Solids 4**9(**2): 341-361.

Renardy, M. (1992). "Ill-Posedness at the Boundary for Elastic Solids Sliding under Coulomb-Friction." Journal of Elasticity 2**7(**3): 281-287.

Rice, J. R. (1983). "Constitutive Relations for Fault Slip and Earthquake Instabilities." Pure and Applied Geophysics 1**21(**3): 443-475.

Rice, J. R. (2001). New perspectives in crack and fault dynamics. Mechanics for a New Millennium (Proceedings of the 20th International Congress of Theoretical and Applied Mechanics, 27 Aug - 2 Sept 2000,). H. Aref and J. W. Phillips. Chicago, Kluwer Academic Publishers: **1**-23.

Rice, J. R., N. Lapusta,, et al. (2001). "Rate and state dependent friction and the stability of sliding between elastically deformable solids." Journal of the Mechanics and Physics of Solids 4**9(**9): 1865-1898.

Rosakis, A. J. (2002). "Intersonic shear cracks and fault ruptures." Advances in Physics 5**1(**4): 1189-1257.

Rosakis, A. J., O. Samudrala,, et al. (1999). "Cracks faster than the shear wave speed." Science 2**84(**5418): 1337-1340.

Rosakis, A. J., O. Samudrala,, et al. (2000). "Intersonic shear crack growth along weak planes." Materials Research Innovations 3**(**4): 236-243.

Rosakis, A. J., O. Samudrala,, et al. (1998). "Intersonic crack propagation in bimaterial systems." Journal of the Mechanics and Physics of Solids 4**6(**10): 1789-1813.

Rubin, A. M. and D. Gillard (2000). "Aftershock asymmetry/rupture directivity among central San Andreas fault microearthquakes." Journal of Geophysical Research-Solid Earth 1**05(**B8): 19095-19109.

Ruina, A. (1983). "Slip Instability and State Variable Friction Laws." Journal of Geophysical Research 8**8(**NB12): 359-370.

Sagy, A., Z. Reches,, et al. (2001). "Dynamic fracturing: field and experimental observations." Journal of Structural Geology 2**3(**8): 1223-1239.

Samudrala, O., Y. Huang,, et al. (2002). "Subsonic and intersonic mode II crack propagation with a rate- dependent cohesive zone." Journal of the Mechanics and Physics of Solids 5**0(**6): 1231-1268.

Samudrala, O., Y. Huang,, et al. (2002). "Subsonic and intersonic shear rupture of weak planes with a velocity weakening cohesive zone." Journal of Geophysical Research-Solid Earth 1**07(**B8): art. no.-2170.

Samudrala, O. and A. J. Rosakis (2003). "Effect of loading and geometry on the subsonic/intersonic transition of a bimaterial interface crack." Engineering Fracture Mechanics 7**0(**2): 309-337.

Scholz, C., P. Molnar,, et al. (1972). "Detailed Studies of Frictional Sliding of Granite and Implications for Earthquake Mechanism." Journal of Geophysical Research 7**7(**32): 6392-&.

Scholz, C. H. (2002). The Mechanics of Earthquakes and Faulting. Cambridge; New York, Cambridge University Press.

Sharon, E. and J. Fineberg (1996). "Microbranching instability and the dynamic fracture of brittle materials." Physical Review B 5**4(**10): 7128-7139.

Sibson, R. H. (1985). "Stopping of Earthquake Ruptures at Dilational Fault Jogs." Nature 3**16(**6025): 248-251.

Sibson, R. H. (2003). "Thickness of the seismic slip zone." Bulletin of the Seismological Society of America 9**3(**3): 1169-1178.

Sleep, N. H. (1995). "Frictional Heating and the Stability of Rate and State-Dependent Frictional Sliding." Geophysical Research Letters 2**2(**20): 2785-2788.

Spudich, P. and E. Cranswick (1984). "Direct Observation of Rupture Propagation During the 1979 Imperial Valley Earthquake Using a Short Baseline Accelerometer Array." Bulletin of the Seismological Society of America 7**4(**6): 2083-2114.

Stein, R. S., A. A. Barka,, et al. (1997). "Progressive failure on the North Anatolian fault since 1939 by earthquake stress triggering." Geophysical Journal International 1**28(**3): 594-604.

Uenishi, K. and J. R. Rice (2003). "Universal nucleation length for slip-weakening rupture instability under nonuniform fault loading." Journal of Geophysical Research-Solid Earth 1**08(**B1): art. no.-2042.

Uenishi, K., H. P. Rossmanith,, et al. (1999). "Rayleigh pulse-dynamic triggering of fault slip." Bulletin of the Seismological Society of America 8**9(**5): 1296-1312.

Wald, D. J. and T. H. Heaton (1994). "Spatial and Temporal Distribution of Slip for the 1992 Landers, California, Earthquake." Bulletin of the Seismological Society of America 8**4(**3): 668-691.

Weertman, J. (1980). "Unstable Slippage across a Fault That Separates Elastic Media of Different Elastic-Constants." Journal of Geophysical Research 8**5(**NB3): 1455-1461.

Wu, F. T., K. C. Thomson,, et al. (1972). "Stick-Slip Propagation Velocity and Seismic Source Mechanism." Bulletin of the Seismological Society of America 6**2(**6): 1621-1628.

Xia, K. W., A. J. Rosakis,, et al. (2004). "Laboratory earthquakes: The sub-Rayleigh-to-supershear rupture transition." Science 3**03(**5665): 1859-1861.

Yomogida, K. and T. Nakata (1994). "Large Slip Velocity of the Surface Rupture Associated with the 1990 Luzon Earthquake." Geophysical Research Letters 2**1(**17): 1799-1802.

Zheng, G. and J. R. Rice (1998). "Conditions under which velocity-weakening friction allows a self-healing versus a cracklike mode of rupture." Bulletin of the Seismological Society of America 8**8(**6): 1466-1483.

Zor, E., E. Sandvol,, et al. (2003). "The crustal structure of the East Anatolian plateau (Turkey) from receiver functions." Geophysical Research Letters 3**0(**24).